Scaling effects in the mechanical behaviour of carbon nanoparticle modified fibre reinforced polymers

Vom Promotionsausschuss
der Technischen Universität Hamburg
zur Erlangung des akademischen Grades
Doktor-Ingenieur (Dr.-Ing.)

genehmigte Dissertation

von

Christian Leopold

aus Lübeck

2018

Gutachter	Prof. Dr.-Ing. habil. Bodo Fiedler *(Technische Universität Hamburg)* Prof. Dr.-Ing. habil. Maik Gude *(Technische Universität Dresden)*
Vorsitzender des Prüfungsausschusses:	Prof. Dr.-Ing. Otto von Estorff *(Technische Universität Hamburg)*

Tag der mündlichen Prüfung: 05.12.2018

Danksagung

Diese Arbeit ist zwischen 2014 und 2018 während meiner Tätigkeit als wissenschaftlicher Mitarbeiter am Institut für Kunststoffe und Verbundwerkstoffe der Technischen Universität Hamburg entstanden.

Ganz besonders bedanken möchte ich mich bei meinem Doktorvater Prof. Dr.-Ing. habil. Bodo Fiedler für die Möglichkeit am Institut zu promovieren und die Betreuung der Arbeit. Die vielen konstruktiven Diskussionen haben maßgeblich zum Gelingen der Arbeit beigetragen und zahlreiche, meist gemeinsame Konferenzteilnahmen gaben mir neue Impulse für die Arbeit. Die vielfältigen Tätigkeiten und der große Freiraum bei der Ausgestaltung meines Forschungsvorhabens ermöglichten es mir, mich nicht nur fachlich sondern auch persönlich weiter zu entwicklen, wofür ich sehr dankbar bin. Somit kann ich auf eine lehrreiche, spannende und schöne Zeit am Institut zurückblicken.

Herzlicher Dank gilt Prof. Dr.-Ing. habil. Maik Gude für die Übernahme der Zweitguachtertätigkeit in meinem Promotionsverfahren. Herrn Prof. Dr.-Ing Otto von Estorff danke ich für die Übernahme des Vorsitzes des Prüfungsausschusses.

Großer Dank gilt meinen Kollegen am Institut, die durch viele anregende Diskussionen und große Hilfsbereitschaft eine sehr angenehme und produktive Arbeitsatmosphäre schafften. Besonderer Dank gilt Wilfried Liebig, Till Augustin, Sergej Harder, Martin Schütt, Björn Riecken, Björn Bosbach und Julia Kosmann. Christian Viets danke ich für die gute Einarbeitung am Institut. Johann Körbelin und Benedikt Kötter wünsche ich viel Erfolg in der Fortführung der Forschung. Meinen Projektpartnern im SPP-1466 Gordon Just und Ilja Koch vom ILK der TU Dresden danke ich ganz herzlich für die vielen spannenden Diskussionen und den guten Austausch, insbesondere bei den gemeinsamen Treffen.
Ich möchte mich bei den von mir betreuten Studenten bedanken, deren Arbeiten zum Gelingen des Forschungsvorhabens beigetragen haben. Insbesondere die Arbeiten von Christina Buggisch, Thomas Schwebler, Andreas Schetle, Timo Philipkowski und Jonas Kürten und die dabei geführten fachlichen Diskussionen waren eine große Hilfe.

Ich danke von ganzem Herzen meiner Familie: Meinen Eltern Ingrid und Fritz Leopold, die mich immer unterstützt und diesen Werdegang möglich gemacht haben; meiner Schwester Katharina für den positiven Zuspruch und besonders meiner Frau Esther für die stetige Unterstützung, insbesondere dann, wenn es mal nicht so gut voran ging. Meinem Sohn Noah danke ich dafür, dass er mich auch an schlechten und schwierigen Tagen stets zum Lächeln bringt.

Abstract

The increasing use of fibre reinforced polymers (FRP) for structural parts requires detailed knowledge about failure initiation and propagation within composite laminates. Due to the complex failure process of the material with different damage mechanisms, the mechanical degradation behaviour under cyclic loads is difficult to predict. For further improvement of FRP mechanical properties and increase of fatigue lifetime, a modification of the polymer matrix with nanoparticles is a promising approach. With such a nanoparticle modification a third, nanoscale phase is added to the system consisting of fibres and the surrounding matrix. This modification provides additional damage mechanisms that dissipate energy during mechanical loading, hence influencing the failure process.

Different groups of nanoparticles exist, each of them exhibiting their own damage mechanism at the nano- or micro-scale depending on the particle morphology. The thesis investigates the influence of a carbon nanoparticle modification on the damage behaviour and resulting mechanical properties of an epoxy matrix and FRP. A comparison of the different nanoparticle morphologies with regard to their potential use in FRP is carried out. Since the volumes between the fibres in FRP are very small, the focus is set on the investigation of size effects of polymer nanocomposites and how local microdamage at the particles influences the mechanical properties in a small volume. The influence on mechanical properties is discussed by comparing the different energy dissipating damage mechanisms in dependence of the nanoparticle morphology. Crack initiation and damage mechanisms at the different nanoparticles can be clearly identified. For layered particles such as few-layer graphene (FLG), it is found that the orientation of the graphene layers with regard to loading direction is critical for local damage mechanisms and mechanical degradation.

In order to develop a better understanding of the influence of FLG nanoparticles in the respective layers of FRP laminates, a tailored modification approach is used. The approach allows exact analysis of the impact of a nanoparticle matrix modification in either 0° or 90°-layers of cross-ply laminates on mechanical properties and damage mechanisms. A modification of the 0°-layers unexpectedly increases the quasi-static tensile strength,

although dominated by fibre properties. However, The applicability of nanoparticle modified resin systems to improve the performance of FRP-laminates is loading-case sensitive. Positive crack stopping effects as well as negative effects, such as accelerated delamination growth, are discussed. The additional microdamage introduced with the nanoparticle modification dissipates energy, leading to a change in transverse cracking behaviour and may thus hinder the initiation and propagation of inter-fibre failure. With it, stress concentrations at free edges could be reduced by distributed microdamage and localised cracking instead of fast growing cracks, resulting in a less brittle failure behaviour and counterbalancing one of the main disadvantages of FRP.

Kurzfassung

Der zunehmende Einsatz von Faser-Kunststoff-Verbunden (FKV) in Strukturbauteilen erfordert genaue Kenntnis über die Entstehung und Ausbreitung von Schäden in Kompositen. Allerding sind innere Schäden und die damit verbundene Degradation der mechanischen Eigenschaften unter zyklischen Lasten schwer vorherzusagen. Dies liegt an dem komplexen Versagensprozess dieser Materialien, der verschiedene Schadensarten beinhaltet. Um die mechanischen Eigenschaften und insbesondere die Lebensdauer von FKV weiter zu verbessern, ist eine Modifikation der polymeren Matrix mit Nanopartikeln ein vielversprechender Ansatz. Mit einer solchen Matrix-Modifikation wird eine dritte, nanoskalige Phase zu dem Werkstoff, bestehend aus den Fasern und der diese umgebenden Matrix, hinzugefügt. Die Modifikation liefert zusätzliche Schadensmechanismen die unter mechanischer Last Energie verzehren und so den Schadensprozess beeinflussen.

Verschiedene Gruppen von Nanopartikeln weisen aufgrund ihrer Morphologie unterschiedliche Schadensmechanismen auf der Mikro- und Nanoebene auf. In dieser Arbeit wird der Einfluss einer Kohlenstoff-Nanopartikel Modifikation auf das Schadensverhalten und die resultierenden mechanischen Eigenschaften von Epoxid-Matrix und FKV untersucht. Die unterschiedlichen Partikelmorphologien werden im Hinblick auf ihr Potential für den Einsatz in FKV miteinander verglichen. Da die Volumina zwischen den Fasern in FKV sehr klein sind, liegt der Fokus auf der Untersuchung von Größeneffekten bei polymeren Nanokompositen und der Betrachtung, wie lokale Mikroschäden an den Partikeln die mechanischen Eigenschaften kleiner Volumina beeinflussen. Der Einfluss auf die mechanischen Eigenschaften wird anhand der energieverzehrenden Schadensmechanismen in Abhängigkeit von der Partikelmorphologie diskutiert. Rissinitiierung und unterschiedliche Schadensmechanismen an den Partikeln können dabei eindeutig identifiziert werden. Für Partikel, die sich aus mehreren Lagen zusammensetzen, wie beispielsweise Few-Layer Graphene (FLG), ist die Orientierung der Lagen in Bezug zur Lastrichtung entscheidend für die Art der lokalen Schädigungsmechanismen und die mechanischen Eigenschaften.

Um ein besseres Verständnis für den Einfluss einer FLG Modifikation in den einzelnen Lagen von FKV Laminaten zu erlangen, wird ein spezifischer Modifizierungsansatz genutzt.

Mittels einer Nanopartikelmodifikation der Matrix entweder in den 0° oder den 90°-Lagen von Kreuzverbundlaminaten kann der Einfluss auf das Schadensverhalten und die mechanischen Eigenschaften dezidiert analysiert werden. Eine Modifikation der 0°-Lagen führte dabei überraschenderweise zu einer Erhöhung der quasi-statischen Zugfestigkeit, obwohl diese von den Fasereigenschaften dominiert wird. Sowohl positive, riss-stoppende Eigenschaften, als auch nachteilige Effekte der Nanopartikelmodifikation, wie ein beschleunigtes Delaminationswachstum, werden aufgezeigt und diskutiert. Die zusätzlich in das Material eingebrachte Möglichkeit von Mikroschäden dissipiert Energie und verändert das Querrissverhalten und könnte somit die Initiierung und Ausbreitung von Zwischenfaserbrüchen verzögern. Durch den Energieverzehr infolge von Mikroschäden an den Partikeln und vereinzelte Mikrorisse anstelle von schnell wachsenden Rissen könnten Spannungskonzentrationen an freien Rändern abgebaut werden, was zu einem weniger spröden Versagen führen würde und damit einen der großen Nachteile von FKV ausgleicht.

Contents

Nomenclature

Symbols

Sign	Unit	Meaning
E	GPa	Young's modulus
E_{cum}	aJ	Cumulated energy
d	mm	Diameter
F	N	Force, Load
G_{Ic}	MPa$\cdot\sqrt{\mathrm{m}}$	Interlaminar fracture toughness under mode I
G_{IIc}	MPa$\cdot\sqrt{\mathrm{m}}$	Interlaminar fracture toughness under mode II
H_{cum}	-	Cumulated hits
K_{Ic}	MPa$\cdot\sqrt{\mathrm{m}}$	Stress intensity factor
l	mm	Length
l_c	nm	Critical length
m	-	Weibull modulus
n	-	Amount of layers
P	-	Probability
R_t	MPa	True failure strength
t	mm	Thickness
T_g	K	Glass transition temperature
V	mm^3	Volume
V_f	%	Fibre volume content
w	mm	Width
ϵ_{IFF}	%	Strain at inter-fibre failure initiation
ρ	$\mathrm{g/m}^3$	Density
σ	MPa	Normal stress
σ_{th}	MPa	Theoretical strength
τ	MPa	Shear stress

Abbreviations

AE	Acoustic emission
CAI	Compression after impact
CB	Carbon black
CFRP	Carbon fibre reinforced polymer
CNT	Carbon nanotubes
DIC	Digital image correlation
DSC	Differential scanning calorimetry
EDX	Energy dispersive X-ray
FLG	Few-layer graphene
GNP	Graphene nano platelets
IFF	Inter-fibre failure
IR	Infrared
FEM	Finite element method
FRP	Fibre reinforced polymer
GFRP	Glass fibre reinforced polymer
HCCF	Hydraulic composite compression fixture
MWCNT	Multi-walled carbon nanotubes
NCF	Non crimp fabric
NDT	Non-destructive testing
OHC	Open hole compression
OHT	Open hole tension
Prepregs	Pre-impregnated fibres
QI	Quasi-isotropic
RTM	Resin transfer moulding
SE2	Secondary electron
SEM	Scanning electron microscopy
SWCNT	Single-walled carbon nanotubes
TUHH	Hamburg University of Technology
UD	Unidirectional
UNC	Unnotched compression
UNT	Unnotched tension
US	Ultrasound
WD	Wideband differential
WLS	Weak link scaling

1 Introduction

Fibre reinforced polymers (FRP) are increasingly used in many industries due to their high density-specific mechanical properties. For applications with high safety and reliability requirements such as in the aerospace or wind energy sector, the increasing use of FRP for structural parts requires detailed knowledge about failure initiation and propagation within composite laminates. But internal damage in the composite or mechanical degradation behaviour under cyclic loads is very difficult to forecast due to the complex failure process of the material with different failure mechanisms. Failure initiates at defects in the material either as cohesion failure in the matrix between the fibres or as adhesion failure at the fibre matrix interface. Matrix cracks propagate between these two characteristic failure types [1]. As internal damage in composites is difficult to monitor during operation, often costly and time consuming non-destructive testing methods are necessary to evaluate damage in composite laminates [2–4]. Early stages of damage like matrix cracks control the design in layers transverse to loading direction [5] and limit fatigue life of composite laminates [6]. Although this type of inter-fibre failure (IFF) corresponds only to a slight stiffness reduction in multi-directional laminates, it is critical as it promotes more severe damage like delaminations and fibre failure. This leads to an oversizing of composite parts and limits the full potential of the material.

For further improvement of FRP mechanical properties and increase of fatigue lifetime, two different approaches among others are extensively discussed in literature. On the one hand, reduction of composite ply thickness allows higher variability in stacking sequence for similar part thickness and suppresses IFF, leading to improved fatigue behaviour [7]. On the other hand, a matrix modification with nanoparticles is a promising approach for increasing fracture toughness and hence mechanical properties of polymers and FRP [8–11]. With a combination of these two approaches, the disadvantages of one approach might be equalised by the other. The fibre-matrix interfacial strength is often the limiting value for crack initiation and a relief of interfacial stress by distributed damage at nanoparticles could improve the resistance of FRP against cracking.

The layer thickness and orientation in a laminate has significant influence on the mechanical properties and damage mechanisms. Due to the high anisotropy of the material, that is the dependency of mechanical properties of each layer on the fibre orientation, edge effects occur with a changing layer orientation within a laminate. Due to the mismatch of the elastic properties, a three-dimensional and in addition singular stress state occurs at free edges (e.g. holes) between two adjacent layers of different fibre orientation [12]. These edge effects imply stress concentrations that can lead to premature damage, such as inter-fibre fracture and delamination at free edges [13, 14]. Tow spreading methods, developed in the last decade [15, 16], allow production of thin-ply prepregs with a ply thickness of less than 50 µm. Thin-ply laminates offer higher strength and fatigue resistance when compared to laminates made of traditional prepregs [7, 17]. In general, reducing the ply thickness of a laminate delays IFF and increases the strength, particularly under tensile loads [5]. In addition, reduction of the ply thickness is a possibility to minimise edge effects and thus to suppress premature damage at free edges [18]. For thin-ply laminates, this damage suppression leads to high stress concentrations at free edges, because stresses are not dissipated by early damage such as IFF or delamination, as is the case in laminates with thicker plies. These high stress concentrations may result in premature, brittle failure at the edges, e.g. a drilled hole [7]. Furthermore, the resistance of thin-ply laminates against delamination at an impact event is inferior compared to traditional thick-ply laminates [17, 19]. An open or filled hole is usually a design feature, therefore free edges are often present in structural composite parts and compression after impact behaviour is a design criteria for aerospace applications. These disadvantages of thin-ply laminates may hinder their use for safety and reliability relevant structural parts. Detailed knowledge about the ply thickness dependence of mechanical properties and damage mechanisms of composite laminates is thus of interest in order to evaluate the potential of thin-ply laminates. The influence of ply thickness and stacking sequence on the failure process and resulting mechanical properties for laminates containing stress intensifications such as an open hole or impact damage under compressive loading is not definitely clarified so far. With reduced ply thickness, different scaling related size effects must be considered.

With a nanoparticle modification of the matrix a third, nanoscale phase is added to the system consisting of fibres and the surrounding matrix. This modification provides additional damage mechanisms that dissipate energy during mechanical loading, hence influencing the failure process. The influence of a nanoparticle modification on the mechanical properties and damage behaviour of different types of polymers is widely investigated [8–10, 20]. Regarding the influence of a matrix modification in FRP though, the mechanisms

and resulting mechanical properties are not fully clear so far and topic of ongoing research [11]. Different groups of nanoparticles exist, each of them exhibiting their own damage mechanism at the nano- or micro-scale depending on the particle morphology. A comparison of the different morphologies with regard to their application as FRP matrix modification has not yet been done. In comparison to the question asked amongst others by Zweben in 1994 "Is there a size effect in composites?" [21] the question that arises now is that of a size effect in polymer nanocomposites and how microdamage at the particles influence the mechanical properties such as failure stress in a small volume. So far, it is not clear, whether the toughening mechanisms reported for nanocomposite bulk volumes in literature [8–10, 20] are valid in small volumes. This is of particular interest for the use of nanoparticles in FRP, because the matrix volume between the fibres in FRP is very small.

A combination of a ply thickness reduction with a nanoparticle modification of the matrix is a promising approach for further improvement of composite materials meeting high requirements in structural parts. The additional microdamage introduced with the nanoparticle modification dissipates energy, leading to a change in transverse cracking behaviour and may thus hinder the initiation and propagation of IFF. With it, stress concentrations at free edges could be reduced by distributed microdamage and localised cracking instead of fast growing cracks, resulting in a less brittle failure behaviour and hence counterbalancing one of the main disadvantages of thin-ply laminates. This is a very complex approach and since for an investigation on the influence of a nanoparticle modification in combination with ply-thickness effects materials are costly and testing effort is time consuming, only the most promising combination of modification variants should be considered. It is thus essential to investigate the respective effects separately in a first step and deviate mechanisms contributing to the material behaviour. Hereby, the most promising particle morphologies regarding FRP matrix modification should be evaluated. In addition, the effects of a modification in the respective layers of multi-directional laminates with regard to damage processes in dependence of the load case are of interest and have not yet been investigated. Despite their potential, usage of nanoparticles in commercial products is rare [22]. A better understanding of the damage mechanisms and the effect of a nanoparticle modification in FRP laminates may help finding possible applications for this promising material.

1.1 Aims and approach

The main goal of this thesis is to evaluate the potential of a matrix modification with different types of carbon nanoparticles for improving mechanical properties and ductility of FRP in general and thin-ply laminates in particular. The influence of layer thickness related scaling effects and nanoparticle modification are regarded separately.

Regarding size effects of a layer thickness variation, high amount of research results are available in literature for laminates with multiple fibre orientations and are compared with experimental results. The general influence of layer thickness on transverse crack initiation for the used material is investigated in tensile tests of cross-ply laminates. A cross-ply laminate lay-up is used, because it is well suited and commonly used for analysing transverse cracking and failure initiation behaviour in composites. A focus is set on an experimental investigation on the influence of layer thickness and stacking sequence in quasi-isotropic carbon fibre reinforced polymer (CFRP) laminates containing stress intensifications under compression loading, because for this load case, partly inconsistent results are reported. The aim is to identify and discuss the different effects that influence the compression failure and the role the stacking sequence has on damage development and the resulting compressive strength. In addition, the formation of fibre matrix debonding and initiation of IFF is investigated micromechanically in a small experimental test campaign with model composites. Model composites are used to reduce the total specimen volume in order to investigate the damage initiation and propagation in dependence of the ply thickness selectively in a in small, defined volume.

According to the main goal, the focus in this thesis is set on the investigation of the influence of nanoparticles with regard to size effects for their potential use in FRP. The answer to the question of a size effect for polymer nanocomposites as well as a better understanding of the different mechanisms of microdamage at nanoparticles are objectives in this context. The aim is further to investigate the influence of nanoparticle morphology and filler content in polymer nanocomposites on the mechanical properties in small elongated volumes, as they are present between the fibres in FRP. The influence on mechanical properties is discussed comparing the different energy dissipating damage mechanisms at the nanoparticles, in dependence of their respective morphology. The approach of using small specimens has the advantage of very small fracture surfaces. Hence, crack initiation and damage mechanisms at the different nanoparticles can be clearly identified, which is very difficult in larger polymer nanocomposite specimens or FRP because of the complex fracture surfaces [23]. In order to develop a better understanding of the effect and damage mechanisms of a modification with graphene based nanoparticles in the respective

layers of FRP laminates, a tailored modification approach is used. The aim is to identify the effects of nanoparticle modification in FRP layers with fibres oriented parallel and transverse to loading direction separately and in dependency of the load case.

The most promising nanoparticle morphology as well as conclusions on which layers of a multi-directional laminate are the most promising to be modified for improving mechanical properties can be used for future investigations on nanoparticle modified thin-ply laminates in order to improve their failure behaviour.

The research questions derived from these aims are listed as follows:

- What are promising nanoparticle morphologies for improving mechanical properties of FRP?
  - Is there a size effect for polymer nanocomposites?
  - How do nanoparticle morphology and filling content influence the mechanical properties and failure behaviour of polymer matrices in small volumes?
- Is a tailored nanoparticle modification of only some layers in a composite laminate promising for improving mechanical properties?
  - How does a nanoparticle modification of the matrix in layers oriented parallel respectively perpendicular to loading direction influence the mechanical properties of FRP?
  - What is the influence of a nanoparticle modification on the damage process in the different layers of cross-ply laminates under static and cyclic loading?
- How does layer thickness scaling influence the mechanical properties and damage behaviour of FRP laminates?
  - How does the transverse layer thickness in cross-ply laminates influence the initiation and propagation of IFF?
  - How does the layer thickness and stacking sequence influence the mechanical properties and damage process of laminates containing stress intensifications under compressive loading?

The thesis is structured in six chapters. The following chapter 2 provides the theoretical background for this work in a literature overview on the size and scaling related effects of FRP and the influence of nanoparticle modification on the mechanical properties of polymers and FRP. The results obtained from the experiments, described in chapter 3,

are presented in chapter 4 and discussed in the context of the theoretical background. In chapter 5 the results are related to each other and put into a broader context and the main conclusions from this thesis are deduced. Chapter 6 presents an outlook on the next steps for continuation of research in this field.

2 Technological and scientific background

Fibre reinforced polymers consist of two different materials, the stiff and strong fibres and the surrounding matrix. The fibres are the load bearing component, while the matrix introduces the load into the fibres, holds them in position and protects them from external influences [24]. For continuous fibre reinforced polymers, typically used for structural parts, the fibres are arranged parallel to each other to form a unidirectional (UD) ply. Composite laminates or parts comprise usually of several of these plies. This way, the fibre orientations within a laminate can be adapted with regard to the main loads via the stacking sequence of the plies, which is one advantage of FRP for lightweight design. One or more neighbouring plies with the same fibre orientation form a layer.

In thermosetting UD-prepregs, used for this thesis, the fibres are impregnated with an epoxy matrix that is only partially cross-linked in a so called B-stage. As long as it is stored at low temperatures (at about $-18\,°C$), further chemical cross-linking of the epoxy system is suppressed, which preserves the processability [25]. Laminates are stacked from defrosted UD-prepregs. Due to their good manufacturing quality and reproducibility and the high achievable fibre volume content, prepregs are for example used in aircraft industry [26]. During curing at elevated temperatures, the matrix cross-links and a consolidated, fully cross-linked composite is the result. Laminates from prepregs are commonly cured in a vacuum bag within an autoclave (a heatable pressure vessel). The vacuum bag minimises entrapped air and thus void content, while the temperature in the autoclave can be set according to the curing profile of the used resin system and quasi hydrostatic pressure on the laminate assures good consolidation and removes excess resin for achieving the desired high fibre volume content [26].

Depending on the fibre orientation of the layers within a laminate with regard to loading direction, they exhibit different types of intra-laminar damage. Furthermore, damage in the form of cracks may propagate between two layers of different orientation. This inter-laminar damage is referred to as delaminations. The damage mechanisms in FRP

under different kinds of loading are presented shortly in the following chapter 2.1. The subsequent chapter 2.2 summarises the effects of scaling and variation in the stacking sequence of FRP on the mechanical properties. In chapter 2.3, a literature review on the influence of a nanoparticle modification on the mechanical properties and damage mechanisms of polymers and FRP is given.

2.1 Damage types in FRP laminates

In general, FRP exhibits brittle failure behaviour. The first damage type to usually occur in FRP under loading is fibre-matrix debonding in layers oriented perpendicular to loading direction at fibres with close inter-fibre distance [27, 28]. Due to the high stiffness difference between fibres and matrix, stress concentrations at the interface lead to an adhesive separation of the matrix from the fibre [29]. In addition, thermal residual stresses after curing, resulting from the different coefficients of thermal expansion of fibre and matrix, may act on the fibre-matrix interface and cause failure initiation by debonding at the interface [30]. After initiation at local defects or flaws, the debonding grows in arc direction of the fibre as well as along the fibre axis [31, 32]. In the debonded area, no further load can be introduced from the matrix into the fibres. The interfacial normal strength governs failure initiation in most composites [27] and for this reason a high interfacial strength, resulting from a strong bonding of fibre and matrix, is desired.

If free edges are present, fibre-matrix debonding initiates at the free surface and propagates into the material [33]. With increasing load, regions of fibre-matrix debonding coalesce and form a transverse crack, referred to as IFF. Mostly, the interfacial strength is lower than the failure strength of the matrix and because of the mentioned stress concentrations, IFF propagates through the thickness along debonded interfaces [1, 27, 28]. If the interfacial strength is higher than the matrix strength, which can for example be achieved by a modification of the interface [34], transverse cracks propagate as cohesive failure through the matrix in thickness direction. Transverse cracking in a multi-directional laminate leads to a small but measurable stiffness decrease. The first analytical models to describe matrix cracking as first ply failure were presented by Dvorak and Laws [35], assuming that IFF initiates from localised fibre-matrix debonding.

Transverse cracks propagating in thickness direction are arrested at the interface to a neighbouring layer of different fibre orientation. This leads to a stress concentration at the interface and if the external load is above the interlaminar interface strength, the crack propagates as a delamination between the two layers (crack tip delamination).

From a fracture mechanics point of view, the interlaminar crack propagation (delamination) type depends on the direction of external loading. Mode I crack propagation is due to tension loading perpendicular to the fracture plane and mode II crack growth is due to in-plane shear forces [36]. Under in-plane compression loading, delaminations are growing due to a combination of normal (buckling) and shear stresses resulting in mode I dominated behaviour, whereas in tension shear stresses dominate, which results in mode II delamination growth.

In layers with fibre orientation parallel to loading direction, rupture of the load carrying fibres initiates final failure when the external tensile load exceeds the tensile strength of the fibres. As the fibres parallel to loading direction carry the main load, larger amount of fibre failures leads to rupture and hence catastrophic failure of the composite. For compression loading, the failure process of FRP is more complex. Due to the geometry of the fibres, they tend to buckle locally and compression properties are often dominated by the matrix, resulting in lower compressive than tensile strength [24]. The damage process of CFRP under compression is described more in detail in the following chapter.

2.1.1 Behaviour of CFRP under compressive loading

The compressive strength is often a design limit of CFRP, as it is significantly lower than the tensile strength. The first model for predicting compressive strength of composite laminates was presented by Rosen [37]. He proposed that compressive failure initiates due to fibre microbuckling and distinguished between two modes of microbuckling: in-phase microbuckling (shear mode) for higher and out-of-phase microbuckling (extension mode) for lower fibre volume fractions [37]. The in-phase microbuckling leads to the formation of a kink-band with increasing load. This is similar to the compressive failure of other fibrous materials like wood. Moran et al. [38] and Poulsen et al. [39] investigated the kinking failure in spruce and compared the damage process with that of CFRP. They identified three stages of compressive kinking. Incipient kinking as the first stage begins on a very small scale and is characterised by localised plastic shearing and buckling of fibres. In the following transient kinking stage, the localised incipient kinking areas grow and coalesce to form a single dominant kink-band across the specimen. The last stage is steady state kinking during which the kink-band broadens laterally [38, 39]. In CFRP, these three stages occur as well in a similar process [38, 40], but they are difficult to clearly identify because of the brittle fracture within a very short amount of time. Incipient kinking occurs when the matrix shear stress in fibre direction reaches a critical value [38].

The analytical model of Budiansky et al. [41, 42] describes the initiation and propagation of a kink-band with the orientation angle β, the kink-band width ω and the inclination angle Φ of the fibres. Initiation of kink-bands is facilitated at defects, e.g. voids [43, 44] or local fibre misalignment [45]. Gutkin et al. [46, 47] described the initiation of microbuckling and the following kink-band as shear driven fibre failure with a distinct shearing angle α. Figure 2.1 sums up the different failure mechanisms of FRP under compressive loading with the nomenclature used in this thesis.

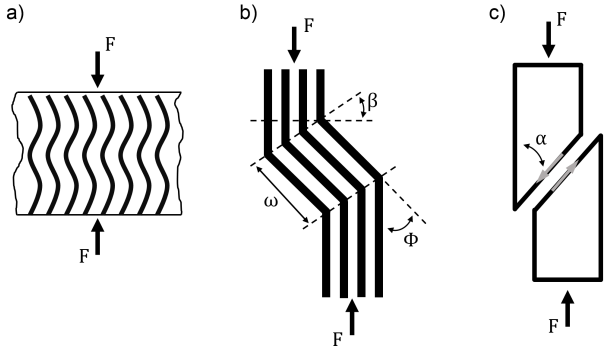

Figure 2.1: Scheme showing the different mechanisms contributing to compressive failure of FRP: a) in-phase microbuckling, b) kink-band geometry, c) shear failure.

2.1.2 Low velocity impact damage in CFRP

Impact events may occur during the lifetime of a composite part. The matrix is designed with regard to high strength and stiffness of the part, which in the case of thermosetting resins involves low ductility. Most composites are brittle and cannot absorb energy via plastic deformation but only via elastic deformation and through damage mechanisms [48]. They are thus susceptible to damage resulting from low velocity impacts as they may occur e.g. in the aircraft or mobility sector from dropped tools, runway stones, or hailstones. An impact damage results in a stress intensification that is difficult to account for in the design process. Impact damages may be barely visible at the surface of a CFRP laminate but result in severe damage such as matrix cracking, fibre breakage, and delaminations. The typical damage shape through the thickness of a multi-layer laminate (often referred to as a "pine-tree damage shape") after a low velocity impact is shown schematically in Figure 2.2. The damage increases with the thickness from the impact side to the back side.

Regarding the damage process at a low velocity impact, matrix cracks are the first type of damage to occur when the object hits the composite surface due to the induced bending

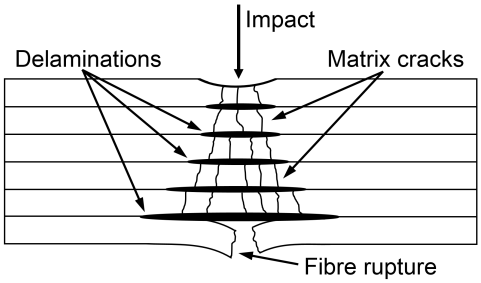

Figure 2.2: Scheme showing damage in FRP after a low velocity impact with matrix cracks, delaminations and fibre breakage.

load. These cracks grow and lead to delaminations between interfaces to layers with different fibre orientations. Interlaminar cracks propagate more easily along fibre direction than transverse to it, leading to a lemniscate shape (or "peanut shape") of these delaminations, with the major axis oriented parallel to the fibres [49]. Fibre damage occurs later in the fracture process than matrix cracking and delamination and at higher impact energies. Fibre failure near the impact surface or under the impactor is due to locally high stresses and indentation effects, whereas on the backside it is attributed to high bending stresses [48]. The introduction of impact damage and compression after impact (CAI) properties are often design limits [50, 51], because impact damage significantly reduces fatigue life of FRP [52, 53]. The reduction of fatigue life depends on the size of the impact damage and the load level and is more pronounced with a compressive loading part [53, 54] and for lower load levels [52]. Under tensile cyclic loading an impact damage may have minor influence [54].

2.1.3 Fatigue behaviour of FRP

Understanding of failure behaviour under cyclic loading and an improvement of FRP fatigue performance is of on-going interest in order to achieve higher efficiency and extended in-service life. In laminates containing 90°-layers, IFF is the first damage mode [5, 55–57]. The fatigue degradation behaviour of multi-layered composites in general is driven by the development of IFF in layers loaded by transverse tension and plane shear stresses. Due to the crack opening under tension and crack sliding under shear, the residual as well as load induced stresses are released locally and redistributed to adjacent layers. Depending on layup and loading, the cracks are formed with crack tip delaminations, which may grow during fatigue loading, leading to an additional release of residual stresses and the separation of layers. Later, longitudinal cracks and fibre failure as a result of the preceded damage processes leads to final failure and rupture [58, 59].

Based on this behaviour, three phases of degradation are distinguished for fatigue damage behaviour of multi-directional FRP laminates [59, 60]. Within the first cycles, the degradation rises steeply due to transverse IFF formation and growth (phase I), before it reaches an almost constant and comparatively slowly increasing damage level (phase II). This plateau can be attributed to saturation in number and following growth of IFF. At the end of the lifetime, final failure is indicated by a steep increase in damage level (phase III) until global failure due to delaminations and fibre fractures [59, 60].

The formation of IFF is critical especially under fatigue loading, as it reduces the stiffness and induces more severe damage like delamination or fibre breakage and therefore limits fatigue life [6, 61]. Macroscopically, all effects leading to a loss of residual stiffness, strength and changes in Poisson‘s ratio are usually called fatigue degradation.

2.2 Size and scaling effects for fibre reinforced polymers

A size effect is present when the strength of a material increases with decreasing volume (or in other words a decrease in strength with increasing volume) due to a statistical distribution of defects. Concerning defects, the principle of the weakest link that determines the strength of a chain is applicable. With increasing number of links in a chain, the probability of having a weak link in the chain increases as well, therefore the strength tends to decrease with increasing number of links. For a volume, the strength under uniform stress is dominated by the largest defect. Since defects are randomly distributed, larger volumes have a higher probability of containing larger defects and thus exhibit lower strength. In general, brittle materials exhibit a size effect [62]. For infinite small volume, assuming a defect free brittle material, the strength approaches the theoretical strength, which is based on the separation of atomic bonds and thus the energy that is necessary to create a new fracture surface [63]. When investigating matrix failure in FRP, size effects of the material should be considered, because volumes between fibres are tiny. Size effects also play an important role in the design and in the prediction of mechanical properties of composite laminates or parts. Size effects are shown in literature to be present from a large to a smaller scale, regarding on laminate level the total volume or the thickness of the layers in a laminate [5, 64–67], which gains increased importance since the development of thin-ply prepregs for producing composite laminates [7].

Regarding the substituents, size effects in fibres were first documented by Leonardo da Vinci for iron wires [68] and are shown to exist for different materials such as glass [62],

carbon [69, 70], acrylic [71] or epoxy [72, 73]. For fibre bundles, when the weakest individual fibre fails, the bundle as a whole does not fail due to redistribution of the load equally among the other fibres [74]. In a composite, the surrounding fibres then carry more load because of load transfer by the matrix [75, 76].

For polymer matrices, the microstructure and the stress state in the pure resin compared to the same material as a matrix in a composite may differ [77], which has to be regarded when comparing experimental data with finite element method (FEM) simulations and for estimation of the local matrix strength in the small volume between the fibres [30]. Towse et al. [72] found a correlation between defect size and failure strain for an epoxy adhesive. In an investigation by Hobbiebrunken et al. [73], a size effect for the RTM 6 epoxy matrix system was identified experimentally. By using dog-bone specimens and fibres of the same material, increasing tensile strength with decreasing volume was found [73].

2.2.1 Size effect for the transverse tensile strength of FRP

First investigations about the size effect concerning the transverse strength of composites were performed by Adams et al. [78]. In this study, a comparison was made between flexural and tensile strengths, in which flexural tests always gave higher values. Further investigations on this topic were made by O'Brien and Salpekar [79] who tested specimens of different widths and different thicknesses in transverse fibre direction. Their test results indicated that matrix dominated strength properties varied with the volume of the material to be stressed, with strength decreasing as volume increased [79]. Both groups [78, 79] used CFRP in their studies, whereas Wisnom and Jones [64] and Wisnom [80] also reported similar results for glass fibre reinforced polymer (GFRP). They compared curved unidirectional beams with the in-plane transverse tensile strength. It was concluded that the lower in-plane strength matched closely the value expected for a much larger volume of material based on the Weibull parameters from the interlaminar tests [64]. Mespoulet [81] compared transverse tensile strengths of carbon/epoxy with different volumes at straight sided and doubly waisted specimens. It could be shown that higher strength of doubly waisted specimens is due to smaller volume. However, it could not be clearly carved out, whether a better surface finish on smaller specimens or the size effect led to these results. O'Brien et al. [82] reported that the trend of decreasing strength with increasing specimen width and hence increasing volume, which would be anticipated from Weibull scaling law, was not clearly apparent in three and four point bending tests. Nevertheless, for increasing span length and hence increasing volume, a strength decrease was observed. But due to a significant panel-to-panel variability in this

study, it could not be clearly figured out, whether the expected scaling was due to the size effect or not [82].

These uncertainties led to the recent, co-authored investigation on the size effect of CFRP transverse strength with a new test approach, carried out together with Liebig et al. [83]. In order to understand whether first failure strength corresponds to the true transverse failure strength of the material, a second transverse tensile test was performed by using a part of the specimen out of the already tested volume. This approach allowed to determine the strength of the second failure and to investigate whether weakest link theory could be applied or not and a size effect within a single specimen volume exists.

Figure 2.3 shows the transverse tensile strength R_{22}^t for all tested specimens versus their volume, which varies according to the different thickness (number of plies n) of the configurations regarded. First failure of a specimen is indicated with open white symbols, second failure strength is represented with filled black symbols. Strength values for second failure are higher for nearly every specimen. The Weibull plot through the minimum values of each volume shows the size effect resulting from a statistical distribution of defects that is according to Weibull's theory of defect distribution [84]. The horizontal line at 86 MPa indicates the ultimate transverse tensile strength of the material for the tested volumes, which results from the maximum interfacial strength of fibre and matrix. Except for one value regarded as an outlier, all values for transverse tensile strength lie in the range or within the ultimate value and that one dominated by the statistical distribution of defects as a Weibull envelope curve. Thus it was shown, that first transverse failure occurs at the most critical defect (weakest link) and second failure strength is higher than first failure strength. The proposed test method provided a more accurate measure of transverse tensile strength, which may be used along with the Weibull scaling law to predict transverse strength in cross-ply laminates or for micromechanical modelling (for further information see [83]).

2.2.2 Influence of layer thickness and stacking sequence under tensile loading

For FRP, not only a volumetric size effect due to a statistical defect distribution, but also scaling related effects are reported. Despite the fact, that thinner specimens or layers tend to contain a smaller amount of manufacturing induced defects [85], the layer thickness and stacking sequence have high influence on the mechanical properties of composites. As discussed above, the transverse tensile strength is determined by the largest defect

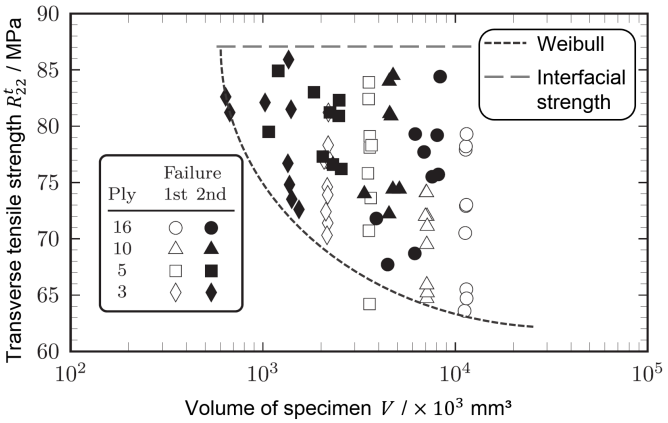

Figure 2.3: Transverse tensile strength of CFRP (M21/34%/UD194/T800S) in dependency of specimen volume with Weibull plot [83].

within the volume under investigation. However, for transverse plies between layers of different fibre orientation, the *in situ effect*, firstly introduced by Flaggs and Kural [86], should be considered. The in situ effect describes the effect of higher transverse tensile or shear strength of a composite ply, if supported by surrounding plies of different fibre orientation, in comparison to the same ply in a UD laminate. The corresponding strength of the transverse ply is called the *in situ strength*. The in situ strength increases with decreasing ply thickness and with increasing stiffness of the surrounding layers [35, 86–89]. Hence, the strength of a layer oriented transverse to loading direction depends on its position within the laminate and by reducing the ply thickness, transverse cracking is suppressed to a certain degree.

When regarding cross-ply laminate specimens or parts, cracks initiate at free edges, where out-of-plane or interlaminar stresses occur [12, 90] and propagate inward through the layers oriented perpendicular to loading direction. At transverse cracks, the stress is zero whereas it reaches a maximum in the middle between two cracks, so that a stress redistribution to the neighbouring layers takes place. With increasing load, additional cracks occur at the location of the maximum stress and this process continues, until a saturation is reached at which the maximum stress between two cracks is lower than the transverse strength of the layer. In this case the minimum distance between two cracks is reached [29]. The ply thickness has an effect on the crack initiation at free edges, described by the *free edge effect* [13, 14]. The free edge effect describes, that at the interfaces between two adjacent, dissimilar laminate plies in the vicinity of free laminate edges of pure cross-ply layups, a three-dimensional and in addition singular stress state is developed. It originates from the mismatch of elastic properties of the layers, especially by the difference in effective Poisson's ratios of the 0°- and 90°-layers [12]. With reduced ply thickness,

peel stresses between two layers of different orientations decrease, which implies increased resistance against delamination initiation and growth at the free edge [18]. However, since stresses are not relaxed by initial damage growth due to the hindering of cracking or delamination damage, stress concentrations at free edges are not reduced for decreasing ply thickness, leading to a higher notch sensitivity of thin-ply laminates [7, 17, 91–93].

The 90°-ply thickness of a laminate influences the strain at damage onset and the crack propagation within the laminate. Experimental investigations by Parvizi et al. [5, 56] showed that transverse cracking in the 90°-layer of GFRP cross-ply laminates is constrained at an inner 90°-ply thickness below 0.4 mm and completely suppressed at 90°-ply thickness below 0.1 mm [5]. Additionally, by varying the ply thickness a change in the propagation of edge cracks is observed, with slowly propagating cracks (slow crack growth) for thinner plies and nearly instantaneous cracks through the width (fast crack growth) for thicker plies [5]. When cracks grow fast through the width, the stress is reduced, which is not fully the case for a low crack growth rate. This leads to the formation of new cracks in thinner plies [56, 57, 88, 94]. Thus, the crack distance is also a function of the ply thickness [5]. Other studies also reported a higher stress at the onset of IFF with decreasing ply thickness. The crack suppression effect for decreasing ply thickness is explained by a decrease of energy release rate at the crack tip due to the close proximity of the stiff 0°-layer [95]. Damage onset and development in 90°-layers of cross-ply laminates in dependence of layer thickness and position within the laminate is analysed by means of acoustic emission (AE) analysis by Baker et al. [96]. They found, that the stress for matrix cracking depends on the ply thickness, its location (internal or surface) and on the fibre orientation of the adjacent plies. Thicker 90°-layers and 90° surface plies tend to have the lowest stresses for cracking initiation within a laminate [96].

With the development of thin-ply laminates by tow spreading techniques [7, 15, 16, 97] lower ply thicknesses in laminates can be achieved. Reduced ply thickness offers increased freedom in design for a given part thickness by larger variants in stacking sequence with regard to external loading. The improved design options with the reduced thickness make thin-ply laminates also promising candidates for multi-material composites for achieving pseudo-ductile behaviour such as combined GFRP-CFRP [98] or metal-FRP combinations [99].

Experimental results for CFRP thin-ply laminates with a ply thickness of less than 50 µm show great potential in the suppression of IFF. Reducing the ply thickness leads to a delay in the onset of damage to higher tensile loads [7, 17, 95, 100, 101]. Saito et al. investigated crack initiation and propagation in CFRP cross-ply laminates experimentally [95] and

with numerical simulation [100] and reported, that cracks run completely through the thickness after initial failure at the fibre matrix interface for conventional prepreg plies. For thin-plies, cracks initiate in the middle but crack propagation is constrained and stress is transferred to the neighbouring layers resulting in a crack propagation through the thickness at higher strains compared to the thicker plies [95, 100]. The damage propagation is significantly reduced in both width and thickness direction with decreasing the ply thickness [5, 7, 95, 100]. Yuan et al. [102] recently presented a failure diagram, in which the failure modes of transverse matrix failure, delamination and fibre breakage are shown as a function of ply thickness, with fibre breakage being the only failure mode for thin-ply laminates. They faced issues of a reduced fibre volume content with decreased ply thickness and thus a competing mechanism on resulting laminate strength. For optimum mechanical properties, fibre volume content should be kept constant with decreasing ply thickness [102]. The suppression of matrix cracking leads to improved fatigue life in the tension-tension regime of thin-ply laminates [7, 17] or non-crimp fabrics (NCF) laminates made of spread tows [103].

For quasi-isotropic (QI) laminates, two common approaches for stacking of the different layers from single plies exist. In a sublaminate scaling, plies with varying fibre orientations are stacked on each other, forming a sub-laminate that is then repeated to half of the desired laminate thickness. The resulting stacking sequence is then mirrored at the neutral plane, thus forming a symmetric laminate. In the ply block scaling approach, plies of the same fibre orientation are grouped to one thicker layer, forming a sublaminate with increased layer thickness that is then mirrored at the neutral plane for symmetry. Laminates containing layers of blocked thin plies behave similar in unnotched tension (UNT) and open-hole tension (OHT) tests compared to sublaminate scaled laminates of thick plies, as long as the layer thickness is equivalent [17]. These two approaches for stacking sequence are compared in this thesis with regard to their notch sensitivity at stress intensifications under compression loading (chapter 4.4).

In Figure 2.4 values from literature showing the influence of layer thickness on UNT strength for QI laminates are given. Values for inner 0°-layers and outer 0°-layers are represented by filled symbols and open symbols, respectively. As expected, the 0°-layer position has no influence on the behaviour in tension. Experimental results from tensile tests with QI specimens manufactured similar as described in chapter 3.2.2 and tested according to DIN EN ISO 527-4 [104] are given for comparison. As shown in the diagram, a clear trend of increased tensile strength for thinner layers (sublaminate scaling) in comparison to ply-block scaled thick layers is reported [7, 17, 105–107]. The diagram

shows also, that absolute values strongly depend on fibre type and manufacturing quality, visible in the large strength range for similar ply thickness.

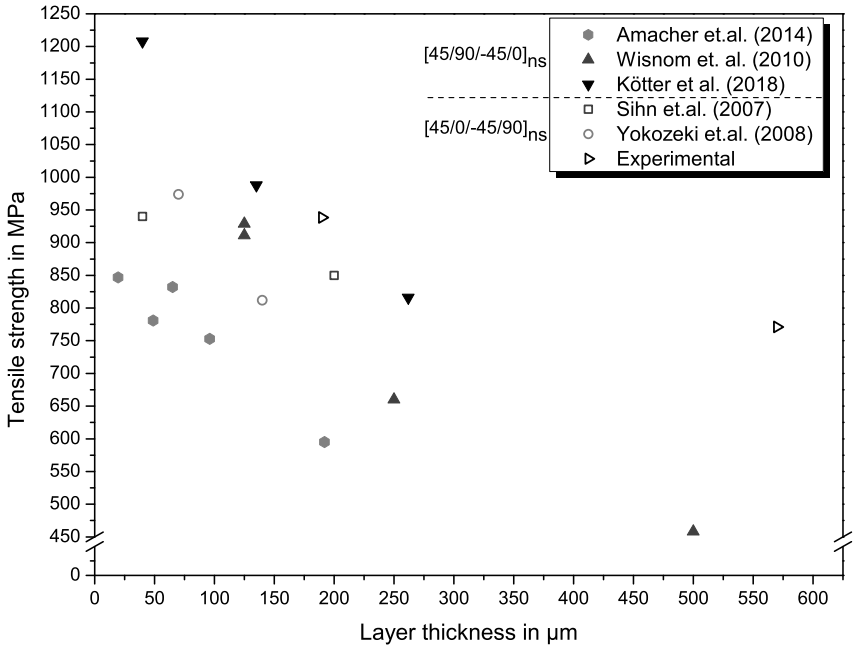

Figure 2.4: Influence of layer thickness on unnotched tensile strength of quasi-isotropic CFRP (values from [7, 17, 105–107]).

2.2.3 Influence of layer thickness and stacking sequence under compression loading and impact damage

The laminate properties and stacking sequence play an important role in damage initiation and propagation and the resulting mechanical properties under compression loading. For composite laminates in general, size effects with regard to scaling of the specimens on one hand and thickness of the constitutive plies on the other hand should be considered [108]. Soutis [109] and Lee and Soutis [65, 110] investigated the influence of specimen and layer thickness on the strength and failure behaviour for unnotched compression (UNC) [65, 109] and open-hole compression (OHC) [110, 111] load cases. They compared the compression behaviour of open-hole specimens with that under tensile loading and found a strength increase with decreasing dimensions or layer thickness [106]. Arteiro et al. [112] showed with micromechanical modelling and FEM simulation, that the in-situ effect known in tension [86] exists as well under compression loading: They reported a higher ply strength with decreasing ply thickness and with increasing the stiffness of the surrounding layers [112]. These ply thickness effects become more and more important

with the possibilities of the thin-ply technology. The damage mechanisms for standard and thin-ply laminates with regard to ply thickness and stacking sequence effects under compression are not yet fully clear [7, 17] and require further research.

Figure 2.5 shows values from literature for UNC strength for QI laminates with varying layer thickness and stacking sequence. Values for inner 0°-layers and outer 0°-layers are represented by filled symbols and open symbols, respectively. Values from the experimental investigation (refer to chapter 4.4) are given for comparison. With decreasing layer thickness, the compressive strength increases.

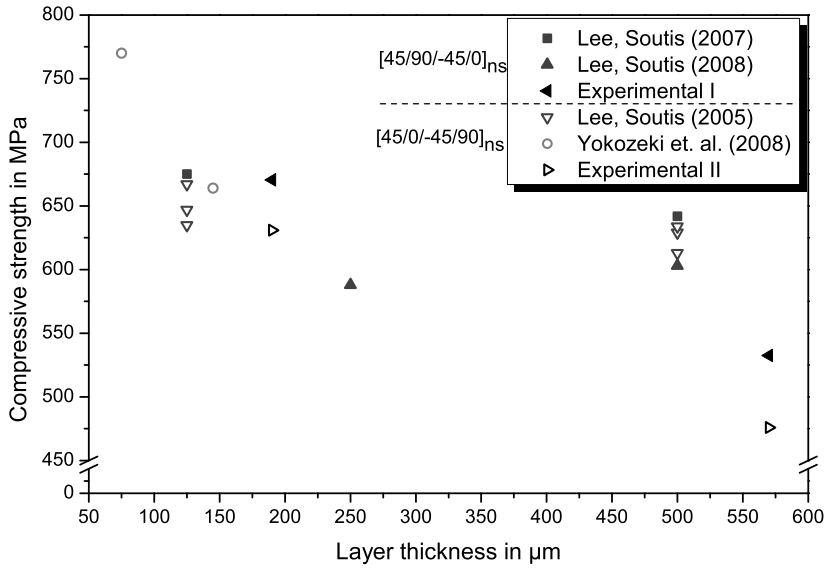

Figure 2.5: Influence of layer thickness on unnotched compressive strength of quasi-isotropic CFRP (values from [65, 66, 105, 110]).

The influence of stress intensifications induced by holes, notches or barely visible impact damage is critical for composite laminates in many applications. At holes or the edges of a laminate, the free edge effect must be considered [13, 14]. Due to high peel stresses, delaminations between two layers initiate at the edges (resulting from a mathematical stress singularity [12]). With decreasing ply thickness, a suppression of these edge delaminations is reported [18]. Under compression, fibre microbuckling initiates at the hole boundary followed by delamination and formation of a kink-band [113]. At free edges, compression failure is hence partly a result of delamination growth. With increasing hole diameter / specimen width ratio, compressive strength decreases [65, 110, 111, 114]. The OHC failure process depends on the interlaminar toughness. A high interlaminar toughness leads to a short crack rest after being initiated at the hole before brittle failure occurs, whereas a weaker interlaminar interface results in sudden failure [115]. Wang et al. [116] compared

experimental results for open-hole tension and compression to predictions of a numerical FEM analysis and pointed out, that the compressive strength of a lay-up with subsurface 0°-plies is higher than that of a UD lay-up due to higher stability of the load bearing fibres [116]. Thus, stacking sequence and optimum support of the 0°-layers carrying the highest load share is critical.

Stacking sequence and scaling of the constitutive layers have also an influence on resistance against impact damage [19, 49, 117–120]. By using the concept of sublaminate and ply-block scaling and by varying the number of layers Guynn and O'Brien [49] showed, that thick laminates exhibit higher CAI failure strains than thin laminates if impacted at the same energy per unit thickness [49]. Fuoss et al. developed guidelines to improve impact resistance of composite laminates via a parametric study [117] and an analytical prediction method [121] and pointed out, that ply grouping (blocking) and stacking of adjacent plies with orientation angles $< 45°$ should be avoided.

A comparison between ply-block scaled and sublaminate scaled laminates reveals that the increase of interfaces available for delamination in the distributed plies of sublaminate scaled laminates results in more, but less large delaminations. Furthermore, the delamination size is a function of the interface position through the laminate [49]. If the number of interfaces available for delamination is reduced, larger delaminations occur [18, 49]. This might be beneficial for thin-ply laminates with distributed plies, because of the high number of interfaces. However, impact tests with different types of thin-ply laminates exhibit equal [7] or larger [17, 19] delamination areas after impact with decreasing ply thickness. CAI strength is slightly improved with a significant decrease in ply thickness [19, 105], with the delamination being less severe [7, 122]. But due to their resistance against matrix cracking and delamination, thin-ply laminates or spread tow NCF are more prone to fibre failure at an impact event [122, 123].

Delamination size is critical under compression, because the constitutive layers are not supported at the delaminated areas. Fractography investigations from Greenhalgh et al. [124] about delamination growth and migration revealed that migration between different interfaces is important, as it is the slower propagating mechanisms, resulting in a smaller projected damage area. When delamination driving force direction and fibre orientation of the adjacent layer are in the same axis this results in fast delamination growth with larger damage areas [124]. In compression, delamination growth is facilitated at interfaces with plies transverse to the loading direction, thus the 90°-layers are most critical for delamination propagation.

As can be seen in Figure 2.6, where results from literature for OHC strength are grouped according to the stacking sequence, the position of the 0°-layers has a major influence in relation to the layer thickness. Values for inner 0°-layers are represented by filled symbols, those for outer 0°-layers with open symbols in the diagram. For outer 0°-layers, the OHC strength increases with decreasing ply thickness, similar to the UNC behaviour (refer to Figure 2.5), whereas for inner 0°-layers, this is only valid for thin-ply laminates [17] and for thicker layers, the contrary is the case [110]. This motivates the more detailed investigation on the influence of layer thickness and stacking sequence with regard to notch sensitivity under compressive loading, presented in chapter 4.4. The experimental values obtained from this investigation are given for comparison in the diagram and show the same trend as observed in literature.

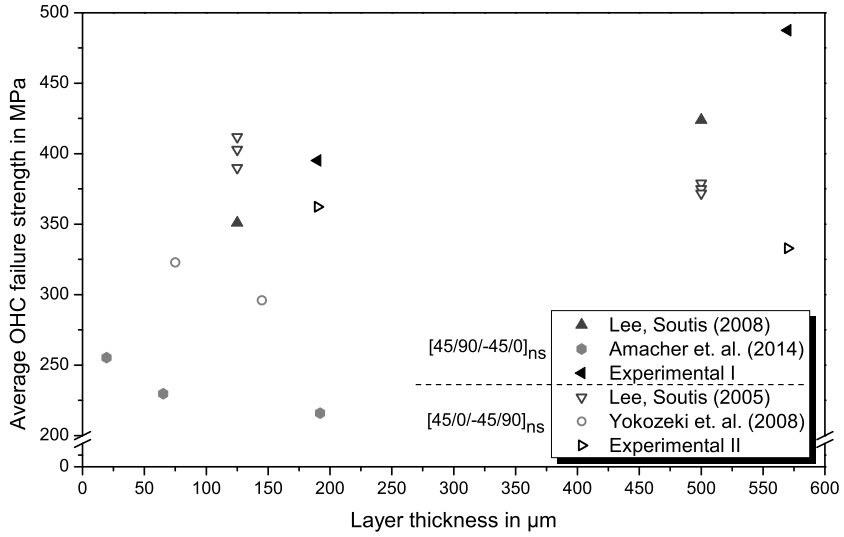

Figure 2.6: Influence of layer thickness on open-hole compressive strength of quasi-isotropic CFRP (values from [17, 65, 105, 110]).

2.3 Matrix modification with nanoparticles

The different allotropes of carbon are shown in Figure 2.7. Graphene consists of a single atomic layer of sp^2-hybridised carbon atoms that are arranged in a honeycomb structure (thickness $\approx 0.35\,nm$). It is a 2D material with unique physical propertied but very difficult to obtain in its single layer form [125, 126]. All graphitic forms of carbon are stacked from graphene layers [8]. Three different nanoparticle types are most commonly used for modification of polymers or FRP matrices. Namely, these are fullerene [127] or other globular particles like carbon black (CB), carbon nanotubes (CNT) and graphene

based particles, such as graphite, few layer graphene (FLG) or graphene nano-platelets (GNP). FLG and GNP consist of several graphene layers, with a higher amount of layers for GNP, stacked together with the covalent bonds between the carbon atoms in plane and Van-der-Waals bonds between the layers. CNTs are further divided into single-walled CNT (SWCNT), consisting of just one layer of graphene rolled up to a tube and multi-walled CNT (MWCNT) with several graphene layers forming the walls of the tube.

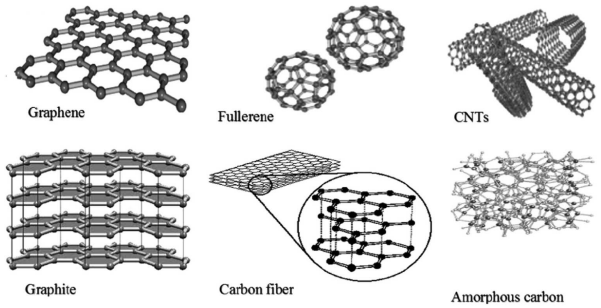

Figure 2.7: Allotropes of Carbon [128].

2.3.1 Mechanical properties of polymer nanocomposites

For improving mechanical properties of polymers, various filler materials have been used, such as silica nanoparticles [129], aluminium nanoparticles [130], nanoclays [131, 132] and a wide range of carbon nanoparticles. A combination of different nanoparticle types, such as MWCNT with mineral fillers, is also a promising approach for improving electrical, thermal or thermo-mechanical properties, as shown in a recent, co-authored investigation with Backes et al. [133]. Besides the filler material itself, the size, morphology, volume fraction and dispersion of the particles have an influence on the resulting properties of the nanocomposites [9, 134]. Singh et al. [130] investigated the influence of particle size and volume fraction in a thermosetting polyester matrix modified with micro- and nanometer-sized aluminium particles and reported that for a given particle size, the fracture toughness increased with the volume fraction and that toughness increase is significantly greater for smaller particles [130]. Liu et al. [131] showed that the fracture toughness of epoxy/clay nanocomposites increased with increasing clay concentration and analysed toughening mechanisms such as shear yielding, debonding and crack deflection [131]. Another important factor is functionalisation of the nanoparticles for improving the particle-matrix adhesion, dispersion and thus the mechanical properties [20, 135–138].

Concerning the morphology of nanoparticle reinforcements, no consistent categorisation is established up to now. Schadler et al. [139] and Marouf et al. [10] classified nano-fillers

in three categories, based on their dimensions on nanoscale, with cubic silica and rubber particles as 3-dimensional (3D), nanotubes as 2-dimensional (2D) and nanoplatelets as 1-dimensional (1D) reinforcement. In contrast, here a nomenclature after Tang et al. [11] is used that defines spherical nanoparticles as 0D, because they can be regarded as a point, with surface area and thus interfacial volume being much smaller compared to tubes or plates of the same volume. Linear particles such as nanotubes are regarded as 1D and planar particles, e.g. graphene or layered structures, as 2D, corresponding to their orientation within a volume [9, 11]. This categorisation is presented in Figure 2.8. Three-dimensional (3D) particles refer to graphite with a high amount of stacked layers [140] or more complex structures such as Aerographite [141, 142] or nano-foams, but these are not regarded within this thesis.

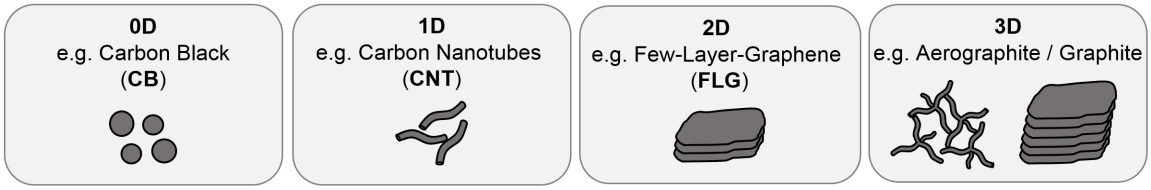

Figure 2.8: Classification of different types of carbon nanoparticles.

The influence of different types of carbon nanoparticles on the mechanical properties of polymers and FRP has been widely investigated by many research groups. Polymer nanocomposites based on spherical carbon nanoparticles such as carbon black were investigated previously with regard to electrical percolation [143, 144] or fracture toughness of nanoparticle modified polymer [135, 144] and FRP [145]. Although no significant improvement in tensile strength is observed for a matrix modification with CB, tensile modulus and fracture toughness are significantly improved, achieving similar fracture toughness values as a modification with MWCNT [135]. An increase in polymer matrix fracture toughness due to incorporation of CB nanoparticles is reported as well by Zhang et al. [144].

Since the rediscovery and popularisation of CNT in the 1990s [146, 147], impressive increase in mechanical properties is reported for CNT modified polymers or FRP [9, 20, 135, 136, 145, 148–151]. Different energy dissipating and thus toughness increasing mechanisms at the CNT are identified. Among these mechanisms are nanotube pull-out, nanoparticle-matrix debonding and nanotube breakage [135, 151, 152]. Nanotube pull-out may result in crack bridging of nanotubes [135, 149, 151, 153]. For double- or multi-walled CNT a shearing of the layers is reported as an additional failure mechanism (sword-in-sheath failure) [135, 154]. The importance of CNT dispersion, length and aggregate size on the mechanical and electrical properties of polymer nanocomposites was experimentally inves-

tigated by Bai and Allaoui [155], who pointed out that in case of a random orientation of nanotubes, high concentrations are not helpful [155]. The importance of MWCNT dimensions and dispersion quality was demonstrated by Zhang et al. [153], who reported that longer MWCNTs with small diameters (higher aspect ratios) achieved the best results for a reduction of fatigue crack growth [153].

Increasing interest is set on graphene nanoparticles after the pioneering work of Novoselov and Geim et al. [125, 126], leading to the EU "Graphene Flagship" research program. Graphene based, layered particles exhibit high potential for improving mechanical properties [9, 134, 137, 156–160]. The addition of small amounts of graphite nanoplatelets or graphene-oxide increases the fracture toughness of epoxy significantly by 25 % respectively 40 % [156]. "Enhanced mechanical properties" such as Young's modulus, tensile strength and fracture toughness due to the addition of graphene nanoplatelets in epoxy even at low nanofiller content are reported by Rafiee et al. [157]. The graphene platelets performed better than carbon nanotubes. Also, higher resistance of epoxy to fatigue crack growth with a graphene modification was shown [157, 158].

The fracture toughness and hence strength increase is explained with stress relief due to micro-damage at the nanoparticles. Different energy dissipating damage mechanisms at the nano- or micro-scale are proposed. At the particles itself, graphene layer separation, layer shearing and plastic yielding of the matrix that results in plastic voids are reported [9, 23, 156]. These mechanisms were already suggested for other layered particles such as silicas [161]. Furthermore, crack pinning and bifurcation, crack deflection as well as crack propagation at different heights at the graphene nanoparticles hinders crack propagation, thereby increasing the fracture toughness [156]. Detailed summaries on the toughening mechanisms for differently shaped nano- or microparticles are given by Quaresimin et al. [9] and by Marouf et al. [10].

An analytical approach regarding the role of length and cross-sectional shape of fillers on strength and toughness of nanocomposites was presented by Greenfeld and Wagner [162]. Whether pull-out failure or breakage of a nanoparticle occurs, depends on the critical length l_c. If the particle length is higher than l_c, the particle will rather break, whereas for a length smaller than l_c a pull-out failure is more probable [163]. For optimum reinforcement regarding energy dissipation, nanoparticle length should be close to but below the critical length. The surface area of the nanoparticle in contact with the surrounding polymer is important for stress transfer and larger for hollow tubes than for solid particles like short fibres. Comparing thin walled CNT and thin flat particles like graphene, the latter have half the critical length due to the double sided bonding [162]. Liu and

Brinson [164] determined the influence of particle orientation by comparing the reinforcing efficiency. They conclude, that nanoplatelets achieve better reinforcement in the case of random orientation, but nanotubes can generate a larger amount of interphase. With their analytical results, they motivate further experimental comparisons of different nanoparticles in the same polymer matrix [164].

Recently, Nadiv et al. [140] investigated the influence of nanoparticle dimension on mechanical and electrical properties as well as rheological behaviour and defined an optimum nanoparticle concentration for the three filler types investigated, namely CNT, GNP and graphite (shown in Figure 2.9). They concluded, that CNT are best suited for multifunctional composites because of their low percolation threshold, while GNP are the best choice for hierarchical composites like modified FRP due to the better processability and broader range of optimum concentration regarding a reinforcement in mechanical properties [140]. However, the influence of nanoparticle dispersion, which has a high influence on mechanical [134, 148, 150, 153, 165] as well as electrical properties [134, 138] and rheological behaviour of nanocomposites, is not regarded in the results and in the context of an optimum concentration.

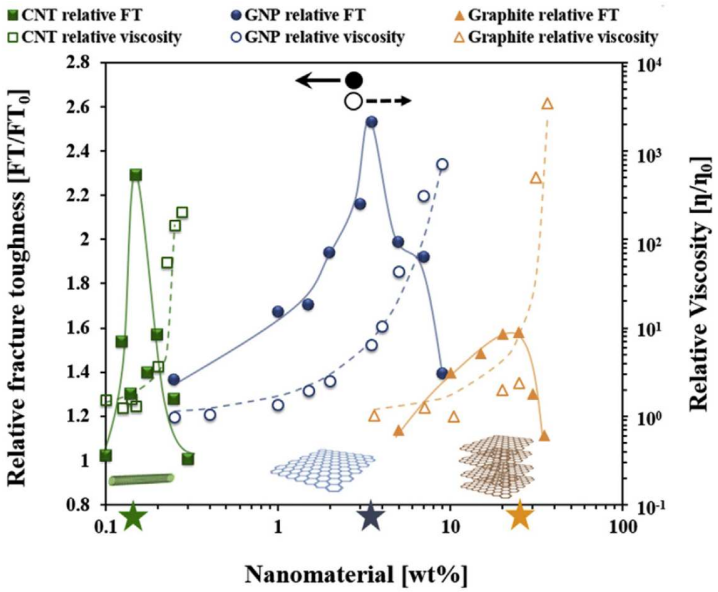

Figure 2.9: Relative fracture toughness and relative viscosity as a function of CNT, GNP and graphite concentrations. The optimum nanoparticle concentration for each filler is denoted by a star [140].

By FEM simulation, the influence of graphene nanoparticle shape, orientation, aspect ratio, filling content and clustering on the strength and stiffness of epoxy is investigated by Dai and Mishnaevsky [166]. As can be seen in Figure 2.10, the highest values for strength and stiffness are achieved, if the particles are oriented parallel to loading direction. For

a random orientation, the load direction has no significant influence whereas the lowest strength and stiffness values are reported for a loading transverse to oriented particles. Furthermore it was found, that the Young's modulus of nanocomposites increases with increasing aspect ratio, volume content and particle-matrix interfacial strength, whereas it decreases with a higher degree of clustering. The tensile strength follows similar tendencies, except for the aspect ratio and clustering degree, where the opposite effects were reported [166].

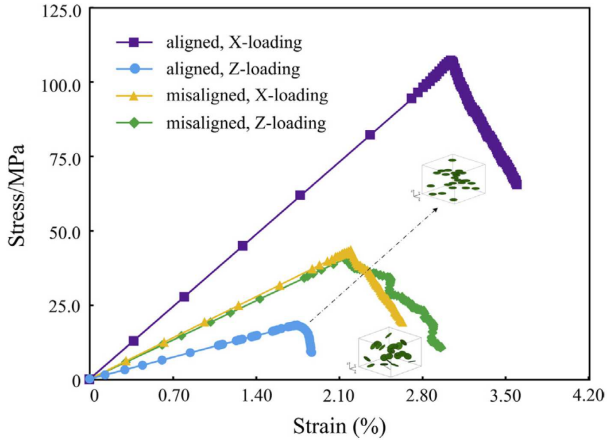

Figure 2.10: Simulation results for stress-strain relationship for nano-composites with aligned and random graphene reinforcement [166].

For multifunctional materials, the requirements for nanoparticles to improve both mechanical and electrical properties may be opposing. For example, the highest enhancement of fracture toughness is achieved with an exfoliation method and individual CNTs in the matrix [150], but for electrical conductivity, networks with CNT being in contact with each other are preferable to obtain electrical conductive paths. A trade-off may thus be necessary when designing multifunctional composites.

Values from literature showing the influence of different types of carbon nanoparticles on the fracture toughness of thermosetting polymers are summarised in Figure 2.11. For all fillers an increase in fracture toughness is reported, if the filling content is high enough. Experimental values from single edge notch bending (SENB) tests, performed according to ASTM D 5045 [167], for two different types of SWCNT (OCSiAl Tuball (75%) and Tuball (purified)) and for FLG (AvanGraphene-2) are given for comparison. The experimental values exhibit the same trends as reported in literature with the highest fracture toughness increase ($+$ 60 %) for FLG at 0.05 wt.%. Compared to the literature, this is the highest value of K_{Ic} increase reported so far for this comparable low filling content, hinting to a very good dispersion. The diagram shows the potential of carbon nanoparticles for

toughness improvement. The used FLG and the Tuball (75%) SWCNT are the respective type of particles also used for the further investigations as described in 3.1. Up to now, only bulk volumes are investigated in SENB tests with cuboid specimen geometries. However, for modification of FRP, it is of particular interest to identify whether or not a size effect for nanoparticle modified matrix exist. Since the volumes between fibres in FRP are tiny, an understanding of the damage mechanisms in small volumes is necessary. These issues are clarified in chapter 4.5.

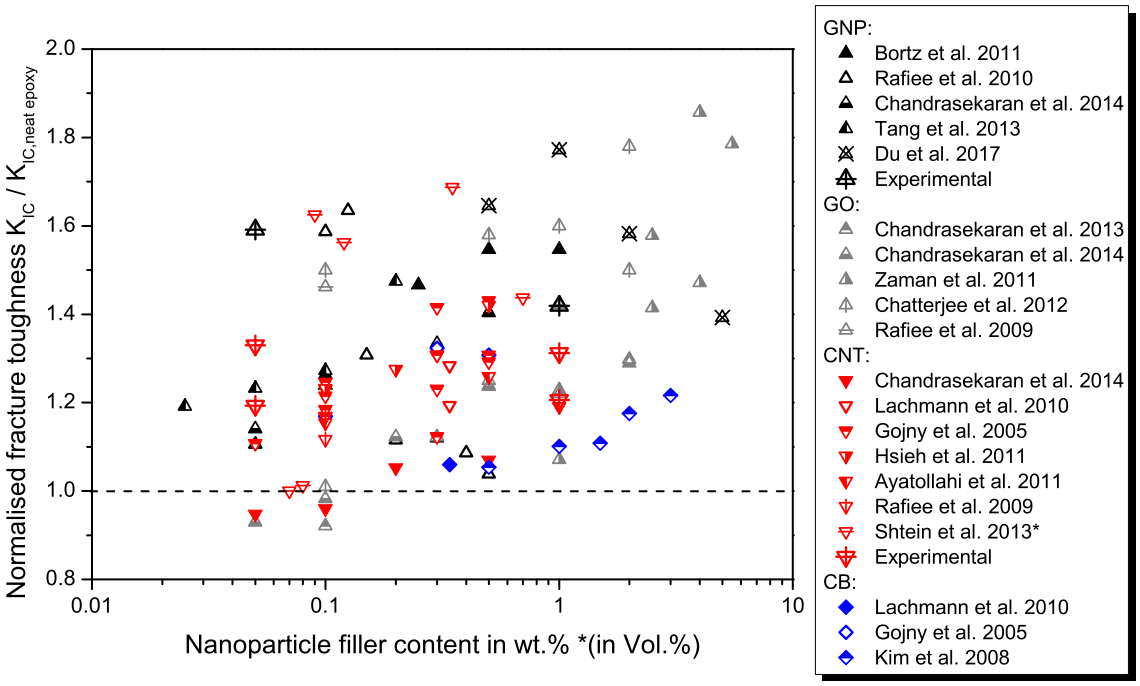

Figure 2.11: Normalised fracture toughness of polymer nanocomposites over nanoparticle filling content for different types of carbon nanoparticles (values from [134, 135, 149–151, 156–159, 168–173]).

2.3.2 Influence of nanoparticle modification on the mechanical properties of FRP

The beneficial influence of a nanoparticle modification on mechanical properties, especially fracture toughness, of polymers makes them promising candidates for improving FRP with regard to a more damage tolerant behaviour. Compared to the huge amount of literature available on nano-composites based on carbon nanoparticles (e.g. summarised in reviews [9, 10]), only few investigations have been carried out on the influence of nanoparticles on the damage behaviour of FRP, with most of them focusing on silica or nanoclays [11].

Some of these studies investigate the influence of nanoparticles on the fibre-matrix-bond with the aim to improve the interfacial strength. Liu et al. [174] achieved enhanced interfacial adhesion and improved mechanical properties of the matrix when modified with silica nanoparticles in single fibre fragmentation tests. In transverse fibre bundle tests with nano-silica modified epoxy, no significant effect on fibre-matrix interfacial debonding but reduced stress concentrations from thermal residual stresses were reported [175]. Results from Tian et al. [176] obtained with micro-droplet, transverse fibre bundle tension and short-beam shear tests indicate, that silica nanoparticles did improve the interfacial properties between carbon fibre and epoxy effectively. This is attributed to a higher energy dissipation and more efficient stress transfer during fracture [176].

The positive influence of nanoparticles on fracture toughness is especially applicable in FRP for load cases where damage initiation and propagation is critical like impact damage and CAI behaviour. Increased resistance against impact damage, visible in a smaller delamination area after impact, and increased CAI strength are reported for CFRP and GFRP for a modification of the epoxy matrix with thermally reduced graphene-oxide [177]. A MWCNT modification of CFRP also increases the CAI strength, although a reduction of delamination area is only visible for impact energies higher than 15 J [178]. It should be noted, that matrix particle toughening with thermoplastic particles shows similar behaviour and suppresses delamination growth, leading to increased CAI failure stress [179].

Regarding mechanical properties under static loading, the influence of nanoparticles on tensile strength and stiffness is small [53]. But the combination of a MWCNT matrix modification with thin-ply technology leads to improved tensile strength as well as resistance against material degradation by a space environment [180]. FRP compressive strength increases with graphene-oxide and pristine graphene matrix modification that also improves the thermal conductivity [181].

In FLG and MWCNT modified CFRP, the stress relieving mechanisms at the nanoparticles increase the fatigue lifetime in the tension-tension regime [23]. The improvement is higher with increased load level and slightly higher for a FLG modification compared to MWCNT. The nanoparticle modification shifts the fatigue degradation to a lower level within phase I and II. The onset of phase II however is not clearly delayed towards a higher number of loading cycles [23], as it is reported by Manjunatha et al. [182] for silica nanoparticle modified GFRP. In the tension-compression regime however, a FLG modification is detrimental to fatigue lifetime, which is explained with lower mode I interlaminar fracture toughness $G_{\mathrm{I}c}$ due to the modification [183, 184]. Fractography analysis of the

tested laminates indicates different types of microdamage at the FLG nanoparticles, but due to the complex crack geometry and large fracture surface, single damage mechanisms are hard to identify in composites [23]. Therefore, an approach of using fibres as specimens for the investigation of very small volumes and thus smaller fracture surfaces is executed within this thesis (refer to chapter 4.5). Yavari et al. [185] reported increased fatigue life of interwoven GFRP due to an incorporation of GNP and different types of nanotubes under flexural bending. This is attributed to the graphene network toughening the fibre-matrix interface and preventing delamination or buckling of the glass fibres under compressive stress. Again, the effect is more pronounced for higher load levels and slightly higher for GNP compared to MWCNT [185]. With an interlayer modification, the interlayer fatigue crack growth resistance may exceed the intralayer crack growth resistance, resulting in the crack propagating through the fibre rich areas instead of the interface between two layers, as shown for a CFRP interlayer toughening with PA12 particles [186]. For 3D numerical simulations of fatigue damage of multiscale fibre reinforced polymer composites with secondary nano-clay reinforcement, higher damage resistance in the compression-compression regime is reported [187]. Simulation cases with particles localised in the fibre sizing exhibit higher lifetime and damage resistance than those with particles dispersed throughout the matrix. Furthermore, crack bridging by nanoparticles was observed mainly for randomly oriented nanoplatelets in the models. However, as only a small unidirectional fibre arrangement is modelled [187], the influence of delamination between different layers and hence the material resistance against buckling of complete layers, which is critical for compression loading cases, are not considered.

Several investigations on the influence of a nanoparticle matrix modification concentrate on interlaminar (delamination) crack growth [183, 188–190], but inconsistent results are reported regarding the influence of graphene based nanoparticles on the interlaminar fracture toughness of FRP under mode I and mode II loading in double cantilever beam (DCB) and end-notch flexure (ENF) tests. Ahmadi-Moghadam et al. [190] reported an increase in crack initiation resistance (onset) but a decrease in propagation fracture toughness for GFRP modified with 0.5 wt.% GNP (25 µm lateral dimension) under mode I loading. Mode III interlaminar toughness was in the range of the unmodified GFRP. For mode II loading, a slight reduction in fracture toughness (onset) is reported, which is explained with lower matrix fracture toughness with GNP modification under mode II [190, 191]. However, no investigation on failure mechanisms under mode II and mode III loading, e.g. by SEM, is carried out and the findings are only explained with the mechanisms observed in mode I. The decrease of mode II interlaminar toughness is contradictory to the findings from Kostagiannakopoulou et al. [189], who presented an increase in both

mode I and mode II energy release rate of CFRP by modifying the matrix with 0.5 wt.% and 1.0 wt.% GNP (5 µm lateral dimension). For slightly smaller GNP particles (1 µm to 2 µm lateral dimension) at 0.5 wt.% filling content, they report an increase in mode I fracture toughness of CFRP as well [188]. In a previous experimental investigation with the same material and production method used in this work, an influence of size and orientation of FLG particles (5 µm to 25 µm lateral dimension) at 0.3 wt.% filling content on the delamination surface roughness respectively on the energy release rate during delamination crack propagation was found that depends on the mode. For mode I, a decrease of $G_{\mathrm{I}c}$ is observed, whereas mode II interlaminar fracture toughness $G_{\mathrm{II}c}$ increases by 68 % [183, 184].

Differences between mode I and mode II efficiency with regard to interlayer toughening are also reported for layered silicate [192]. Over 100 % improvement of $G_{\mathrm{II}c}$ was measured and explained with the high aspect ratio of the nano-additive that helps to constrain the growth of the micro-cracks and delays failure. Mode I ($G_{\mathrm{I}c}$) performance decreases however, as a result of the fibre tows preventing optimum dispersion of the modifier, leading to a high clay concentration in the resin rich interlayer region, which results in promotion of the propagating crack rather than inhibition [192].

When comparing these findings, the particle size plays a crucial role for toughening. Furthermore, nanoparticle dispersion [148] and the degree of filling may have an additional influence. High filling content may reduce the toughness of polymers [156] and to some extent also of FRP. Surface modification to achieve better bond between matrix and nanoparticles may also be beneficial with regard to fracture toughness [137, 171, 190] but its investigation is beyond the scope of this work.

Up to now it has not been clarified, how the local damage mechanisms reported for nanoparticles in bulk polymers [9, 156] act in the small volumes between the fibres and influence the damage behaviour in the differently oriented layers of FRP. These issues are considered by the experimental investigation in chapters 4.5 and 4.6. The differences regarding the effect of nanoparticle modification on interlaminar crack propagation will be addressed with a theoretical concept explaining the differences in chapter 4.6.3.

3 Experimental methods

In this chapter, the materials, specimen preparation, and the experimental test set-ups are introduced. In order to assure representativeness and reproducibility of test results, manufacturing quality is controlled by various methods during specimen preparation. Different non-destructive testing (NDT) methods are used during mechanical testing in order to gain insight on the damage process with increasing loading. Failure mechanisms are analysed by fractography in light microscopy and scanning electron microscopy (SEM). Full traceability is given by specimen planning and documentation throughout the manufacturing and testing process.

3.1 Materials

The different types of carbon-nanoparticles used are listed in Table 3.1. Classification of the nanoparticles is according to Figure 2.8. Dimensions are given considering the morphology of the particles: for the SWCNT diameter d and length l, for FLG width w and thickness t and for CB the BET surface area (after Brunauer, Emmett, Teller [193]).

Table 3.1: Types of carbon nanoparticles used in this investigation (values from the respective data sheets).

Category	**Type**	**Name**	**Supplier**	**Dimensions**
0D	CB	Printex 300	Evonik industries, Germany	BET surface area $= 80\,\mathrm{m^2/g}$
1D	CNT	Tuball (75%)	OCSiAl, Russia	$l \geq 5\,\mu\mathrm{m}$ $d \leq 1.9\,\mathrm{nm}$
2D	FLG	AvanGraphene-2	Avanzare, Spain	$5\,\mu\mathrm{m} \leq w \leq 25\,\mu\mathrm{m}$ $t \leq 2\,\mathrm{nm}$ $n_l \leq 6$ layers

For manufacturing epoxy fibres and model composites as described in the following, the resin Momentive Epikote RIMR 135 with the hardener Momentive Epikure RIMH 134

for the fibres and RIMH 137 for the model composite is used as matrix system (density $\rho = (1.13 \text{ to } 1.17)\,\mathrm{g/m^3}$). It is an epoxy matrix system with an amine hardener and has a glass transition temperature of $T_g = 93\,^{\circ}\mathrm{C}$. The epoxy equivalent for RIMR 135 is 166-185 g/equivalent and the average amine equivalent for RIMH 134/137 is 52 according to the manufacturer. The components are mixed in a ratio of 10:3 weight proportion according manufacturer's recommendation. E-glass fibre rovings Hybon 2002 with a silane sizing from PPG Fiber Glass are used as fibres for the model composites. Nominal roving tex is 600 g/km and the fibre diameter is 12 µm.

The UD prepreg HexPly-*M21/34%/UD194/T800S* (Hexcel, Germany) is used for producing CFRP laminates with various lay-ups in order to investigate the influence of layer thickness. The fibre is a *T800S* intermediate modulus carbon fibre (yield: 24k). *M21* is a toughened B-stage epoxy matrix system with a glass transition temperature of $T_g = 195\,^{\circ}\mathrm{C}$ (onset). Cured ply thickness is $t_{ply} = 190\,\mu\mathrm{m}$ and the fibre volume content is $V_F \approx 57\,\%$.

The cross-ply laminates for investigating the impact of a tailored FLG modification in the respective layers are produced with a custom-made prepreg machine. *T700S* carbon fibres (Toray, Japan) with an epoxy resin compatible sizing are used in the form of a 12k roving with the epoxy prepreg system Ludeko R470 / H471 (Ludeko, Germany) at a mixing ratio of 100:16 as matrix material. Planar FLG avanGraphene-2 (refer to Table 3.1) are used for nanoparticle modification of the matrix with a filling content of 0.3 wt.% based on the complete matrix system.

3.2 Specimen manufacturing

For modifying an epoxy resin with carbon nanoparticles either for producing polymer nanocomposites or for use as nanoparticle modified matrix in FRP, in a first step the appropriate amounts of nanoparticles and epoxy resin are mixed inside a glove box and dispersed by using a three roll mill (EXAKT Advanced Technologies GmbH 120E) that works on the principle of applying high shear rates on the mixture to disperse the nanoparticles homogeneously. Previous studies have proven, that using a three roll mill to disperse carbon nanoparticles in epoxy leads to an excellent dispersion quality without disturbing size and morphology of the particles [148]. The mixture is fed into the three roll mill at the feed roll and collected at the apron roll. This process is repeated seven times with the gap widths being adjusted from 120 µm to 5 µm (refer to Figure 3.1). The rotational speed of the rolls is kept constant at $33\,\mathrm{min^{-1}}$, $100\,\mathrm{min^{-1}}$ and $300\,\mathrm{min^{-1}}$, respectively. After dispersion, the hardener is added and the mixture is stirred for approximately 10 min and

then degassed under vacuum (15 mbar abs) for 15 min to remove any air inclusions. Uniform nanoparticle dispersion is obtained for the different morphologies and filling contents investigated.

3.2.1 Manufacturing of single epoxy fibres and model composites

The complete manufacturing process is depicted schematically in Figure 3.1. The method of using epoxy fibres is adapted from Hobbiebrunken et al. [73]. Unmodified or nanoparticle modified epoxy, as it is obtained after the dispersion described above, is used. In order to increase the viscosity for producing the fibres, the degassed matrix system is heated in an aluminium cup on a heating plate at a constant temperature of 50 °C for about 40 min. When the matrix starts to vitrify, the fibres are pulled with a needle. By dipping the needle into the matrix and lifting it, thin fibres stick to the needle. These fibres are wound around two rods (refer to Figure 3.1). Via the pulling speed of the needle, the fibre diameter can be adjusted to a certain point. Fibres with diameters between 20 µm and 350 µm after curing are obtained. The fibres are cut and glued at one end on paper sheets based on ASTM D3379 for single fibre tensile tests [194] and then cured in an oven at 20 °C for 24 h and at 80 °C for 15 h, as recommended for this matrix system. Only one side is fixed in order to avoid tension stresses or morphology changes (e.g. by chain orientation) in the fibres because of thermal or chemical shrinkage during curing. It is assumed, that any axial orientation of the molecule chains, which may have been occurred during stretching the resin into the fibre shape is lost during the curing process. With differential scanning calorimetry (DSC) measurements it is assured that the matrix system is completely cured. Since the manufacturing process, including the curing cycle, is the same for all fibrous specimens and differences in the overall surface area of the fibres are small, the hardening reaction at atmospheric conditions is not considered for discussion of the test results.

After curing, the second end of the fibre is fixed on the paper at the ends of a hole with dimensions of 10 mm × 25 mm [194]. Behind the glue for fixation on the paper, the fibres are electrically contacted with silver conductive paint for measuring the electrical resistance change during tensile testing. The investigation of the electrical properties is beyond the scope of this thesis but is described and discussed in [195]. The free test length is 25 mm (refer to Figure 3.3). In order to compare the obtained results with the strength of specimen with larger volume, dog-bone specimens of all four configurations are manufactured according to DIN EN ISO 527-2 [196] with a gauge length of $l = 30$ mm and a median gauge width of $w = 3.93\,\text{mm} \pm 0.07\,\text{mm}$. In addition some dog-bone

specimens with dimensions of $l = 13\,\text{mm}$ and $w = 4\,\text{mm}$ are produced for a broader range of volume.

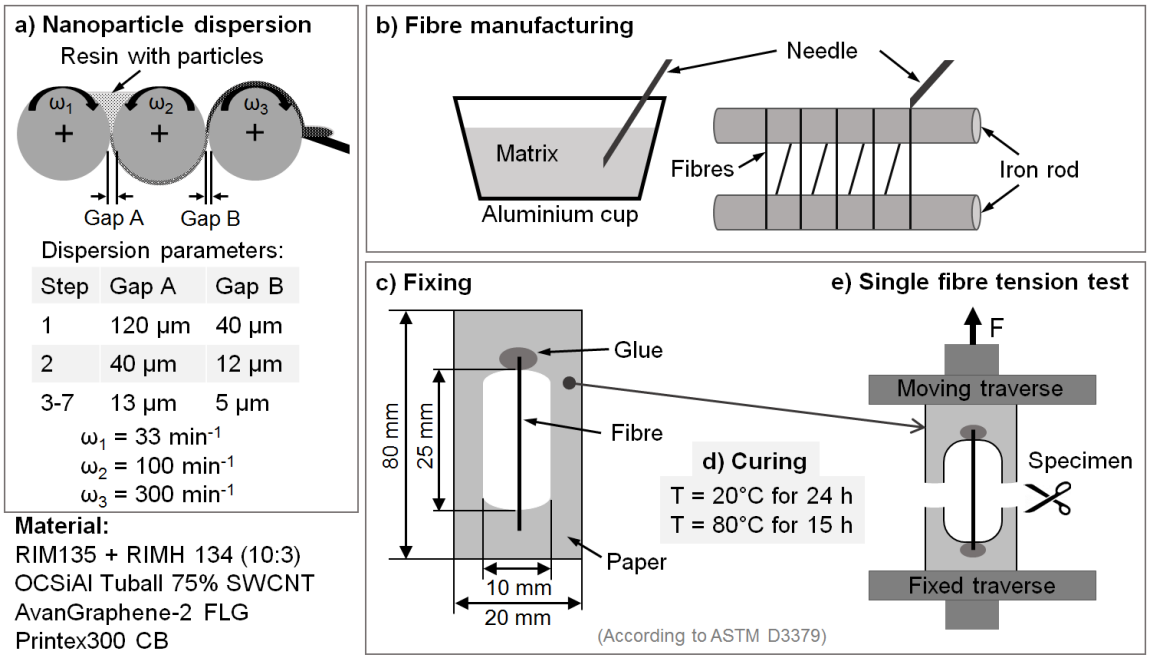

Figure 3.1: Schematic representation of fibre specimen manufacturing process: a) dispersion of nanoparticles in the resin (only for modified fibres), b) epoxy fibre manufacturing, c) specimen preparation for curing, d) curing parameters, e) scheme of specimen mounted in universal test machine.

Model composites are used to observe the influence of ply thickness of failure initiation in small, defined volumes. The width and thickness of the glass fibre rovings used as fibrous reinforcement are varied in order to represent different ply thicknesses in the model composites. Some specimens were manufactured using the rovings as delivered. The roving width is between 2.5 mm and 3.0 mm with a thickness of approximately 130 µm to 150 µm. A part of the roving is spread between two rollers of a three roll mill (Exakt Advanced Technologies GmbH). The gap between the rollers is set to 100 µm with a ratio of rotational speed of 3:1. Due to the difference in rotation speed, shear loads are introduced into the roving, but with the chosen set of parameters no damage of the fibres is detected in light microscopy analysis carried out after the spreading. The rovings are spread to a median width of 3.84 mm (+40 %), the thickness decreases about 30 % down to 100 µm.

Model composites are produced with a casting set-up, shown schematically in Figure 3.2 a). The fibre rovings are placed in the centre of a silicone mould. The resin and hardener are mixed and degassed as described above. The matrix is infused via channels in the mould. The specimens are cured at room temperature in the mould for 24 h, demoulded

and cured for 15 h at 80 °C in an oven. Void free specimens with the dimensions given in Figure 3.2 b) are produced. A crucifix-shape, introduced by Ogihara et.al. [197] to evaluate the glass fibre/epoxy interfacial transverse strength, is chosen for specimen geometry to avoid early failure due to stress increase at the specimen edges and assure damage initiation in the centre (0/90/0) section of the specimen, where damage initiation and propagation is observed under transmission light microscopy.

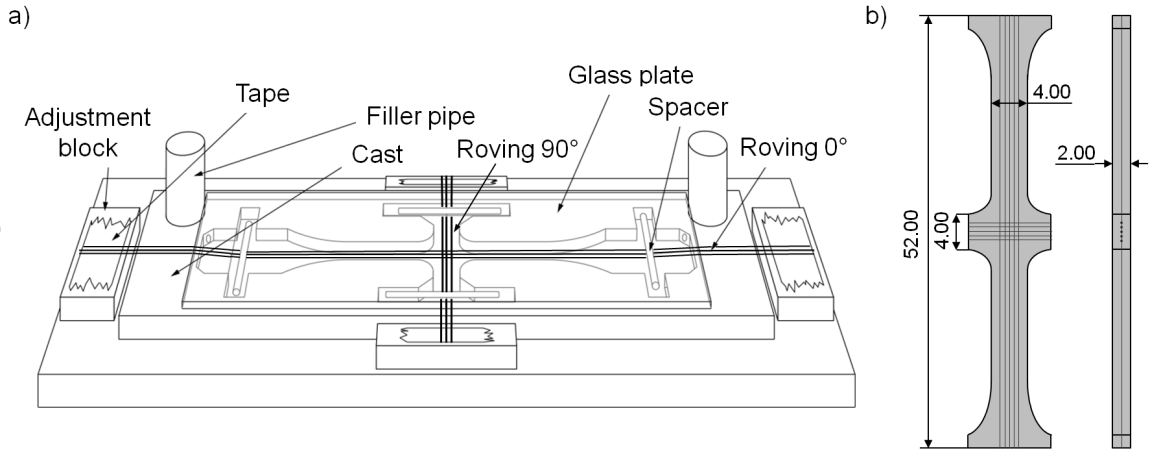

Figure 3.2: Scheme of the casting set-up for manufacturing of model composites a) and specimen geometry b).

3.2.2 Manufacturing of CFRP specimens

Laminate plates of 300 mm × 300 mm are laid-up by hand from UD prepreg (HexPly-M21/34%/UD194/T800) with a cross-ply lay-up for quasi-static tensile test and a QI lay-up for UNC, OHC and CAI tests, as detailed below. Laminates are cured in an autoclave at a maximum temperature of 180 °C, an applied vacuum of 800 mbar abs and a maximum pressure of 7 bar with a curing cycle recommended for this prepreg system by the manufacturer. Quality inspection of all laminates with ultrasound inspection confirms, that there are no manufacturing induced defects such as voids or delaminations. Specimens are cut from these plates with a diamond saw (ATM Brillant 265). For each test case, two or more plates of each configuration are produced in order to regard statistical variations of the manufacturing process within the test results.

Quasi-isotropic lay-ups of $[45_n/0_n/-45_n/90_n]_{ms}$ and $[45_n/90_n/-45_n/0_n]_{ms}$, with $n = 1, 3$ and $m = 3, 1$ are selected in order to investigate the influence of both the layer thickness and the position of the 0°-layers (stacking sequence) on the compressive properties.

Thickness of the laminates after curing is 4.56 mm with a theoretical cured ply thickness (CPT) of 190 µm. The specimen width for UNC and OHC tests is according to aviation standard AITM 1-0008 [198] $w = 32\,\text{mm}$. Tab length is chosen to be 55 mm resulting in a total specimen length of $l = 142\,\text{mm}$. 2 mm thick GFRP end tabs are applied on the specimen with 2-component epoxy adhesive (UHU Endfest-300), leaving a gauge length of $l_0 = 32\,\text{mm}$ between the tabs [198]. The specimen side edges are polished to minimise edge effects. For the open-hole specimen, a hole with a diameter of $d = 6.34\,\text{mm}$ is drilled with a carbide drill through the thickness at the centre of test area. The specimen geometry for CAI tests is according to ASTM-D-7136 [199] and ASTM-D-7137 [200] standard with length and width: $l \times w = 150\,\text{mm} \times 100\,\text{mm}$.

For quasi-static tensile tests, the lay-up is $[0/90_n/0]$, where n is varied with n=1,2,3,4,8,10, in order to investigate the influence of the 90°-layer thickness. The specimen geometry is according to DIN EN ISO 527-4 [104] with length $l \geq 250\,\text{mm}$ and width $w = 25\,\text{mm} \pm 0.5\,\text{mm}$. As the 90°-layer thickness is varied, specimen thickness deviates from the normative reference and only the dimensions of the specimens with $n = 8$ fulfil this requirement [104]. End tabs with a length of 50 mm consisting of respectively 1 mm thick GFRP and aluminium strips are glued on the specimens by using a 2-component epoxy adhesive (UHU Endfest 300), leaving a distance of $l_0 = 150\,\text{mm} \pm 1\,\text{mm}$ between the tabs.

To avoid moisture influence on the test results, all specimens are conditioned according to DIN EN 3615 [201]. Drying is in several steps with specimen weight being measured after each step and compared to the weight two steps before, until the weight difference divided by last measured weight is smaller than $5 \cdot 10^{-4}$. If the calculated value fulfils this criterion, the specimens are regarded as dry [201]. Afterwards the specimens are stored in the test environment until testing.

3.2.3 Manufacturing of CFRP specimens with tailored FLG modification

FLG nanoparticles are dispersed in the resin without hardener as described above. The hardener is added before impregnation of the fibres. The components are degassed for 1 h at 30 °C and then mixed by automated stirring in vacuum for 20 min to remove any air inclusions.

Unmodified and FLG modified prepregs are produced with a custom-made prepreg machine, successfully used before to produce nanoparticle-modified prepregs [23]. The dry

carbon fibre roving is impregnated with the unmodified or FLG modified matrix system in a continuous process and winded up on a hexagonal roll. With this method, a unidirectional tape with straight, aligned fibres of 300 mm width is produced. Transmission light microscopy of thin micro section samples confirmed, that the nanoparticles are equally dispersed in the matrix between the fibres. After B-staging according to the recommendation for this material system, the prepregs are stored at −18 °C until lamination and the following curing process. Cross-ply laminates with the stacking sequence $[0/90_2]_s$ and thickness $t = 2\,\text{mm}$ are stacked from the produced prepregs and cured in an autoclave for 2 h at 120 °C with an applied vacuum of 800 mbar abs and an autoclave pressure of 3 bar. Three different configurations are produced this way, as listed below. The "N" stands for a neat layer and the "G" for a graphene (FLG) modified layer. The unmodified laminates (NNN) are used as a reference. With this approach, the influence of the FLG modification in either 0°-layers (GNG) or 90°-layers (NGN) on the mechanical properties and the damage process can be experimentally determined.

- NNN - Unmodified
- NGN - 90°-layers modified with 0.3 wt.% FLG
- GNG - 0°-layers modified with 0.3 wt.% FLG

The fibre volume content is determined according to DIN EN 2564 [202] to be approximately 65 %. Ultrasound inspection is performed after curing and assures manufacturing quality without any larger voids or delaminations. End tabs consisting of 50 mm wide and 2 mm thick GFRP/Aluminum stripes are applied on the cured laminates by using 2-component epoxy adhesive (UHU Endfest-300) leaving a gauge length of $l_0 = 150\,\text{mm}$ between the tabs. Specimens for static and cyclic tensile tests are cut with a diamond saw (ATM Brillant 265) to dimensions according to DIN EN ISO 527-4 [104] with total length $l = 250\,\text{mm}$ and width $w = 25\,\text{mm}$. Specimen edges are polished to minimise edge effects.

3.3 Test methods

Since the prepreg for the tailored FLG modified CFRP specimens is produced in house with a custom-made prepreg machine, fibre volume content of the laminates is determined after curing. Samples of each laminate are given to the Central Laboratory of Analytical Chemistry of Hamburg University of Technology (TUHH). The fibre-mass-content is determined according to DIN EN 2564 [202] by removing the matrix in a chemical etching

process. With the density values of fibres and matrix from the data sheets, the fibre volume fraction is calculated.

Differential scanning calorimetry measurements (DSC 204 F1 Phoenix, Netzsch, Germany) are carried out to assure complete curing of epoxy fibre specimens by checking that the polymer's glass transition temperature T_g of the specimens is in the range given by the manufacturer for a completely cured matrix system. With DSC, the heat flow between the sample and a reference is analysed during heating or cooling down and allows to conclude from the signal to internal changes in the material structure such as glass transition, crystallisation, melting or decomposition. A detailed description of the DSC principle can be found for example in [203, 204]. The T_g is determined by analysing the slope of the DSC heat flow signal at a heating and cooling rate of 20 K/min. No significant influence of the nanoparticle modification on the T_g of the matrix is found with an onset of $T_{g,onset,\mathrm{CB}} \approx T_{g,onset,\mathrm{CNT}} \approx T_{g,onset,\mathrm{FLG}} \approx T_{g,onset,\mathrm{neat}} \approx 80\,°\mathrm{C}$. The inflexion point of the heat flow curve is at approximately 92 °C for all configurations and corresponds well with the value of $T_g = 93\,°\mathrm{C}$ given by the manufacturer of the resin.

3.3.1 Single fibre tensile test

Figure 3.3 shows a scheme of the developed set-up for tensile tests of epoxy fibres including the measurement of the electrical resistance during mechanical testing (for further information see [195]). The specimens, consisting of the fibres glued on the paper, are mounted in a universal testing machine (Zwick Z10 / Zwick Z100) with a 10 N / 50 N capacity load cell. For availability reasons, two different machines are used, but no influence of the testing machine on the results is observed, as expected. The side bars of the paper, connecting the upper and lower part of the specimen, are cut before testing (refer to figure 3.1). Test speed is set to 25 mm/min in order to minimise plasticity effects with very high strains with necking and assure a more brittle failure mode of the fibres. The cross section of the fibres after failure is lower than the original cross section because necking cannot be completely avoided during the test. Therefore, the cross section after failure is measured for each specimen in an optical microscope. The true failure strength R_t is calculated from the measured force at failure and the cross section area obtained by microscopy. The fracture of the fibres is regarded as brittle.

The dog-bone specimens are tested with a universal testing machine (Zwick Z2.5) using a load cell with a capacity of 2.5 kN at a test speed of 1 mm/min according to DIN EN ISO 527-2 [196]. As the testing speed may influence the strain at break and

tensile strength, some dog-bone specimens of the neat configuration are tested with the cross-head speed of the fibre specimens of 25 mm/min. No significant influence of testing speed on the failure strength of the dog-bone specimens is observed. The cross section after failure is analysed for each specimen by using an optical microscope and by SEM to determine the damage mechanisms at the different types of nanoparticles and the influence of particle size, filling degree and morphology on failure initiation and propagation.

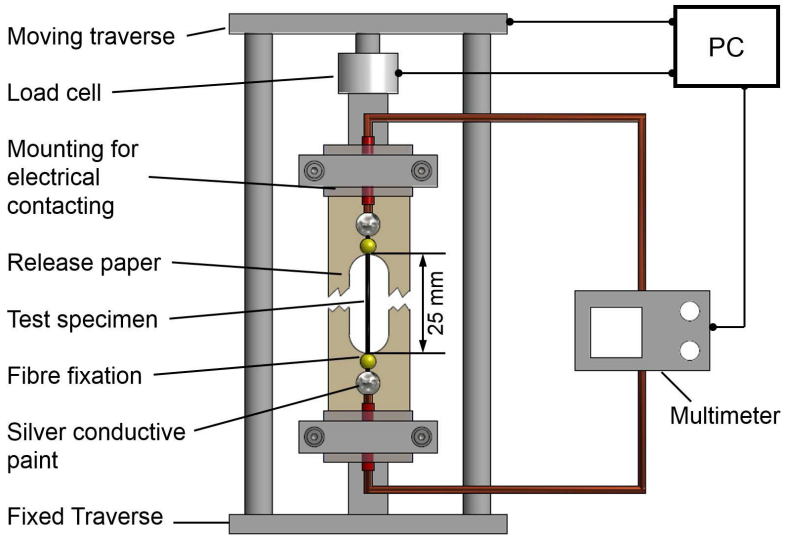

Figure 3.3: Schematic representation of the tensile test set-up for single epoxy fibres in the universal testing machine.

3.3.2 Tensile tests with model composites using light-microscopy

The influence of the 90°-ply thickness in (0/90/0) model composites on the initiation and propagation of transverse cracks under quasi-static tensile loading is analysed under transmission light microscopy. Model composites are used to reduce the total volume of the specimen and to investigate the damage initiation and propagation in a small volume. This approach was already successfully used to analyse matrix cracking and fibre matrix load transfer [205], first ply failure [28], glass fibre-epoxy interfacial transverse strength [197] and the influence of voids on fibre matrix debonding and damage propagation [43, 44, 206]. The model composites are tested in a custom-made tensile test rig equipped with an extensometer and a load cell with a maximum load of 5 kN. The rig is positioned under a transmission light microscope. Load and displacement are continuously measured and recorded. The test is carried out at a constant crosshead speed of 0.03 mm/min. The fracture initiation and propagation is monitored on a screen.

3.3.3 Quasi-static, impact and cyclic tests

Quasi static tensile tests are performed according to DIN EN ISO 527-4 [104] by using a universal testing machine type Zwick 1474 (Zwick, Germany) with a 100 kN load cell at a cross-head speed of 2 mm/min. Strain is measured with a long-travel extensometer on the specimen surface (measuring distance 50 mm). Acoustic emission analysis is used to analyse the damage process regarding the correlation of cumulated energy with damage development.

Impact damage is introduced in a drop weight tower by using a semi-spherical hardened steel striker with a diameter of 20 mm and a weight of 1.46 kg. Clamping of the specimens and the energy during the impact event deviates slightly from the ASTM D-7136 standard [199], but is selected to accommodate for impact damage where delaminations do not reach the specimen sides, as demanded in the standard. Contact force is measured by a strain gauge full bridge. Anti-rebound after the first impact is ensured with a photo sensor activated clamp mechanism. All specimens are subjected with an impact of 10 J. The induced energy related to the specimen thickness is 2.2 J/mm. Impact damage is assessed with ultrasound inspection and radiography.

Compression tests are executed by using a Zwick-Roell Z400 testing machine with a hydraulic pressure of 80 bar damping for clamping the specimens at the end tabs. Data is recorded with the Zwick/Roell software *TestXpert*. The UNC and OHC specimens are mounted in a hydraulic composite compression fixture (HCCF) and are mainly loaded by compressive force on their end surfaces. Via the end tabs, a small amount of shear loading is applied as well. CAI tests are carried out according to the ASTM D-7137 standard [200]. The cross-head speed is set to 0.5 mm/min for the UNC and OHC and 1.0 mm/min for the CAI tests. The compressive load is measured by a 400 kN load cell, whereas displacement is measured via the traverse of the machine. The deformation and force are continuously recorded to determine elongation, compressive strength and the modulus of elasticity. Strain gauges are fixed on the specimen to measure local strain in the centre in order to determine whether global bending or out of plane buckling occurs. A scheme of both test set-ups is given in Figure 3.4, with the set-up for UNC, OHC tests in Figure 3.4a) and for CAI tests in Figure 3.4b).

Fatigue tests are performed on a servo-hydraulic test machine (Instron/Schenk, Germany) with alternating loads in the tension-compression (t-c) regime ($R = -1$) at a frequency of 6 Hz. This frequency is low enough to avoid heating issues of the polymeric matrix. Two load levels are selected. The higher load level is at 228.8 MPa (23.0 % of mean tensile strength), the lower is at 215.0 MPa (21.6 % of mean tensile strength). The upper load

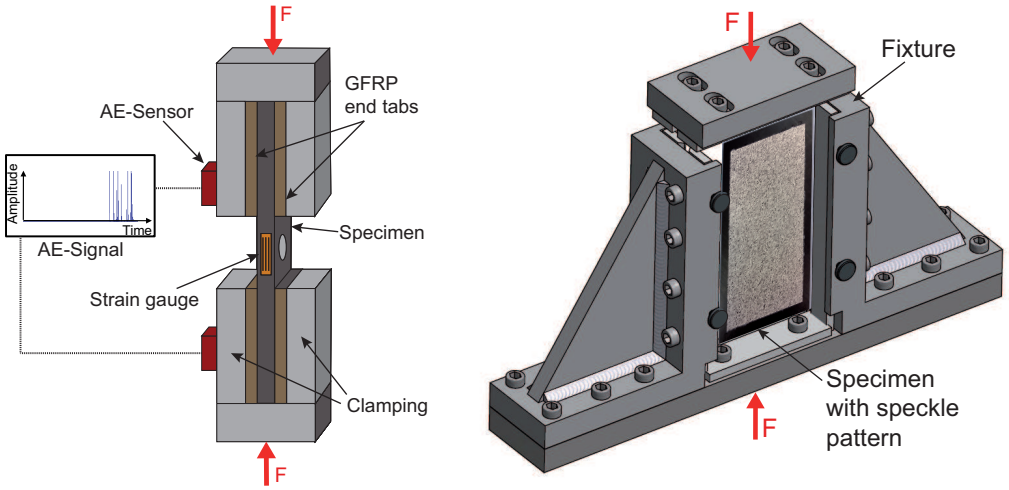

Figure 3.4: Scheme of the test set-up a) for UNC and OHC tests, here shown for a specimen with a central hole and b) for CAI tests.

level lies in the stress range of transverse crack initiation in quasi-static tensile tests, as it is determined with the AE-analysis. The tests are performed at standard conditions of 23 °C and 50 % relative humidity. Specimens are mounted in an anti-buckling device to prevent global specimen buckling during the compressive loading. Via a cut-out in the anti-buckling device, outer layers are allowed to buckle locally as a consequence of delamination within a defined region, for a more realistic representation of compression behaviour of structures. Passive thermography with an infrared (IR) camera is carried out for monitoring specimen surface temperature during fatigue tests to ensure that no critical heating of the matrix occurs. Interrupted tests with exemplary specimens of each configuration are carried out in order to observe the damage propagation with increasing load cycles. After defined numbers of loading cycles, specimens are demounted from the test machine, their damage state is analysed by using radiography and they are then remounted and tested further until the next defined load cycle. This process is repeated until final failure of the specimens. The loading cycle intervals between damage analysis vary with the number of cycles. Shorter intervals are used during the first cycles to investigate the initiation and propagation of IFF and shortly before final failure to observe delamination growth. The number of loading cycles are given in Table 3.2.

Table 3.2: Loading cycle intervals for interrupted fatigue tests.

Interruption no.	Number of cycles	Interruption no.	Number of cycles
I	50	VII	7500
II	250	VIII	10 000
III	500	IX	15 500
IV	1000	X	25 000
V	2500	XI	50 000
VI	5000	XII	100 000

3.3.4 Non-destructive testing methods

Acoustic emission analysis

In order to determine damage initiation during quasi-static testing and for analysing differences regarding the damage process in tensile as well as compression tests, acoustic emission analysis is used. With AE analysis, acoustic waves generated at irreversible deformation of the material, i.e. cracking, are detected with piezoelectric sensors and the wave-signal is conditioned and recorded by using amplifiers and filters as well as a respective software. One signal recorded this way is called a hit. The signal characteristics, such as the amplitude (the maximum peak in the AE signal waveform) can be analysed and correlated to damage mechanisms. The signal's energy (the area under the squared signal envelope) is a measure for the accumulated elastic energy in the material released at deformation. The more severe the damage, the larger the energy released and recorded [207, 208]. Detailed information about AE-analysis technique and principles can be found in the literature, e.g. [207, 208]. The cumulative energy of the signals can be used to analyse instants at which damage like matrix cracking initiates and to compare the damage process of different specimen configurations via the correlation of cumulated energy with damage development. Previous studies showed the usefulness of the AE-method for analysing failure mechanisms in composite laminates [209–211] or for determining the effects of voids on the compression behaviour in GFRP [212]. A detailed AE-signal interpretation for the different damage modes of cross-ply laminates, as it is carried out by Mizutani et al. [210] or a detailed frequency analysis as performed by Groot et al. [213] and combined with a pattern recognition by Gutkin et al. [214] is beyond the scope of this thesis.

For the AE analysis, a Micro II multi-channel acquisition system from *MISTRAS Group Inc.* is used to record AE data. Two wideband differential (WD) sensors are used for AE wave detection. In tensile tests, both sensors for AE wave detection are fixed on one side of the specimen. For the compression tests, the sensors are mounted on the surface of

the HCCF clamping elements. This distant sensor attachment might result in a loss of AE-parameter accuracy, but is indispensable to protect the sensors from damage during the compression tests. As the sound waves are disturbed and deflected at the interfaces on the way from the damage location to the sensor, frequency analysis or localisation results would be unreliable, but the test-set-up was successfully used before for comparing signal energy [212]. In both attachment cases, silicon grease is used as a coupling agent between the sensor and the specimen respectively the fixture. Internal filters and a static threshold are used to reduce disturbance variables such as machine vibrations and ambient noise. Before each test, a pencil lead break test with a Hsu-Nielsen Source [207, 215] is carried out with the specimen mounted in the clamps to assure adequate mounting of the sensors.

The settings of the AE acquisition system for tensile tests of cross-ply specimens and for compression tests of QI specimens are given in Table 3.3. In tensile tests, the focus is set on the investigation of IFF initiation in the 90°-layer of cross-ply laminates and the subsequent damage process with a tailored FLG modification. In addition, the IFF initiation and damage process is analysed for cross-ply specimens with varying 90°-layer thickness. In compression tests, the cumulative energy from the AE-signals is used for analysing differences regarding the influence of layer thickness on the damage process. A more detailed investigation on the damage initiation at an open hole under compressive loading by using AE-signals for determination of a distinct damage state is presented in [216].

Table 3.3: Parameters of the AE acquisition system for tensile tests of cross-ply specimens and compression tests of QI specimens (sensor: WD).

Parameter	**Cross-ply**	**Quasi-isotropic**
Frame rate / MHz	5	5
Preamp gain / dB	20	40
Threshold / dB	45	45
Hit definition time (HDT) / µs	250	200
Hit lockout time (HLT) / µs	800	300
Peak definition time (PDT) / µs	150	50
Maximum hit duration / µs	100	100

Ultrasound inspection and radiography

Ultrasound (US) inspection works on the principle of inducing acoustic signals into a material with a transducer that are reflected from an interface, such as the back wall of the object or from an imperfection within the object. The time of the echo after sending the signal is collected with a receiver and then analysed. The amplitude of the received signal represents the intensity of the reflection and the arrival time of the reflection represents the distance. The visualisation of the signal versus time at one point of the sample is called the A-scan. A series of A-scans along a line on the sample surface is called a B-scan and allows to measure localised differences through the thickness along that line. The failure echo, reflected from defects within the material, is distinguished from the back side echo, resulting from the signal's reflection at the interface between the backside of the sample and the surrounding medium. When B-scans are executed along both surface coordinates of the sample, the echo can be visualised for the complete sample as a 2D image, called a C-scan, although some depth information is lost. For a detailed description of the method, the reader is referred to the literature, e.g. [204].

US inspection in the form of C-scans is performed after autoclave curing of composite laminates for quality assessment. The laminates are placed in a water bath. The water works as a couplant to minimise signal loss by reflections. For each laminate, three C-scans are generated. These are the defect echo, based on signal attenuation at defects within the material, the backside echo, based on the attenuation of the signal from the backside and the defect depth map that is based on the change of speed of sound at defects. The speed of sound for the material is adjusted via thickness measurements using the US inspection device and comparison with values measured with a sliding calliper. Impact damage in QI specimens after drop weight impact tests as well as the damage state of OHC specimens shortly before and after final failure are evaluated via US inspection using the method described above. A USPC 3040 DAC C-scan system (Dr. Hilger Ingenieurbüro, Germany) with a resolution of 20 MHz and an amplification of up to 106 dB in 0.5 dB steps is used with a STS 10 MHz probe (Karl Deutsch GmbH, Germany). The probe works as a transceiver that can both transmit and receive ultrasound signals. The US-signals are visualised and adjustments regarding the measurements and the speed of sound are set with the software *Hilgus* (Dr. Hilger Ingenieurbüro, Germany).

In interrupted fatigue tests, the influence of a tailored FLG modification on crack density is analysed via radiography by comparing X-ray images of the specimens after the defined loading cycles given in Table 3.2. X-ray analysis is also used to identify the influence of layer thickness on IFF initiation and propagation in interrupted tensile tests of cross-ply specimens and for analysing damage states in OHC and CAI tests. For radiographic

measurements, a HP X-ray cabinet Faxitron Model 43855a (Faxitron Bioptics LLC, USA) with the intensity set to 20 keV is used. Zinc iodide is applied as contrast medium before the measurement to highlight cracks.

Digital image correlation and thermography
The digital image correlation (DIC) system ARAMIS 4M (GOM, Germany) with two cameras is used to ensure no global buckling occurs and to analyse the strain field at the location of the impact in the CAI tests. For DIC measurements, a speckle-pattern is applied on one side of the specimen. The frame rate during the first seconds of the test is set to 2 Hz. For analysing the brittle final failure process, high frequency measurements are necessary for it occurs instantaneously. Therefore, during some tests, final failure is recorded using the ring buffer of the system with a frame rate of 300 Hz.

Passive thermography is carried out for monitoring specimen surface temperature during fatigue tests with an IR NDT system from Automation Technology GmbH. A Flir Photon 615 infrared camera measuring in a spectral band of 7.5 lm to 13.5 lm at a frame rate of 8.33 Hz and with a thermal resolution of 50 mK NEdT at f/1.0 is used. Measurement parameters and recording is facilitated with the Automation Technology software *IrControl*.

3.3.5 Fractography using light microscopy and SEM

The cross section of the unmodified and nanoparticle modified epoxy fibres after failure is analysed for each specimen by using an optical microscope (Olympus BX51) and by scanning electron microscopy to determine the damage mechanisms at the different types of nanoparticles and the influence of particle size, filling degree and morphology on failure initiation and propagation. The fracture surfaces of tailored FLG modified cross-ply specimens are analysed by SEM in order to evaluate the influence of the FLG modification on damage propagation under static and alternating cyclic loading.

In SEM, a focused electron beam is used to scan across the surface of the sample systematically, producing electron signals generated by the electron-specimen interaction. These signals are converted to a visual signal and displayed on a cathode ray tube [217, 218]. All SEM investigations are carried out with a Leo Gemini 1530 electron microscope (Zeiss, Germany) by using the secondary electron (SE2) detector with a working distance between 5 mm and 9 mm. The edges of all samples are prepared with silver conductive paint to minimise charging issues but without the use of sputtering on the failure surface. For the epoxy fibres and the fracture surfaces of neat and FLG modified CFRP specimens,

an acceleration voltage of 1 kV is used. For some CNT modified fibres, a mixture of the SE2 detector with the inLens detector at an acceleration voltage of up to 8 kV is used.

4 Results and Discussion

In this chapter, the results obtained from the experimental campaign are presented and discussed. Sections 4.2, 4.3, and 4.4 deal with the influence of layer thickness in multi-directional composites, whereas in sections 4.5 and 4.6 the influence of a carbon nanoparticle modification of the polymeric matrix in FRP is discussed regarding size effects and damage mechanisms. Firstly, some short comments on quality assessment and reproducibility of the obtained test results are given.

4.1 Quality assessment

The *Hexcel* prepreg system used for producing CFRP specimens for tensile and compression tests is a commercial system used in aircraft industry and thus underlies strict quality control. During cutting and lamination of the prepreg, it is assured that the shelf life is not exceeded to avoid undesired matrix cross-linking at room temperature before curing. All laminates used for the presented tests are autoclave cured with the recommended curing cycle and are thus assumed to be completely cured. US inspection after curing is carried out for all laminates and confirmed that no manufacturing induced defects such as delaminations or voids are present.

For model composites and epoxy matrix fibres, DSC measurements of small samples that underwent the same manufacturing routine as the produced specimens assure complete curing of the matrix and constant and similar specimen quality. The determined glass transition temperature T_g is an indicator for the degree of cross-linking. Incomplete cross-linking leads to inferior mechanical properties of the polymer, because of the smaller amount of atomic bonds between the polymer chains. Via the DSC measurements it is confirmed, that the T_g of all specimens is similar to the value given by the resin manufacturer for complete curing.

The prepreg used for investigating the influence of a tailored FLG modification is produced with a custom made prepreg machine and although the same parameters are used for every

process, differences regarding fibre volume fraction V_f or orientation of the fibres cannot be completely excluded. Therefore, the fibre volume fraction is determined for each laminate as described in chapter 3.3. Similar V_f for each laminate is measured.

4.2 On IFF initiation and propagation in model composites

The findings on IFF initiation and propagation in model composites presented in this section were published in [219]. Crucifix shaped specimens are loaded continuously and damage initiation and propagation is observed in-situ in transmission light microscopy. With the chosen geometry, damage initiates in the centre of the specimen, as already described by Ogihara et.al. [197] and the onset of IFF is observable in the microscope. Characteristic load-displacement diagrams for specimens with as-received and spread rovings are given in Figure 4.1 and Figure 4.2, respectively. The damage development in a representative specimen under the applied static tensile loading at certain characteristic loads is given in the diagrams as well. First IFF occurs at higher loads in the spread-roving specimens. Differences in the damage propagation are observed as well. Referring to Figures 4.1 and 4.2 it is shown, that matrix cracks are smaller and shorter in the spread-roving specimens at a load above 800 N. The load at IFF initiation is noted for each specimen. The results are shown in Figure 4.3, in which the applied load at the first visible matrix crack over the roving width is plotted.

Figure 4.3 shows a clear trend: The load, at which first matrix cracking occurs, increases with increasing roving width. For the specimen made with the rovings as-delivered (roving width $w_{R0} < 3.00\,\text{mm}$), a load at initial matrix cracks of $371\,\text{N} \pm 116\,\text{N}$ is measured. For the specimens containing spread rovings (roving width $w_{RS} > 3.75\,\text{mm}$), the onset of the first matrix crack is shifted to higher external loads of $621\,\text{N} \pm 99\,\text{N}$.

The maximum tensile strength of the tested specimens is $1539\,\text{N} \pm 213\,\text{N}$. No significant influence of roving width on failure strength is observed. Since the maximum tensile strength is dominated by the fibres in 0°-direction, the initiation of matrix cracks has a negligible influence on the load at final failure in the tested configuration. The maximum tensile strength is influenced by several other factors such as possible deviations of the fibres in load direction from the 0°-axis or variations in the manufacturing process. In Figures 4.1 and 4.2, the damage shortly before final failure in representative specimens for rovings with a width below, respectively above 3 mm is shown. Multiple matrix cracks

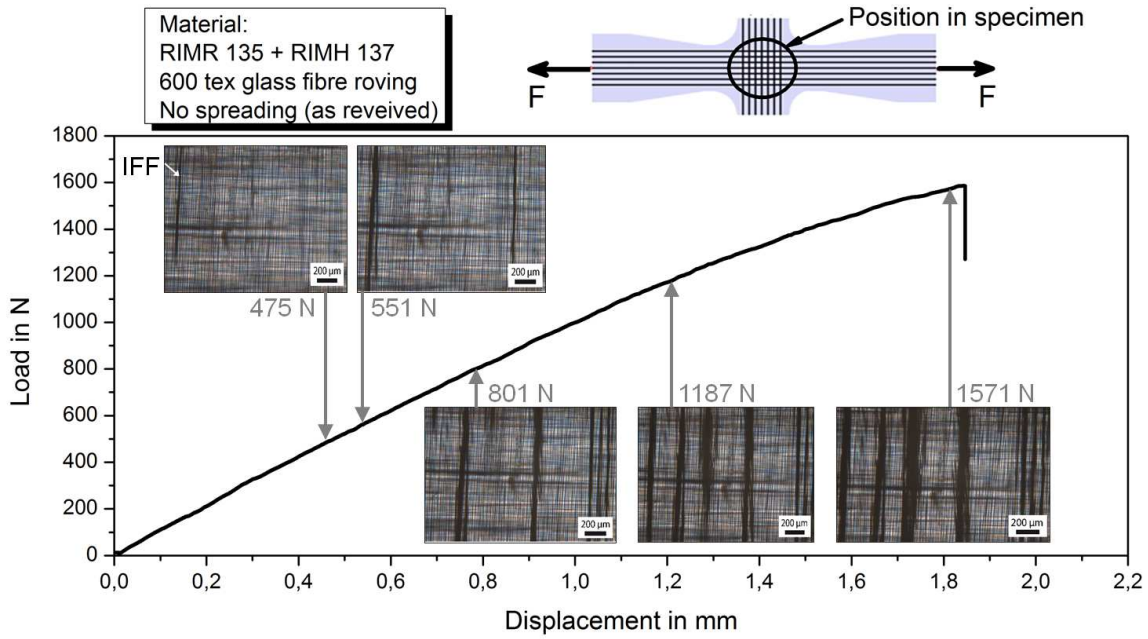

Figure 4.1: Representative load-displacement diagram for a model composite made of 2.50 mm wide rovings (no spreading) with images taken at different stages of damage.

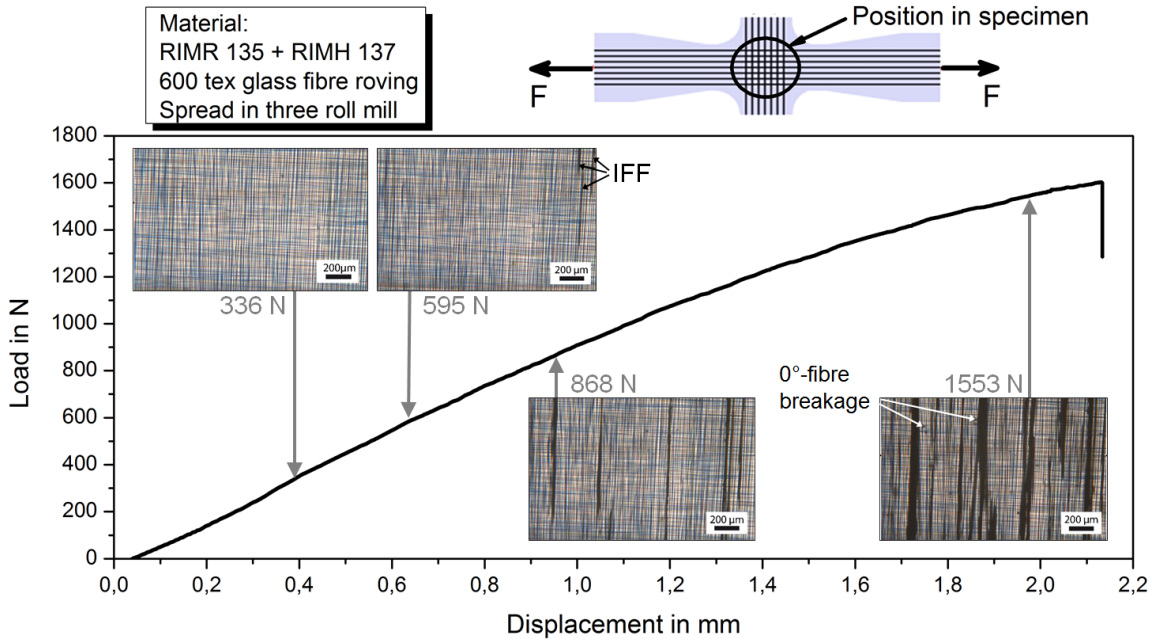

Figure 4.2: Representative load-displacement diagram for a model composite made of 3.85 mm wide spread-rovings with images taken at different stages of damage.

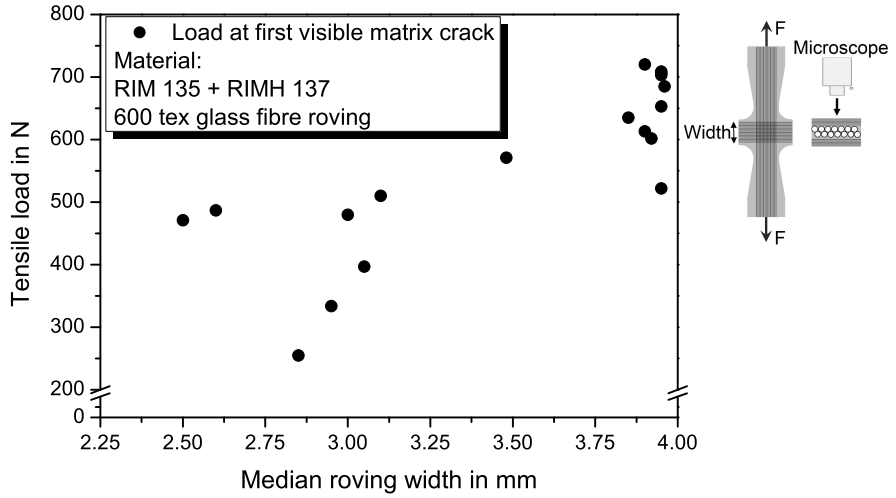

Figure 4.3: Tensile load at first visible matrix crack for (0/90/0) model composites containing glass fibre rovings of different width.

between the fibres in the 90°-direction as well as fibre breakage of 0°-fibres occur. After a saturation in the number of matrix cracks, damage develops firstly as broadening and prolongation of the existing cracks and secondly as fibre breakage. Final failure initiates in a region where a larger amount of 0°-fibres are broken by a crack transverse to loading direction, separating the specimen next to the broadening of the cross section. As this cross section is the smallest due to the specimen geometry, higher stresses per unit area occur and specimens are expected to fail in these regions.

With the spreading of the rovings, the thickness of the fibre layers in model composites is successfully reduced. The advantage of using model composites is, that in the small volume the failure process of the 90°-layer is observable more in detail and in-situ, compared to standard specimen sizes. With decreasing layer thickness, onset of IFF is shifted to higher loads. This is in good agreement with previous investigations on the layer thickness effect from other authors [7, 17, 86, 88, 100, 105]. Despite the fact that the possibility of having a critical defect within the layer is smaller in the thinner layers, the in-situ strength is also an explanation for the observed phenomena. The transverse tensile or shear strength of the 90°-layer between two adjacent 0°-layers is higher for decreasing layer thickness [5, 86–88, 100]. The crack initiation and propagation is restricted by the neighbouring 0°-layers carrying most of the load. More but less severe matrix cracks in the 90°-plies occur with reduced ply thickness. This was shown by other authors by FEM analysis [88, 100] and is confirmed with the experimental results to be valid for model composites as well, allowing for conclusions from model composites to larger scale FRP.

4.3 Influence of layer thickness on damage development in cross-ply laminates

In this section, the experimental results on the influence of 90°-layer thickness on damage development in cross-ply laminates are presented. Figure 4.4 shows representative load-strain curves together with AE amplitude signals plotted over tensile strain for a 90°-layer thickness of $t_{90} = 190\,\mu m$ ($n = 1$) in 4.4a) and $t_{90} = 1900\,\mu m$ ($n = 10$) in 4.4b). Load instead of stress is used to exclude trends resulting just from the geometry of the specimens because of the thickness variation (larger cross-section area with increasing thickness). To avoid AE sensor damage at final failure, the sensors are unmounted shortly before final failure. That is the reason why the amplitude signals end before the load-strain curve. In the tested configurations, no significant influence of 90°-layer thickness on stiffness or tensile strength, both normalised with the thickness of the specimens to exclude geometric influences, is observed. The mean tensile load at failure is $F_{failure} = 28.367\,kN \pm 1.448\,kN$, which is less than 5 % variance for more than 120 tested specimens. The 0°-layers dominate both strength and stiffness and although scaled up by a factor of up to 10, the 90°-layer thickness leads to no significant change regarding final failure.

Nonetheless, differences in damage development and final failure mode are observed. Thinner specimens with $t_{90} = 190\,\mu m$, $t_{90} = 380\,\mu m$ and $t_{90} = 570\,\mu m$ fail in a brittle way with mainly 0°-fibre breakage resulting in a clear fracture crack perpendicular to the loading direction. Specimens with larger 90°-layer thickness ($t_{90} \geq 760\,\mu m$) exhibit a more progressive failure mode with large delaminations and fibre splitting.

AE analysis shows a trend, that damage initiates at lower strains with increasing ply thickness. Initiation of IFF is detectable with the increased amount of high amplitude signals, as shown in Figure 4.4, as well as a significant increase in cumulated energy. For thicker 90°-layers ($t_{90} \geq 570\,\mu m$), a pronounced decrease in the slope of the load-strain curve, also referred to as a "knee" and typical for IFF initiation [55, 220], is observed that correlates with an increase in cumulated energy.

For $n = 10$ 90°-layers, an overflow of the AE acquisition system is often observed, leading to gaps in the acquisition and thus incorrect absolute values. Therefore, the configuration $n = 8$ is used as an example for large 90°-layer thickness regarding interpretation of AE results. First transverse cracks initiate at a strain of approximately 0.15 % for the $[0/90_8/0]$ specimens and at approximately 0.45 % strain for the [0/90/0] specimens.

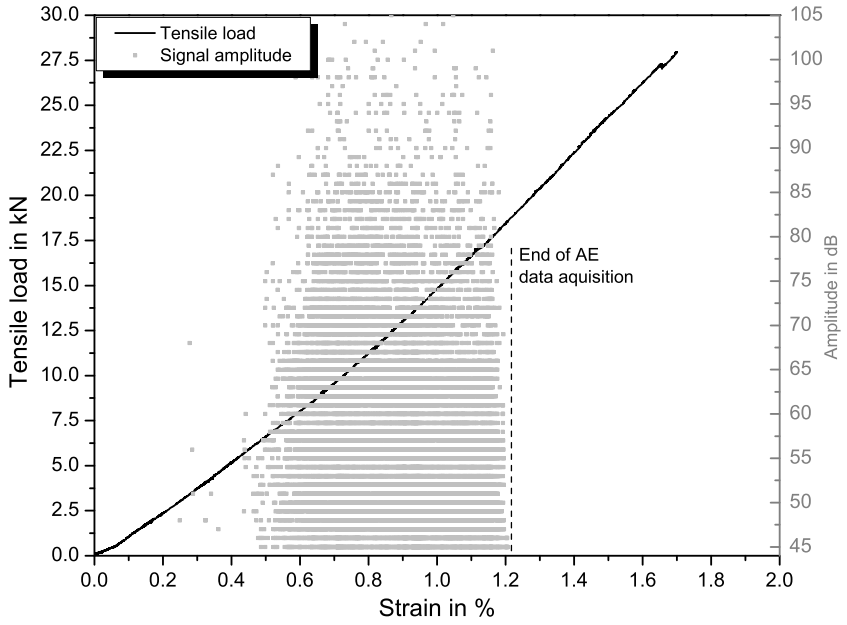

a)

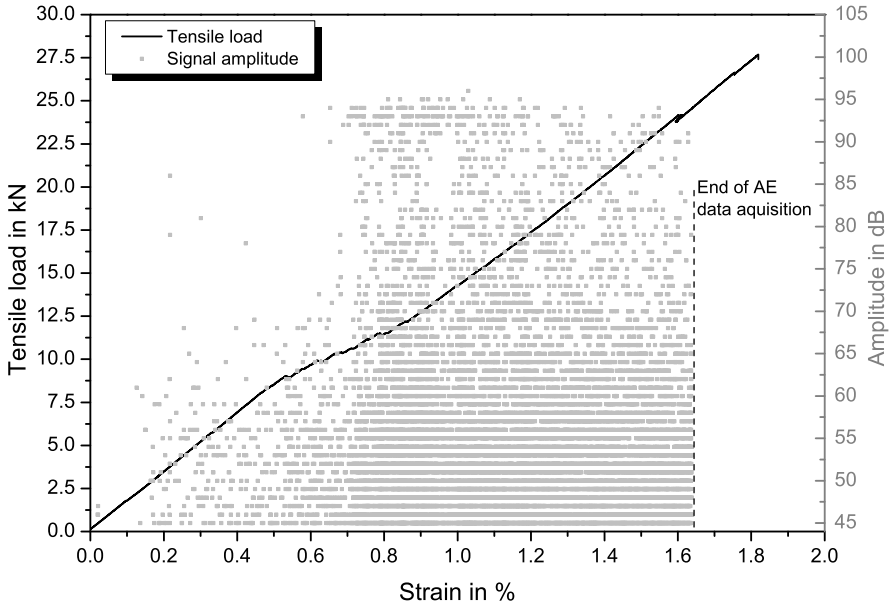

b)

Figure 4.4: Representative load-strain curves and AE amplitude signals over tensile strain for CFRP cross-ply laminates with a) $t_{90} = 190\,\mu m$ ([0/90/0]) and b) $t_{90} = 1900\,\mu m$ ([0/90$_{10}$/0]) 90°-layer thickness (material: HexPly-M21/34%/UD194/T800S).

AE analysis and interrupted tests with radiography show good agreement regarding the strain at failure initiation. Figure 4.5 presents the amount of AE events between the two sensors over specimen length during a tensile test until final failure for $t_{90} = 190\,\mu m$, $t_{90} = 760\,\mu m$ and $t_{90} = 1520\,\mu m$ 90°-layer thickness together with X-ray images of the respective configuration at 1 % strain. One may assume, that thicker specimens generate more events due to the higher amount of material available for cracking, but the contrary is the case, so that a normalisation with the thickness would only increase this effect and is not necessary for explaining the general behaviour. The configurations with t_{90} values between those shown in the diagram confirm the trend of increasing amount of AE events with decreasing layer thickness. The X-ray images (refer to Figure 4.5) show, that cracks perpendicular to loading direction initiate at the edges of the specimen and grow inward. For the [0/90/0] specimen, transverse cracks are highlighted in red in the image for better visibility. Polishing of the edges increases the strain at crack initiation. The higher number of AE events hints toward slower crack propagation through the thickness. A slowly propagating crack generates a higher number of cracking noise, detectable with the sensors, than an instantaneous growing crack, which is assumed to generate just one or two events in AE. This observation agrees well with the X-ray images. With increasing 90°-layer thickness, a change in transverse crack geometry from thin, slowly growing edge cracking for thinner 90°-layer thicknesses ($n = 1, 2$) to broad cracks through the width that grow instantaneous ($n = 8, 10$) is observed. Until 1.0 % strain, no cracks through the width of the laminate are observed for $t_{90} \leq 380\,\mu m$, whereas for $t_{90} \geq 1520\,\mu m$ first cracks penetrating the width are observed at a strain of 0.2 %. These cracks through the width of the specimen have a larger crack opening compared to the edge cracking observed in the thinner specimens. Hence, thicker transverse layers exhibit a more severe damage state at a given external strain.

The total amount of cracks as well as the cracks penetrating the specimen width, counted from X-ray images of representative specimens (refer to Figure 4.5) are presented in Figure 4.6 for the investigated configurations. Cracks are counted at four defined strain levels during interrupted tests. The crack density, transverse cracks per length, as well as the crack length through the width depend on the 90°-layer thickness. The specimens with one 90°-layer have more than twice as many transverse cracks as the thickest specimens with eight or ten 90°-layers at strains between 0.7 % and 1.0 %.

In Table 4.1 the mean cumulated energy at 1 % strain both as absolute value E_{cum} and normalised with the number of 90°-layers E_{cum}/n for representative specimens, the median strain at failure initiation ε_{IFF} as detected with AE analysis and the median values for cumulated hits per layer H_{cum}/n are presented. A contradicting trend is observed for

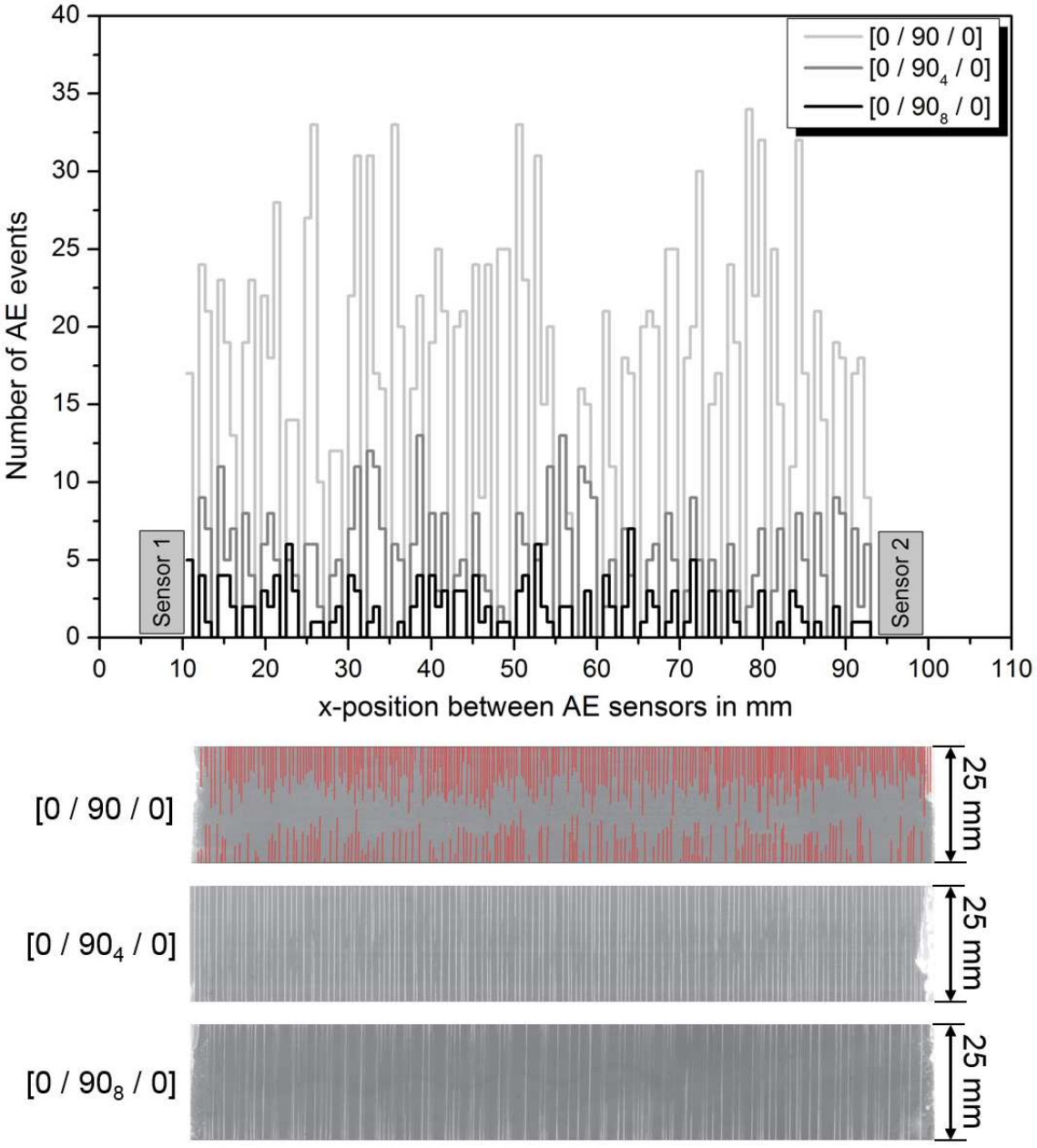

Figure 4.5: Amount AE events over specimen length during a tensile test until final failure for 190 µm, 760 µm and 1520 µm 90°-layer thickness together with X-ray images of the respective configuration at 1 % strain (material: HexPly-M21/34%/UD194/T800S).

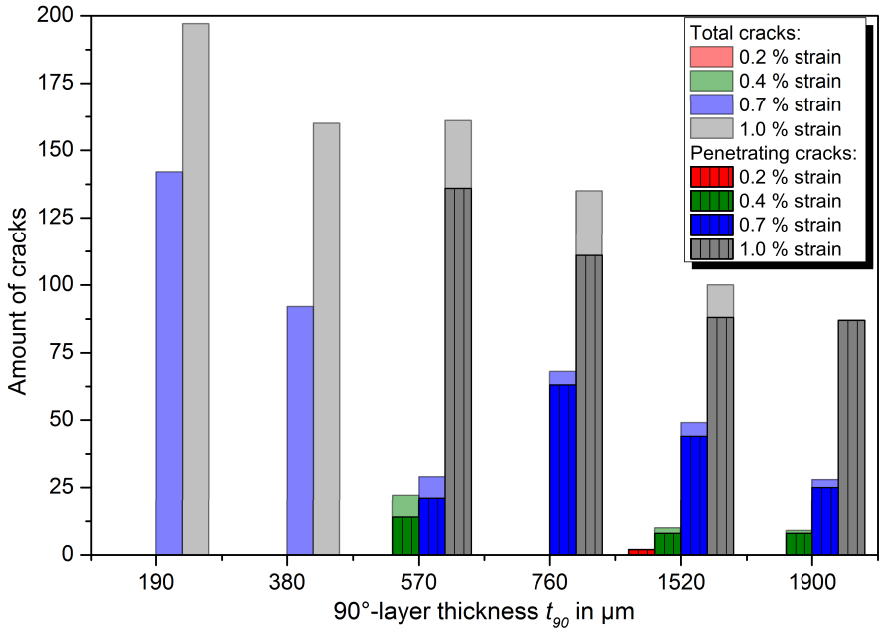

Figure 4.6: Amount of transverse cracks as a function of 90°-layer thickness (material: HexPly-M21/34%/UD194/T800S).

normalised cumulated energy and hits per layer. For a decreasing number of hits per layer, an increase in normalised cumulated energy is observed. Highest values for normalised cumulated energy are measured for $t_{90} = 570\,\mu m$ ($n = 3$ layers) and $t_{90} = 760\,\mu m$ ($n = 4$ layers). The larger crack opening displacement and increased crack height and width, observed for thicker 90°-layers, result in higher energy consumption compared to small, slowly growing cracks. However, the higher amount of comparable large cracks for $n = 3, 4$ layers dissipates the highest amount of energy during crack initiation and propagation, with even higher values compared to the few, but large cracks observed in thicker 90°-layers.

Table 4.1: Acoustic emission results for CFRP cross-ply laminates of varying 90°-layer thickness.

	$[0/90/0]_s$	$[0/90_4/0]_s$	$[0/90_8/0]_s$
E_{cum} at 1 % strain / aJ	$\approx 3.5 \times 10^8$	$\approx 2.5 \times 10^{10}$	$\approx 3.2 \times 10^{10}$
E_{cum}/n at 1 % strain / aJ	$\approx 3.5 \times 10^8$	$\approx 6.25 \times 10^9$	$\approx 4.0 \times 10^9$
H_{cum}/n at 1 % strain	3231.3	1063.0	2256.2
ε_{IFF} / %	0.48	0.39	0.16

In contrast to these results, a significant change in tensile strength with decreasing ply thickness is reported in literature for thin-ply laminates with a ply thickness below 50 µm [7, 17]. With the 90°-layer thickness between 190 µm and 1900 µm, the speci-

mens tested here are in the region of conventional prepreg laminates. The mechanisms being beneficial in thin-ply laminates, such as the increased in-situ strength [86, 87], do not apply for the tested configurations. Comparing results for thin-ply laminates with the results for large ply thicknesses, size effects due to a volume increase based on the weakest link theory [84, 221] can be excluded as the only explanation for the strength increase of thin-ply laminates. Tensile strength of these laminates is determined by the 0°-layers and can only be significantly increased with thin-plies. However, as is shown here, tensile strength does not decrease when increasing the thickness further, which may be of relevance when regarding thick laminates as for example used in wind turbine industry.

Damage initiates in cross-ply laminates at lower strains with increasing layer thickness. This is the case for a broad range of 90°-layer thickness from 20 µm up to 1900 µm when considering as well the findings reported in literature [5, 7, 17, 100]. It is valid for both the initiation of inter-fibre fracture at the free edges and the penetration of the 90°-layer width. With an FEM approach it could be shown, that transverse crack initiation and propagation in thickness direction follows the same trend of slower growing and less broad cracks for reduced 90°-layer thickness [222]. The crack density and crack growth rate depend on layer thickness. The observed change of crack distance with lower distance for thinner layers can be explained by the stress redistribution at a crack through the thickness, which is a function of layer thickness, as predicted by different analytical models [35, 55, 223–227] and shown via simulation [94, 100, 228] and experimental methods [55, 56, 223, 225]. No further reduction in strain at damage initiation for layer thickness $t_{90} > 1520$ µm is observed. The 90°-ply strength without the enclosing 0°-layers is the lower limiting value for transverse crack initiation and presumably reached in the experiments for the large thicknesses. For thicker layers, the positive influence of stiffer surrounding layers (in situ effect) diminishes. From the larger crack opening, resulting in broader cracks with increasing layer thickness, it is clear, that not only damage initiation but also damage propagation and crack geometry depend strongly on the 90°-layer thickness. A reduction of layer thickness increases the resistance against IFF and thus offer great potential for increased fatigue lifetime.

AE analysis results for strain at crack initiation show good agreement with X-ray images in interrupted tests up to defined strain levels. In addition, it could be shown that differences in transverse crack propagation rate are detectable by evaluating the amount of AE events, if a set-up with adequate location of events between two sensors is used. Therefore, with carefully chosen parameters, the damage state inside a cross-ply laminate can be well monitored by using AE analysis.

4.4 Influence of layer thickness and stacking sequence on FRP compressive properties regarding stress intensifications

The influence of layer thickness under compressive loading with stress intensifications being present in the laminate is investigated in OHC and CAI tests for four different QI layups. OHC tests offer the advantage, that the exact shape of the stress intensification as well as the stress state is well known. CAI tests are executed to compare the OHC results to a different type of stress intensifications and for analysing the influence of layer thickness on damage propagation after an initial damage. UNC tests are carried out for comparison as a reference. Furthermore, the influence of the 0°-layer position with regard to damage initiation and the resulting mechanical properties is examined. Most of the results were published in [216].

4.4.1 Impact damage

Impact damage is evaluated by comparing the mechanical behaviour after impact, the projected damage area as well as delamination areas in the interfaces between the layers. Figure 4.7 shows the average force-time curves for the four configurations at an impact event. The first load drop, referred to as the beginning of irreversible damage and deformation [50, 229], is identical at approx. 4300 N force after 0.2 ms after the impactor hitting the surface. The further slope of the curve depends on the layer thickness. Thinner layers (sublaminate scaled) exhibit a steeper increase with a maximum impact force of 8300 N, compared to 7800 N for the ply-block scaled laminate, but a shorter contact time of 1.9 ms compared to 2.2 ms. The induced energy during the impact event is calculated by integrating the respective force-time curve and multiplication with the measured speed of the impactor above the specimen. The results of the impact tests are summarised in Table 4.2. In addition, the projected damage areas given by the outer damage shape as well as the delamiantion areas, defined as the sum of all delamination are given. Both are measured from the backside echo of the US C-scans taken after the impact event. For the laminates with sublaminate-scaled stacking sequence, shorter contact time and higher maximum contact force are measured, indicating towards a higher stiffness in thickness direction and against bending during the impact event. Despite the slightly higher induced energy during the impact event, the projected damage area is significantly smaller ($\approx -65\%$) compared to ply-block scaled specimens.

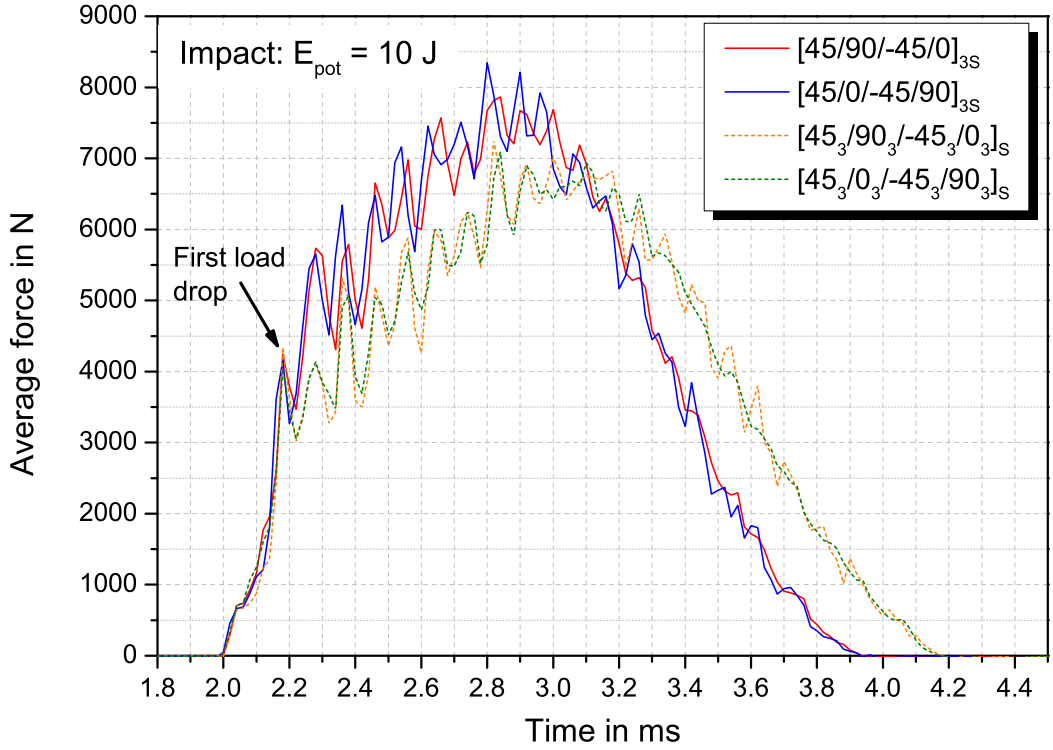

Figure 4.7: Average force-time curves during the impact event of the tested configurations (material: HexPly-M21/34%/UD194/T800S).

Table 4.2: Results of impact test for CFRP (HexPly-M21/34%/UD194/T800S).

	$[45/0/-45/90]_{3s}$	$[45_3/0_3/-45_3/90_3]_s$	$[45/90/-45/0]_{3s}$	$[45_3/90_3/-45_3/0_3]_s$
Contact time / ms	1.90 ± 0.02	2.14 ± 0.05	1.92 ± 0.02	2.16 ± 0.03
Max. contact force / N	8552 ± 104	7292 ± 111	8217 ± 240	7484 ± 323
Induced energy / J	5.48 ± 0.20	4.92 ± 0.64	5.21 ± 0.32	5.15 ± 0.35
Delamination area / mm^2	510 ± 80	792 ± 148	493 ± 29	822 ± 112
Damage area / mm^2	650 ± 79	1894 ± 129	646 ± 26	1937 ± 46

The higher resistance against a low velocity impact damage with decreasing layer thickness, visible in the smaller projected damage area for sublaminate scaled specimens, can be explained by the higher number of interfaces available for delamination. Induced energy at the impact is dissipated mostly by matrix cracking and delamination damage. For a sublaminate scaling in the tested configuration, the delamination damage is distributed over 22 interfaces in the pine-tree shape, typical for impact damage in FRP (refer to Figure 2.2). This is in accordance with the findings from other researchers on the development of damage mechanisms in QI CFRP laminates leading to CAI failure [120]. For the investigated ply-block scaled specimens only six interfaces between layers of different fibre orientation are available for delamination. As the induced energy is in the same range, it is dissipated by larger delaminations, in contrast to a higher number of smaller size delaminations, with increasing layer thickness. Due to the measuring principle, only the projected damage area and not the sum over all delaminated areas can be measured in the US C-scan analysis. This results in the significantly higher projected delamination area for the ply-block scaled specimens. The total summation of delamination area over all interfaces is assumed to be of equal size for both configurations because the induced energies are similar and the matrix properties that determine the resistance against delamination crack propagation are the same. Similar findings are reported for thin-ply laminates compared to laminates with conventional ply thickness [17, 19]. Reducing the ply thickness can thus improve the impact resistance of composite parts.

4.4.2 Compression tests

Linear stress-strain behaviour is observed until shortly before final failure in UNC and OHC tests. Figure 4.8 shows representative OHC stress-strain curves together with AE amplitude signals and cumulated energy plotted over compressive strain for both, sublaminate (Figure 4.8a)) and ply-block (Figure 4.8b)) scaled specimens. For UNC, similar behaviour is observed. A slight decrease of the stress-strain curve slope is simultaneous to an increase in high amplitude AE-signals, indicating the beginning of severe damage. For ply-block scaled specimens this damage initiation occurs at lower strains compared to the sublaminate scaled configuration. Sublaminate scaled specimens fail in a brittle way, whereas a more progressive failure with a higher amount of matrix cracks and delaminations before rupture is observed for ply-block scaled specimens. This difference in damage development is detectable via the AE amplitude signals. In sublaminate scaled specimens, AE-signals with amplitudes higher than 80 dB are detected only shortly before final failure (at about 0.75 % strain), whereas for ply-block scaled specimens amplitudes

higher than 80 dB are measured starting between 0.4 % and 0.6 % strain. Amplitudes equal to or higher than 80 dB correspond well with a significant increase of cumulated energy. The slope of the cumulated energy curves exhibit a sudden increase at the end of the test for sublaminate scaled and a continuous increase after approx. 0.5 % strain for ply-block scaled specimens, confirming the more progressive failure behaviour of the latter. Results from UNC, OHC and CAI tests in terms of compressive strength and strain at initiation of severe damage ε_{init} (detected with AE analysis) are summarised in Table 4.3. With DIC measurements, the buckling behaviour in the impact region is analysed. Buckling in Table 4.3 is defined as the maximum local out-of-plane extension of the specimen surface at the impact region. Within similar layer thickness, specimens with outer 0°-layers are more prone to buckle in the impact region. Ply-block scaled specimens exhibit larger amount of buckling, especially for outer 0°-plies.

Table 4.3: Test results from UNC, OHC and CAI tests. Strain at initiation of severe damage ε_{init} is defined as the strain value at which first AE-signals with amplitudes $>$ 80 dB occur and E_{cum} exhibits a significant increase.

	$[45/0/-45/90]_{3s}$	$[45_3/0_3/-45_3/90_3]_s$	$[45/90/-45/0]_{3s}$	$[45_3/90_3/-45_3/0_3]_s$
UNC strength / MPa	681 ± 27	533 ± 68	640 ± 23	564 ± 35
UNC ε_{init} / %	≈ 1.40	≈ 0.70	≈ 1.60	≈ 0.80
OHC strength / MPa	362 ± 7	336 ± 16	399 ± 10	488 ± 31
OHC ε_{init} / %	≈ 0.70	≈ 0.60	≈ 0.77	≈ 0.50
CAI strength / MPa	296 ± 11	204 ± 9	313 ± 12	296 ± 27
Buckling / mm	0.31 ± 0.12	2.68 ± 0.60	0.26 ± 0.10	0.34 ± 0.18

The size of the respective delamination areas between the layers after the impact event and the fibre orientation next to the largest delamination are critical for compression after impact properties of FRP. A larger delamination area results in a weakening of the laminate against compression in general and a smaller support of the 0°-layers in particular, due to the delamination crack opening being mode I dominated in compression. The 0°-layers carry most of the load if oriented in loading direction but are prone to kinking and buckling. Analogues to an Euler buckling column, higher thickness increases the resistance against kinking [230]. Hence, the higher layer thickness of ply-block scaled specimens contributes to higher CAI strength. To minimise fibre kinking and global buckling, the 0°-layers should be supported against it by surrounding layers of different fibre orientation. Less supported 0°-layers are more prone to buckle. This explains the larger buckling, measured with the DIC, for ply-block scaled laminates with outer 0°-plies compared to inner 0°-plies. The latter are better supported by the higher amount of surrounding layers and thus less prone to buckling. Moreover, the influence of the 0°-layer position, with inner 0°-layer exhibiting higher CAI strength, can be explained with the pine-tree delamination shape.

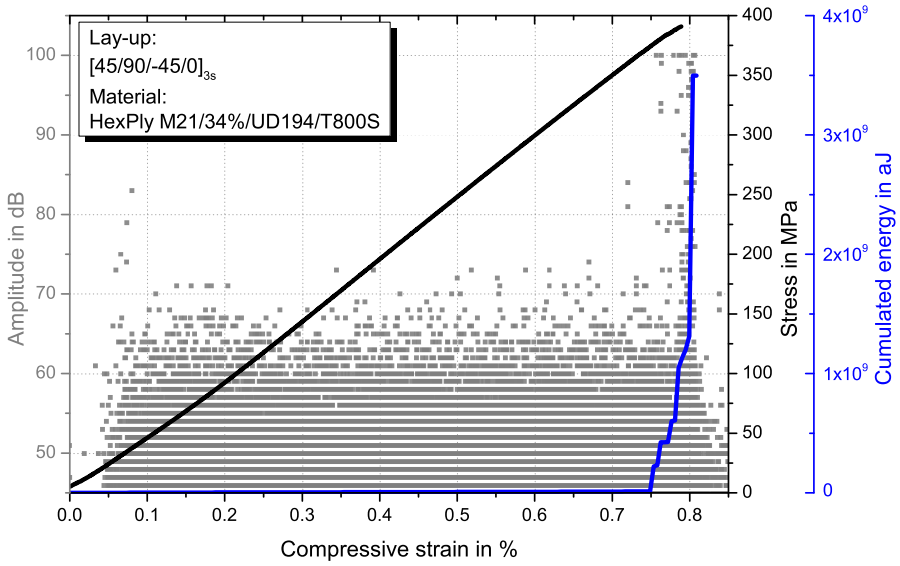

a)

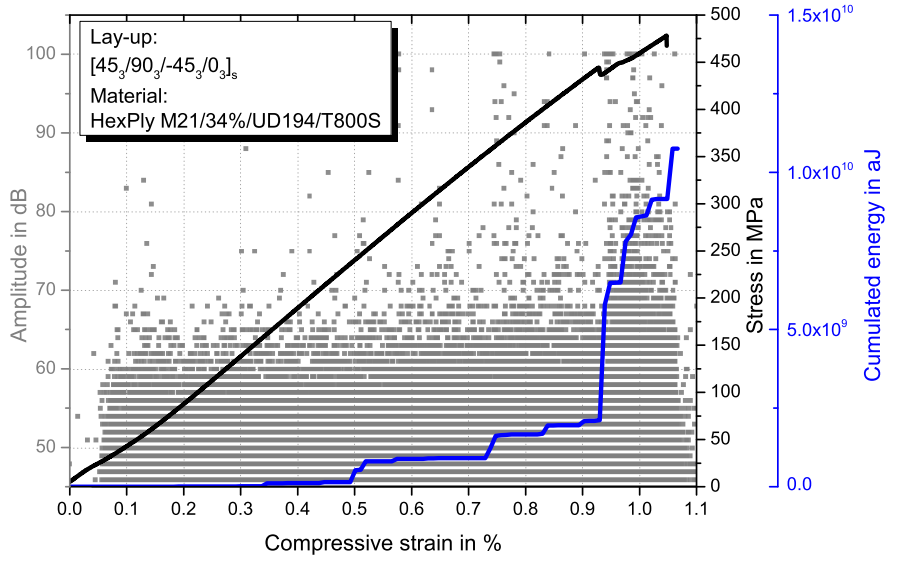

b)

Figure 4.8: Representative OHC stress-strain curves, AE amplitude signals and cumulated energy over compressive strain for sublaminate a) and ply-block b) scaled specimens.

Outer 0°-layers at the back side sublaminate from the impact position are not supported over a large delamination area compared to inner 0°-layers. The unsupported length of the sublaminate increases due to delamination growth [120]. Consequently, specimens with larger delaminations exhibit lower resistance against global buckling, resulting in lower CAI strength with increasing delamination areas between the outer 0°-layers.

The strain at damage initiation depends on layer thickness. Thicker layers exhibit damage onset at lower strains and a more progressive failure behaviour. In the UNC tests, a clear influence of layer thickness on compressive strength is observable. Increasing layer thickness results in lower compression strength. The ply-thickness effect is more dominant than any influence of the stacking sequence. The position of the 0°-layers has no significant influence for the ply-block case, where standard deviations overlap for specimens with inner and outer 0°-layers. For sublaminate scaling, higher UNC strength values are measured for specimens with inner 0°-layers.

In OHC tests however, the position of the 0°-layers has a significant influence on the mechanical properties. Specimens with the 0°-layers inside exhibit higher OHC strength, with the highest value for the ply-block scaled configuration where all 0°-plies are concentrated in one thick layer in the centre of the specimen around the neutral plane ($[45_3/90_3/-45_3/0_3]_s$).

In Figure 4.9, the damage initiation at the hole is compared by C-scan back-wall echo and X-ray images taken in interrupted tests. The specimens are tested until shortly before final failure and the test is stopped at the first significant increase in high-amplitude AE signals at approx. 0.7 % strain. Matrix cracking initiates at the hole due to the high local stress concentration. For further details on crack initiation at the hole see [216]. The layer thickness determines the orientation of IFF at the hole. IFF in sublaminate scaled specimens (thinner layers) occurs first in the 90°-layer transverse to loading direction whereas in the ply-block scaled specimens, it occurs first in the 0°-layers in loading direction. Similar behaviour is observed for initial delaminations starting at the hole. They are oriented perpendicular to loading direction for sublaminate scaled and in loading direction for ply-block scaled specimens.

Regarding final failure, UNC specimens mostly fail in the gauge area between the tabs by a splitting type of damage accompanied by delaminations. Ply-block scaled specimens show larger delaminations at final failure, which corresponds to the progressive failure process with increased delamination growth before final failure, as it was observed and detected with AE analysis. A kink-band can be visually identified at the line of splitting.

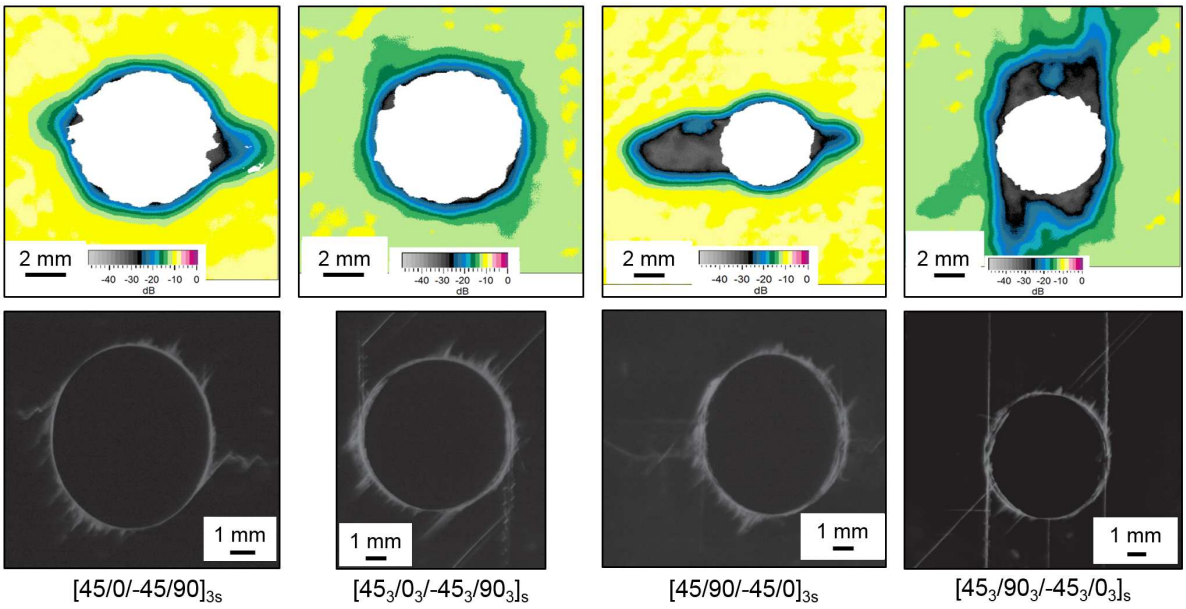

Figure 4.9: C-scan back-wall echo and X-ray images of failure initiation at approx. 0.7 % strain for representative OHC specimens (material: HexPly-M21/34%/UD194/T800S).

Few specimens fail under the end tabs or by splitting at the upper edge where the load is introduced by the test machine, but these are not regarded for the results.

All OHC specimens failed in the centre of the gauge area with a visible kink-band originating from the hole. Final failure of all CAI specimens originates at the impact damage. In both tests, ply block scaled specimens exhibit larger delamination damage than sublaminate scaled specimens at failure. X-ray images taken after final failure for representative OHC and CAI specimens of the four configurations are presented in Figure 4.10. Final failure initiates at the stress intensification, i.e. the hole or the impact damage, and is perpendicular to loading direction. For the sublaminate scaled specimens final failure occurs as brittle fracture in the 90°-direction in a broad, split crack through the stress intensification that spans the width of the specimen. The stacking sequence or the shape of the stress intensification, cut out hole with clear sharp edges versus blunt impact damage, has no visible influence on final compressive failure. For thick layers, the perpendicular crack broadens before leading to final failure, as can be seen in the images for the ply-block scaled specimens. Fracture is not strictly perpendicular to loading direction. Delamination and cracking fracture propagates at an angle of 45° from the stress intensification and then changes its orientation to 90° with regard to loading direction. In addition, larger delaminations are visible compared to the specimens with thinner layers.

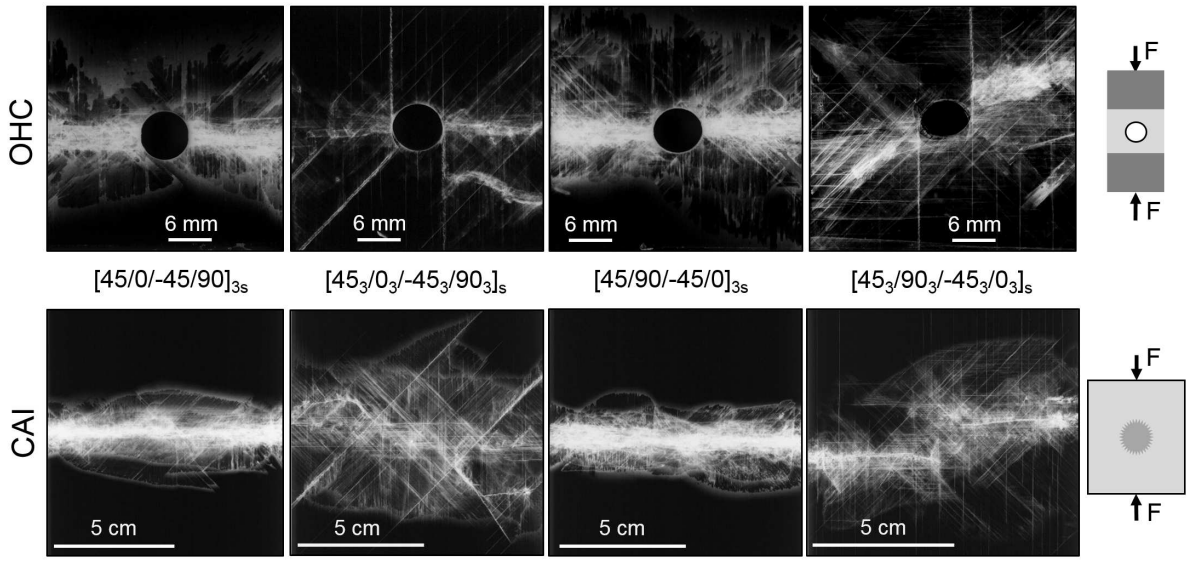

Figure 4.10: X-ray images of final failure for representative OHC (top row) and CAI (bottom row) specimens (material: HexPly-M21/34%/UD194/T800S).

Compression failure in FRP in general is dominated by the matrix properties [24]. All specimens are produced from the same prepreg system to exclude this influence. The damage onset at lower strains with increasing layer thickness, observed in UNC and OHC tests, is in accordance with results from literature for compressive [65] and tensile behaviour [7, 17] of QI CFRP laminates. The higher UNC strength for sublaminate scaled specimens with inner 0°-layers can be attributed to a better support of the load bearing 0°-layers by adjacent plies, leading to a delay of the onset of microbuckling and the resulting kink-band initiation and rupture. This implies, that out-of-plane microbuckling is the dominating mechanisms for inner 0°-layers. This effect is more pronounced when a stress intensification is present. Here, the stacking sequence has a higher impact on strength than the layer thickness. Accordingly, inner 0°-layers result in higher OHC and CAI strength for constant ply thickness.

In Figure 4.11 the OHC and CAI strength with regard to the influence of ply thickness and stacking sequence (0°-layer position) are compared. The highest OHC strength and comparably high CAI strength are measured for the configuration with one central 0°-layer consisting of six plies and surrounded by all other layers. It has to be mentioned, that this configuration would results in lower bending stiffness and strength compared to the other configurations investigated. But in the OHC case the surrounding layers support the load bearing 0°-layers the most, resulting in the highest measured OHC strength values. Regarding CAI strength, specimens with distributed plies exhibit similar

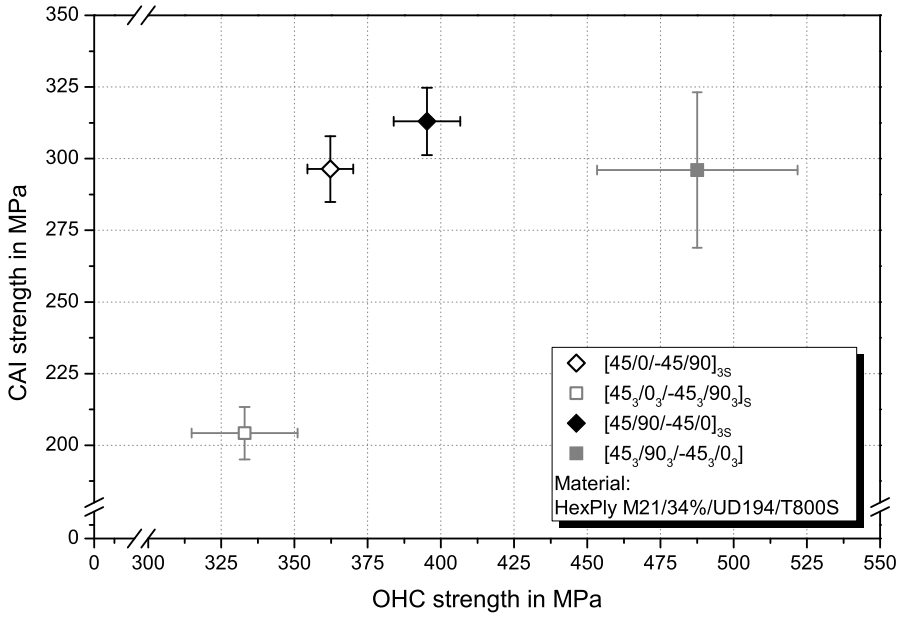

Figure 4.11: Comparison of CAI strength and OHC strength for the investigated configurations.

or higher strength values than this configuration, which can be attributed to the smaller delamination between the layers after the impact event.

An open hole or impact damage reduces the bending resistance and has therefore a negative influence on global buckling. Central 0°-layers increase the bending resistance under compression and show higher OHC strength. For CAI properties, central 0°-layers are advantageous because of the conic delamination damage shape resulting from a low velocity impact with the largest delaminations at the backside from the impact surface. The delamination area at the load carrying 0°-layers should be preferably small so that these layers should be arranged in the centre of a laminate. However, for flexural bending load cases, outer 0°-layers are an optimum. Regarding the 0°-layer position, a trade-off between bending and compression strength has thus to be made, whereas for the CAI case, a trade-off between delamination area and support of the 0°-layers has to be made.

Considering these results, decreasing the ply thickness down to thin-ply laminates ($t_{ply} \leq 50\,\mu m$) may not be the optimum in laminates with stress intensifications under pure compression loading. Further investigations with thin-ply laminates might be necessary to verify these findings with thinner layers, because a positive influence of a ply thickness below 50 µm is reported in literature [7, 17, 19]. However, if the main loads of a composite part are compressive loads, the part is badly designed anyhow, so that a design only against a compressive load case is rarely applicable. Considering the more realistic design

case of mostly tensile or bending loading with a compressive load part, a sublaminate scaled lay-up is most suited to fulfil these design loads.

OHC failure process depends on layer thickness, whereas the stacking sequence has no significant influence. Failure originates at the free edge of the hole in all tests and is perpendicular to loading direction in the 90°-direction for the ply-block scaled and in 0°-direction parallel to loading direction for the sublaminate scaled laminates. This can be explained by the difference in transverse contraction. Sublaminate scaled laminates with thinner layers fail brittle at comparable high strains whereas ply-block scaled laminates exhibit a damage process that initiates at lower strains and is more continuous and thus less brittle. Less brittle materials have a lower notch sensitivity, because early 0°-layer fibre matrix splitting in the ply-block scaled laminates acts as notch blunting mechanism at the free edge [114]. Although a more progressive failure process might be advantageous in some materials, as it may result in the possibility to take measures for repair of replacement of the damaged part, a damage initiation at lower strains is mostly not acceptable for FRP as first ply failure is often a design criterion.

4.5 Influence of carbon nanoparticle modification on strength of epoxy regarding size effects

In this chapter, the influence of nanoparticle morphology and filler content in polymer nanocomposites on the mechanical properties in small elongated volumes with regard to size effects is investigated. Most of the results were published in [195, 231]. With an experimental approach representing small volumes, as they are present between the fibres in FRP, the most promising particle morphologies for improving mechanical properties are discussed and the influence of specimen volume and nanoparticle modification on true failure strength is shown. It is analysed whether or not a size effect for nanoparticle modified epoxy exists and how the nanoparticle morphology influences the mechanical properties in small volumes. These results are presented in the following section 4.5.1. With this approach, the failure initiation as well as local failure mechanisms at the nanoparticles can be identified in detail for different nanoparticle morphologies in the small fracture surfaces. The influence on mechanical properties is discussed by comparing the different energy dissipating damage mechanisms at the nanoparticles, in dependence of their respective morphology. The results from the fractography analysis are given in section 4.5.2. The influence of nanoparticle morphology on the damage process in small volumes is discussed in section 4.5.3.

4.5.1 Size effect of carbon nanoparticle modified epoxy

Representative load-displacement curves for neat epoxy as well as with FLG nanoparticles modified dog-bone and fibre specimens are presented in Figure 4.12. Load-displacement instead of stress-strain curves are given for better comparability among the specimens, because in the case of the fibres, necking is visible during the test and has to be accounted for. The diagram for the fibres in Figure 4.12a) shows an increased elongation at break for the neat specimen in contrast to the comparable brittle failure of the FLG modified fibres. For this diameter range, maximum load of the neat matrix is significantly ($\approx 50\,\%$) higher. For larger fibre diameters however, maximum load can be in the same range for neat and modified fibres, as is shown in Figure 4.12b), in which representative load-displacement curves for a larger fibre diameter are given. For the dog-bone specimens (refer to Figure 4.12c)), a similar trend regarding the elongation is observed. The neat matrix exhibits higher ultimate strain. Nonetheless, maximum stress and failure stress are higher for the FLG modified specimens. The FLG modification shows the highest influence on tensile strength of dog-bone specimens, whereas CNT or CB modified dog-bone specimens behave similar to the unmodified ones. These results are summarised in Table 4.4 and discussed later in this chapter. The influence of nanoparticle morphology on the load-displacement behaviour is shown in Figure 4.13, in which representative load-displacement curves for fibre diameters of $150\,\mu m \pm 25\,\mu m$ are given. Thicker fibres exhibit higher failure loads, as expected. The FLG modified fibres exhibit the shortest elongation at break, which hints to a hindering of the polymer to deform plastically and develop necked areas due to the comparable large FLG particles. CNT modified fibres have slightly lower elongation at break compared to the unmodified ones, but show slightly higher maximum load values for similar fibre diameter. The CB modified fibres behave very similar to the unmodified ones. Thus it is concluded, that the small CB nanoparticles have no significant influence on the load versus displacement and accordingly stress-strain behaviour of an epoxy matrix. With the force at failure and the cross section after failure, the true failure strength R_t is calculated as described in section 3.3.1.

Figure 4.14 shows the true failure strength R_t for the unmodified (neat) fibres and dog-bone specimens as a function of specimen volume. The median value for failure stress of the dog-bone specimens is independent of their volume $R_t = 61\,\text{MPa} \pm 7\,\text{MPa}$, which is in the typical range for the used matrix system. According to the data sheet, the strength is in the range of 60 MPa to 75 MPa. The unmodified epoxy shows a clear size effect. A decrease in volume leads to a significant increase in true failure strength, with an improvement of up to 237 % for the thinnest $22\,\mu m$ fibre ($R_t = 209\,\text{MPa}$) compared to the dog-bone specimens. The median value with standard deviation of true failure

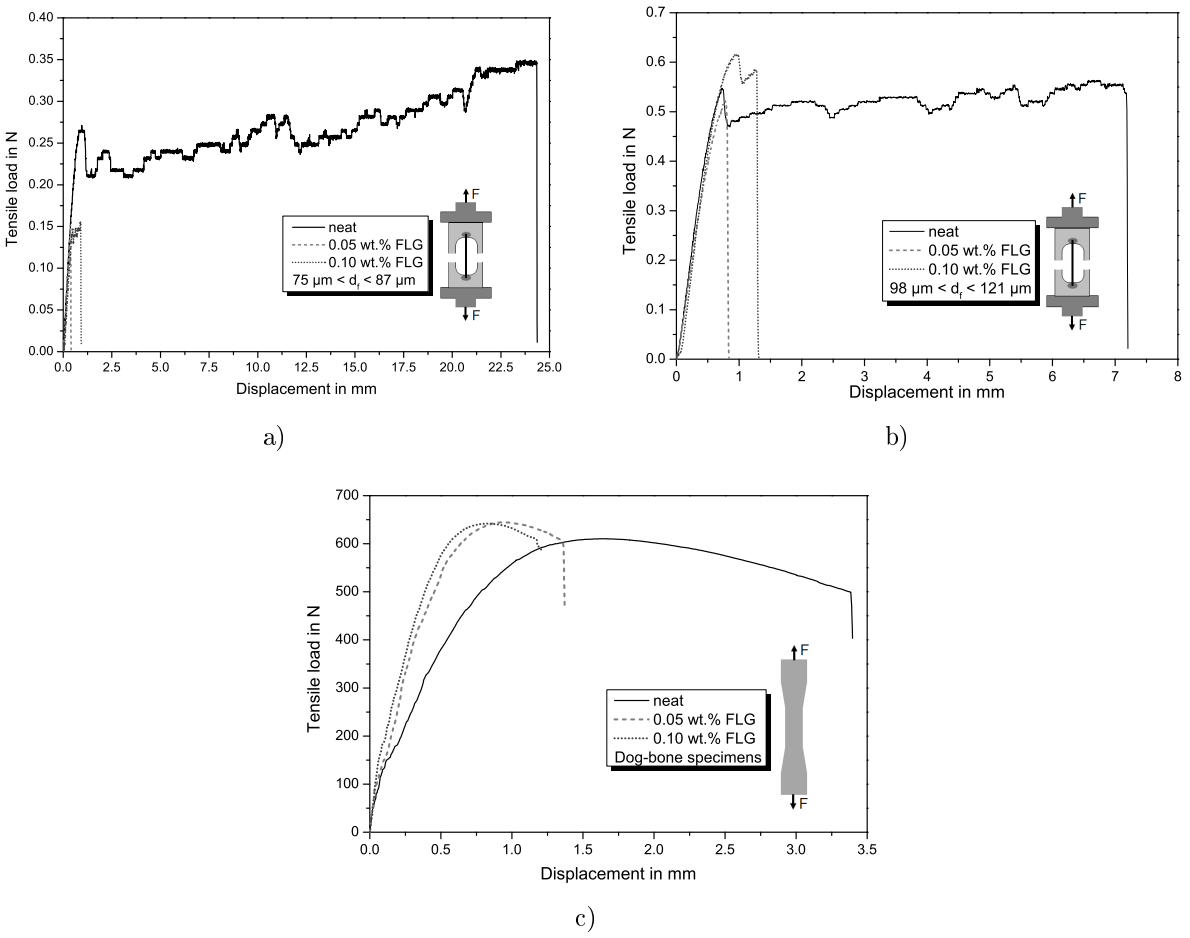

Figure 4.12: Representative load-displacement curves from tensile tests for:
a) Neat and FLG modified fibres of comparable diameter between 75 µm and 87 µm,
b) Neat and FLG modified fibres of comparable diameter between 98 µm and 121 µm,
c) Neat and FLG modified dog-bone specimens.

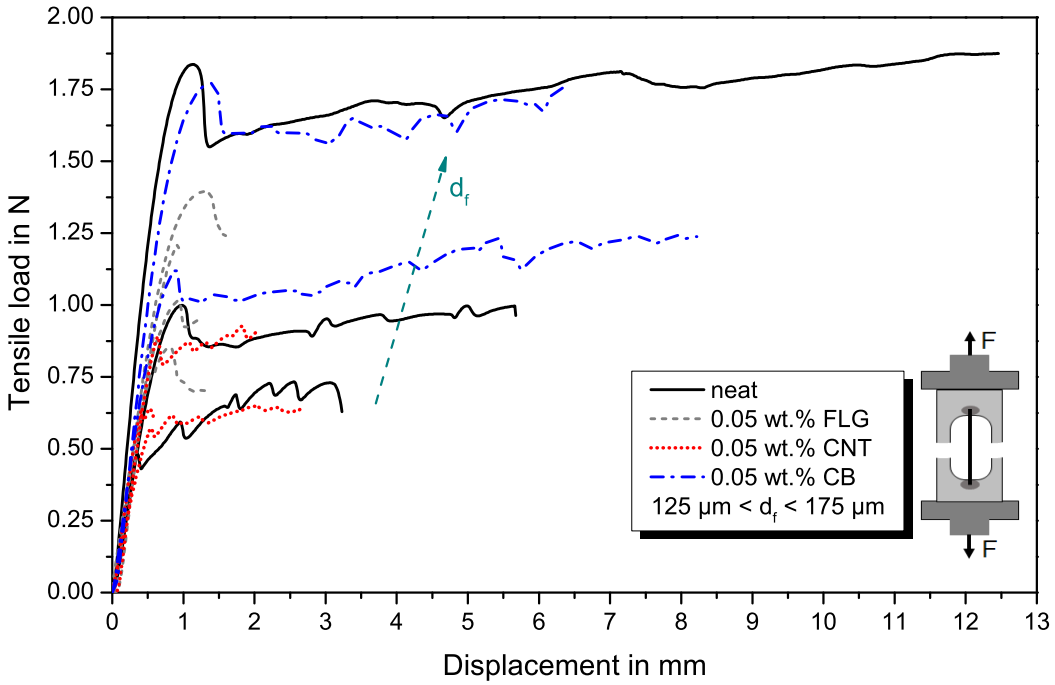

Figure 4.13: Representative load-displacement curves for neat and carbon nanoparticle modified fibres of comparable diameter between 125 µm and 175 µm.

strength for the fibrous specimens is $R_t = 119\,\text{MPa} \pm 38\,\text{MPa}$, which is approx. 95 % higher than that of the dog-bone specimens. Even the lowest strength values for the fibres are approximately 20 MPa higher than those of the dog-bone specimens. The large scatter for fibrous specimens is attributed to the statistical defect distribution and the manual manufacturing process. The cross-head speed seems to have no influence on the true failure strength for dog-bone specimens, because all values lay in the same range independent of the testing speed (refer to Figure 4.14, dog-bone specimens tested at 25 mm/min are marked with open symbols). One specimen tested at 25 mm/min exhibits a slightly higher R_t value, but this is attributed to manufacturing quality rather than cross-head speed.

The clear size effect of the neat matrix is in accordance with the theory of defect distribution that results in an increased strength with decreasing volume, as observed for the rupture of solids and brittle materials [62, 84, 221]. The strength for a brittle material under uniform stress is dominated by the largest defect, the so called "weakest link". Defects are randomly distributed so that larger volumes have a higher probability of containing larger defects that result in lower strength. The size effect in solids with

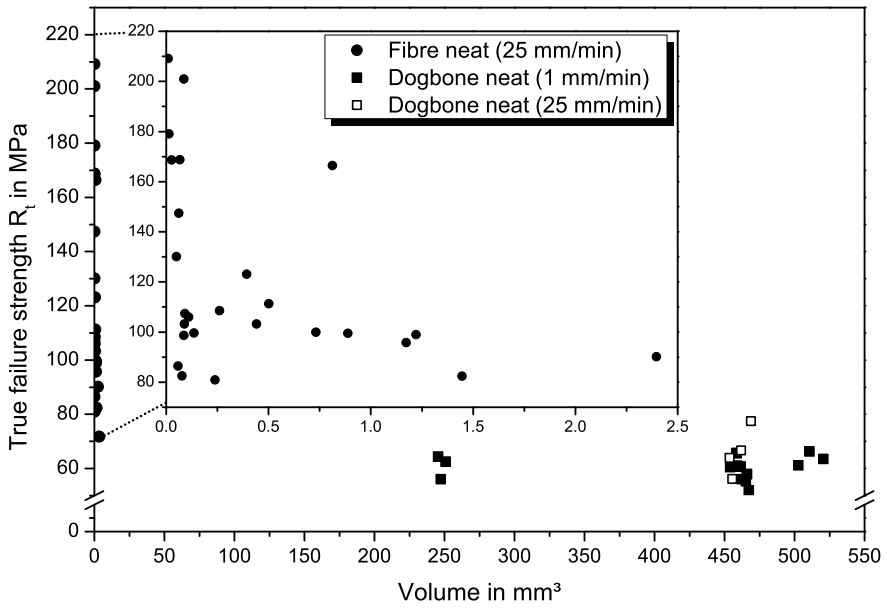

Figure 4.14: True tensile failure strength R_t versus gauge volume V for neat epoxy matrix system.

probability $P_i(\sigma)$ and critical stress σ_c as a function of the stress σ is described according to Weibull's theory of defect distribution with equation 4.1 [84]:

$$P_i(\sigma) = 1 - \exp(-\left(\frac{\sigma}{\sigma_c}\right)^m) \tag{4.1}$$

Where m is the Weibull-modulus. Figure 4.15 shows the size effect in a Weibull weak-link-scaling (WLS) diagram for the used epoxy, in which the minimum values for true failure strength are plotted against volume on a log-log scale. The curve through these values to determine the Weibull-modulus m for the strength minima should be a straight line with a slope of $-1/m$. A Weibull modulus of $m = 0.17$ is calculated. In order to compare the tensile strengths $\sigma_{t,1}$ and $\sigma_{t,2}$ of two different volumes V_1 and V_2 equation 4.2 is used.

$$\frac{\sigma_{t,1}}{\sigma_{t,2}} = \left(\frac{V_1}{V_2}\right)^{-\frac{1}{m}} \tag{4.2}$$

Besides Weibull's theory, the Griffith criterion for the strength of a brittle material [62] can be applied as an analytical approach for estimating failure stress. According to this theory, the strength depends on flaws in the material. With an energy based criterion,

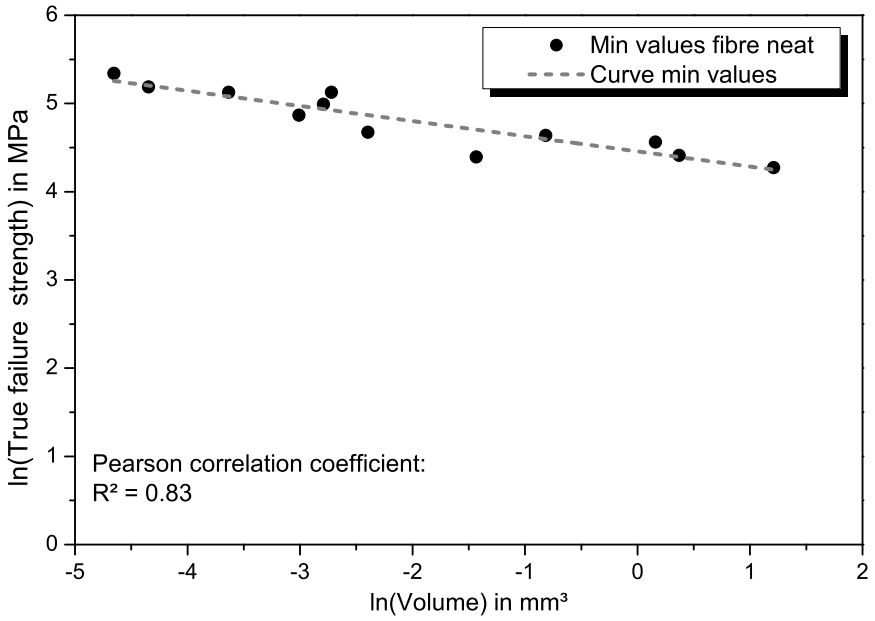

Figure 4.15: Weibull weak link scaling diagram ($m = 0.17$).

the ultimate strength σ_{ult} of a material can be approximately calculated with its stress intensity factor $K_{\mathrm{I},c}$ according to the following equation 4.3 [36, 62]:

$$\sigma_{ult} = \frac{K_{\mathrm{I},c}}{\sqrt{\pi \cdot d_f}} \tag{4.3}$$

Where d_f is the diameter of the fibre in the case at hand.
The maximum strength of a material is the theoretical strength σ_{th}, which is based on the separation of atomic bonds and thus the energy that is necessary to create a new fracture surface. It can be calculated with equation 4.4 [63]:

$$\sigma_{th} = \sqrt{\frac{E \cdot G_0}{2h_p}} \tag{4.4}$$

Where G_0 is the energy required to create a new fracture surface, h_p is the separation of the atomic planes, and E is the Young's modulus of the material. For most solids the theoretical strength is $\sigma_{th} \approx E/10$ [63]. The measured strength values are lower than $E/10$ because of the presence of flaws. For plastic materials a theoretical strength of $E/30$ is derived, which is also postulated and applied as a lower bound for brittle ceramics [232, 233].

In Figure 4.16 the statistical (Weibull) or analytical (Griffith) approaches to determine the strength of a brittle material in dependency of its volume are shown together with the experimental results for the neat epoxy. A fracture toughness of $K_{\mathrm{Ic}} = 1.51\,\mathrm{MPa} \cdot \sqrt{\mathrm{m}}$ for the used matrix system is experimentally determined in SENB tests according to ASTM D 5045 [167] and used to plot the line. True tensile strength is plotted versus diameter in a ln-ln diagram. The theoretical strength, here assumed as $E/10$ [63], is shown in this diagram as well. For larger volumes, the experimental data is in good accordance with Weibull's theory of defect distribution, whereas for smaller volumes, as in the fibres, Griffith's failure criterion shows better agreement. For reaching the theoretical strength $E/10$, the volume of the fibres is still too large. Flaws can be found in every fracture surface, so that the theoretical strength cannot be reached. The highest measured strength values are higher than $E/30$, hence this approximation for theoretical strength is not meaningful for epoxy matrix systems. With the presented approach, the strength to volume relation for polymers is described by different scaling laws and experimentally confirmed. It can be shown, that different scaling laws are valid for a polymer, depending on the range of specimen volume. Bauer et al. [233] presented this behaviour for ceramics on the nanoscale. Their investigations for nanoscale ceramics show, that when decreasing the volume further down, strength values are close or equal to the theoretical strength of the material [234] in compression or push to pull tension tests [233, 234].

For nanoparticle modified epoxy, test results regarding the influence of specimen volume as well as nanoparticle morphology and filling content on true failure strength are presented in the following. Figure 4.17 shows the true failure strength R_t for neat and with 0.05 wt.% carbon nanoparticles modified epoxy as a function of specimen volume. Values obtained in tests with dog-bone specimens are given for comparison representing larger volumes. The experimentally measured values for true failure strength of the dog-bone specimens are summarised in Table 4.4. Slightly higher R_t values (+10 %) are observed for some FLG modified specimens, but since the other values are within the standard deviation for all configurations, the positive influence is small. Despite this, no significant influence of a carbon nanoparticle modification on true failure strength is observed at this volume. This can be attributed to the comparably low filling content. Other studies report an increase of tensile strength with a higher filling content of 0.1 wt.% for different types of graphene based nanoparticles such as graphene platelets [157], graphene oxide [159] or mechanically exfoliated graphene [235]. For 0.05 wt.% FLG modification used here, the mechanical properties of the matrix dominate and hence no significant improvement in tensile strength is observed.

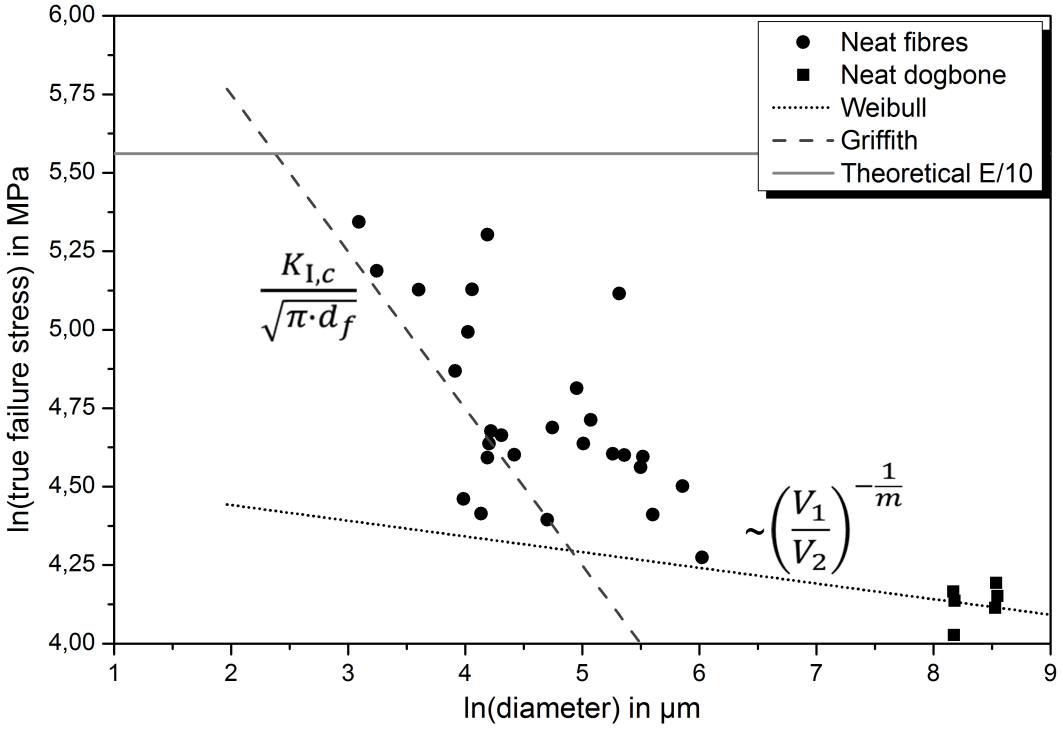

Figure 4.16: Comparison of different analytical and statistical approaches for determining the size effect in polymers with experimental results.

Table 4.4: True tensile strength of unmodified and with 0.05 wt.% carbon nanoparticle modified dog-bone specimens.

Specimen	**True failure strength / MPa**
Unmodified	61.1 ± 6.5
CB modified	58.2 ± 2.6
CNT modified	60.2 ± 5.0
FLG modified	64.7 ± 7.1

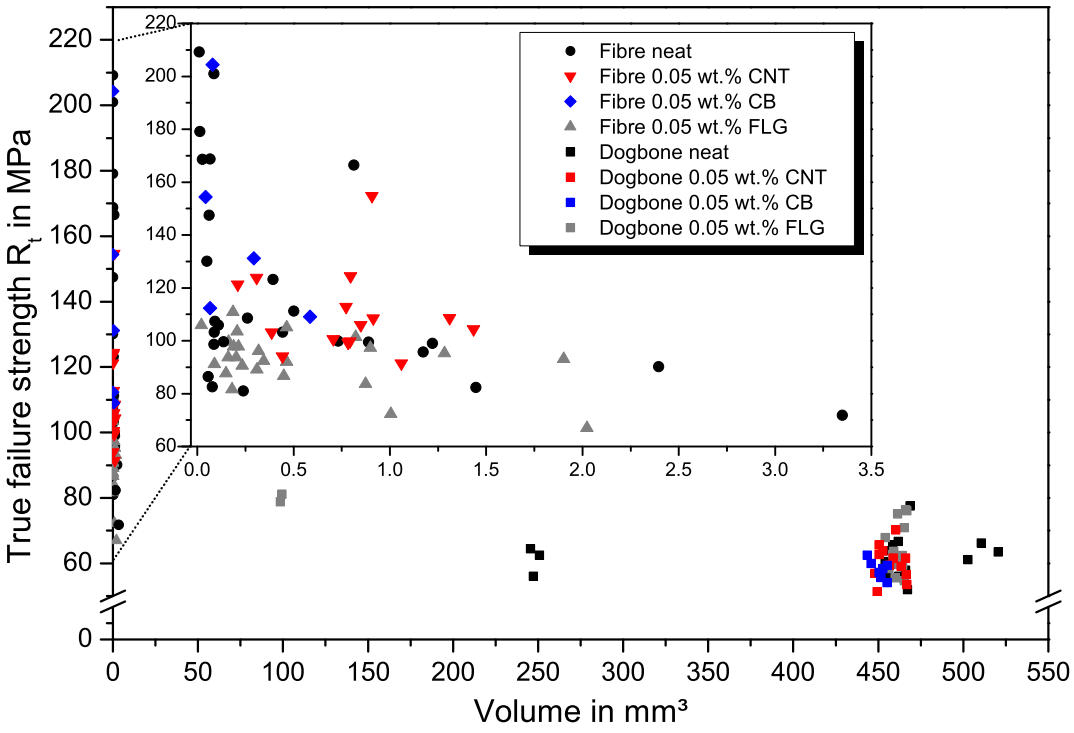

Figure 4.17: True failure strength versus specimen volume for neat and with carbon nanoparticles modified epoxy showing the influence of nanoparticle morphology at 0.05 wt.% particle concentration. The enlargement shows values for fibre specimens

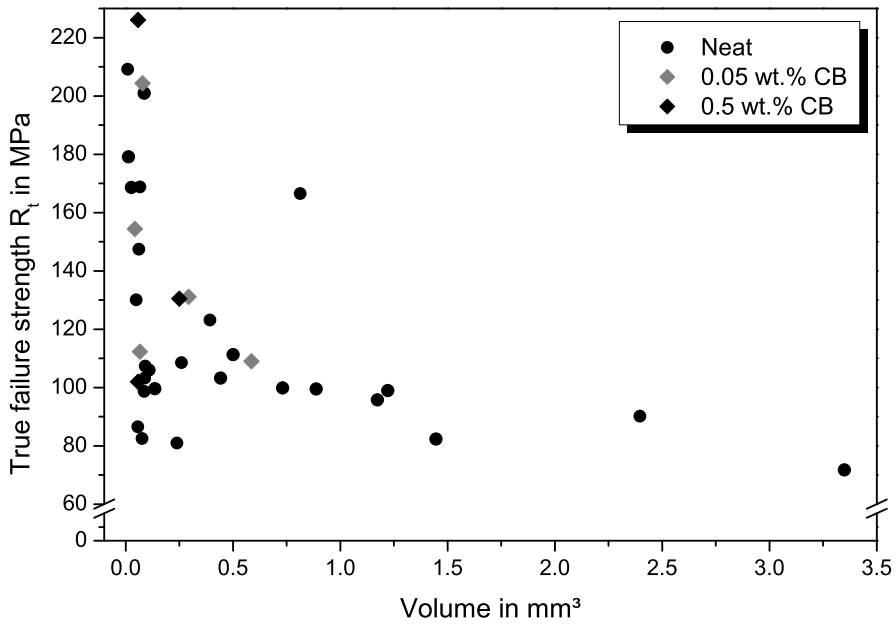

Figure 4.18: True failure strength versus specimen volume for neat and with CB modified epoxy fibres showing the influence of nanoparticle filling content.

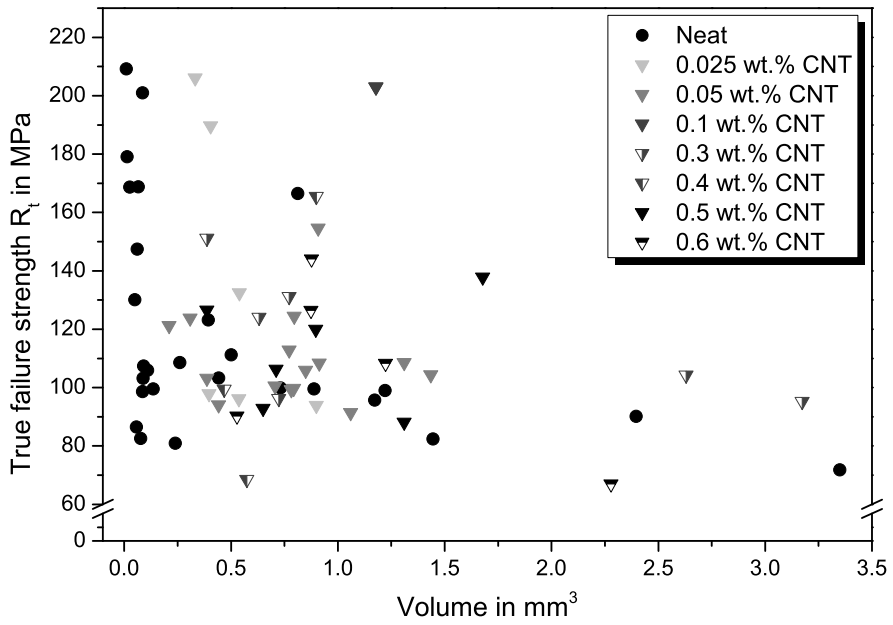

Figure 4.19: True failure strength versus specimen volume for neat and with CNT modified epoxy fibres showing the influence of nanoparticle filling content.

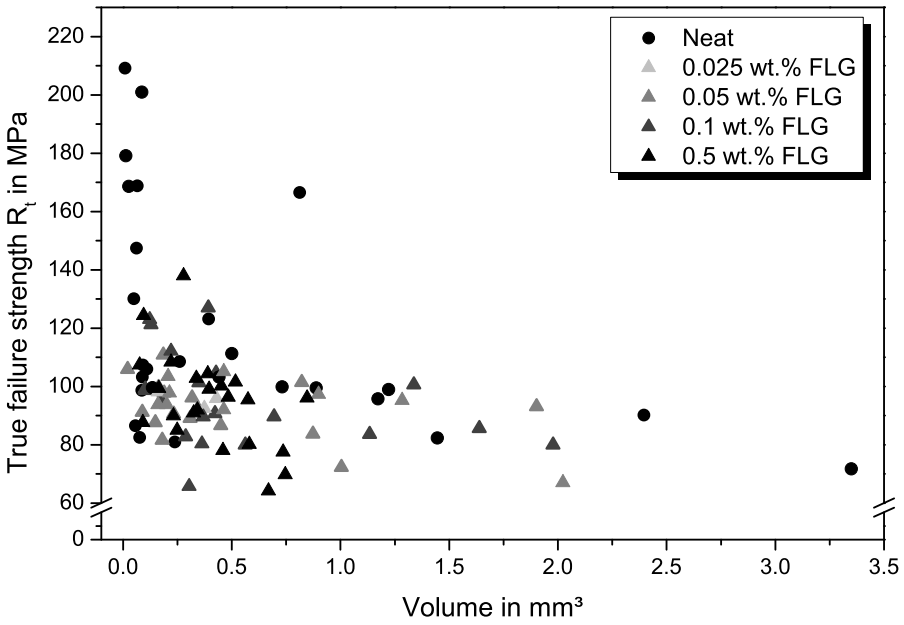

Figure 4.20: True failure strength versus specimen volume for neat and with FLG modified epoxy fibres showing the influence of nanoparticle filling content.

In the enlargement in Figure 4.17, true failure strength versus specimen volume only for the fibrous specimens is plotted for better visualisation of the strength behaviour for small volumes. Strength values exhibit a size effect for neat epoxy and a limitation in true failure strength at approximately 110 MPa for fibres modified with 0.05 wt.% FLG. The CB modified epoxy exhibits a clear size effect, comparable to the neat material. For small volumes, an increase in true failure strength of approximately 100 MPa is observed. In comparison to the neat epoxy fibres, the CNT modified fibres exhibit slightly higher true failure strength at similar volume. One CNT fibre with volume of $V = 0.91\,\mathrm{mm}^3$ exhibits a high true failure strength of $R_t = 154.7\,\mathrm{MPa}$ for the comparable high volume. The fracture surface of this fibre is further examined in fractography in section 4.5.2 to identify possible reasons for this behaviour (refer to Figure 4.23). For a CNT content of 0.05 wt.%, no significant size effect is visible, but for lower particle content, increasing strength with decreasing volume and therefore a clear size effect is observed as well (refer to Figure 4.19).

The influence of nanoparticle volume fraction with regard to true failure strength is shown in Figure 4.18 for CB, in Figure 4.19 for CNT and in Figure 4.20 for FLG modified fibres. For CB modified epoxy, configurations with 0.05 wt.% and 0.5 wt.% nanoparticle content are investigated. No influence of nanoparticle weight content on true failure strength of the specimens is observed in this range of filling content. Although the number of tested specimens for this type of modification is comparably small, especially for 0.5 wt.% (3 specimens), the highest value of all specimens for true failure strength of $R_t = 226\,\mathrm{MPa}$ is measured at a volume of $V = 0.06\,\mathrm{mm}^3$. The lowest R_t value of this modification is measured for a specimen with similar volume, which is comparable to the behaviour of neat epoxy fibres. The unmodified specimens also exhibit large scatter at low volumes due to the statistical distribution of defects owing to the fact, that only the largest defect initiates final failure. The similar behaviour of neat epoxy and CB modified epoxy is explained with failure initiation at surface defects that is observed in SEM images for both types. A larger defect results in lower true failure strength. This is analysed in detail in section 4.5.2.

A broad range in filling content of CNT modified epoxy is tested from 0.025 wt.% to 0.6 wt.%. For the CNT modification values of true failure strength in the range of 200 MPa are observed for the lowest filling content of 0.025 wt.% CNT and for one fibre with 0.1 wt.%. This indicates that with lower filling content, a size effect for CNT modified epoxy exists as well. Failure initiation is analysed more in detail by fractography analysis of the fracture surfaces described in section 4.5.2. It should be highlighted, that the highest strength values of $R_t \approx 200\,\mathrm{MPa}$ for CNT modified epoxy are in the range

of the maximum values for the neat epoxy, but for specimens with significantly higher volume. Furthermore, most CNT modified fibres exhibit higher R_t values compared to the unmodified resin at similar volume for all investigated filling contents. This implies that despite of a size effect, the CNT modification has a positive influence on tensile failure strength.

For FLG modified epoxy, the true failure strength of the fibres is only slightly higher (max. 25 %) compared to the dog-bone specimens. The FLG modified matrix system shows only a small size effect, with a slight increase in strength with decreasing volume. When compared to the high increase for the neat epoxy, the maximum failure strength for the FLG modified epoxy seems to be limited, even in very small volumes. These results implicate, that the nanoparticle modification may act as an enhancement in larger volume, such as it is observed with the slightly higher R_t values of the FLG modified dog-bone specimens and reported in literature [157, 159, 235], but initiate failure and thus weaken the material in very small volumes regarding the true failure strength. No significant influence of the amount of nanoparticles in the matrix is found. Most values for true failure strength are between 60 MPa and 110 MPa. For higher FLG filler content, R_t values rise up to 130 MPa for 0.1 wt.% FLG and 140 MPa for 0.5 wt.% FLG. Hence, only a small increase in R_t but no significant size effect when compared to neat or CB modified epoxy is observed. This is attributed to failure initiation at the largest FLG particle or aggregate, which is larger than any material defects, thus always available within the fibre and independent of specimen volume. As a consequence, true failure strength of FLG modified epoxy depends on two factors. Firstly, the size of the largest FLG particle that initiates failure and secondly, the orientation of this particle with regard to loading direction. This will be analysed more in detail by SEM of the fracture surfaces (refer to section 4.5.2).

4.5.2 Influence of nanoparticle morphology on failure initiation and local damage mechanisms

The fracture surfaces of the fibres after tensile testing are analysed by SEM with regard to failure initiation and damage mechanisms at the nanoparticles. Figure 4.21 shows the fracture surfaces of four representative fibres of different diameter d_f and thus volume V, that failed at the stress given in the caption of the figure. Fracture surfaces are smooth. The crack may nonetheless propagate at different heights, as it is visible in Figures 4.21b) and 4.21d).

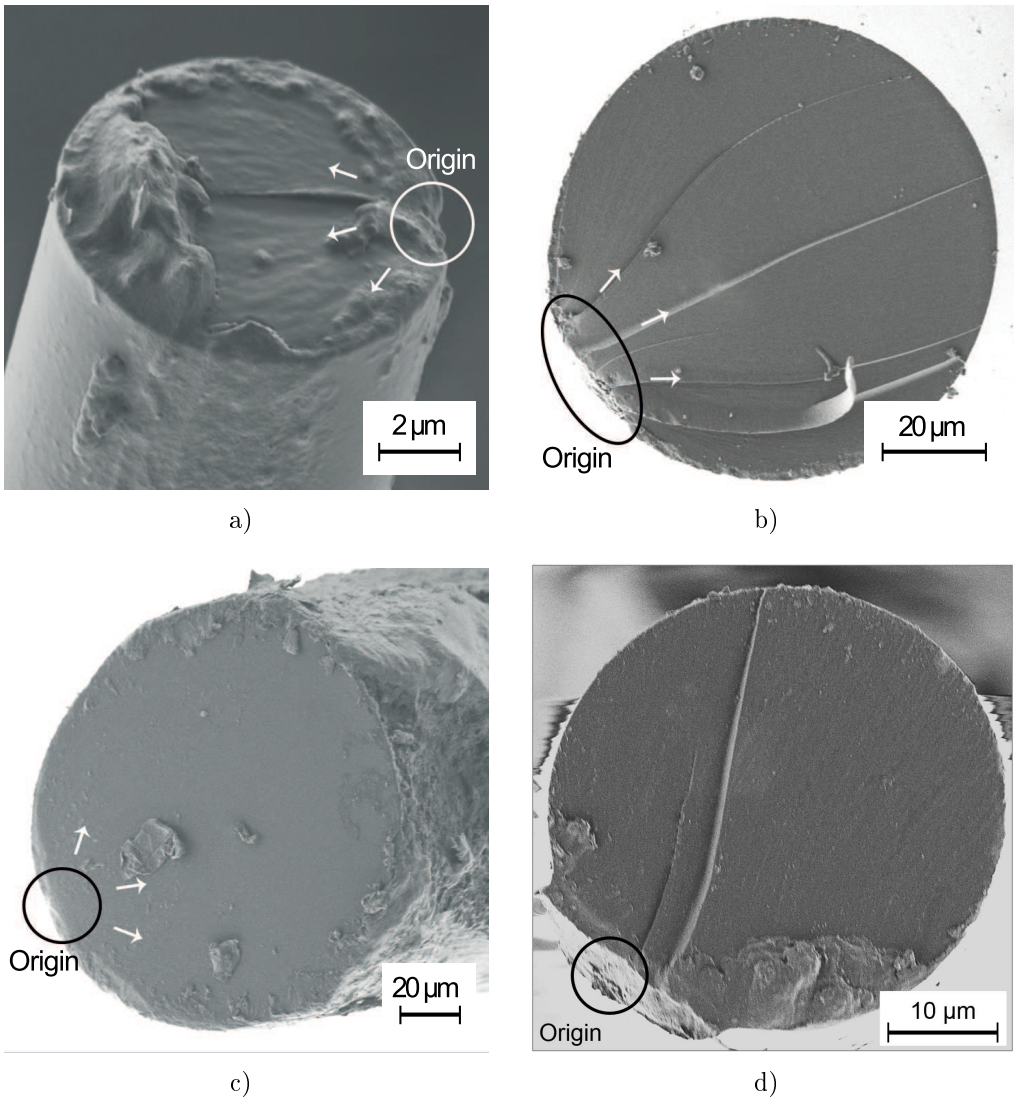

Figure 4.21: SEM images of the fracture surface of unmodified matrix fibres of different volume V:
a) Fibre with volume $V = 0.01\,\mathrm{mm}^3$ ($d_f = 22\,\mu\mathrm{m}$), $R_t = 209\,\mathrm{MPa}$
b) Fibre with volume $V = 0.24\,\mathrm{mm}^3$ ($d_f = 110\,\mu\mathrm{m}$), $R_t = 81\,\mathrm{MPa}$
c) Fibre with volume $V = 0.81\,\mathrm{mm}^3$ ($d_f = 203\,\mu\mathrm{m}$), $R_t = 167\,\mathrm{MPa}$
d) Fibre with volume $V = 0.09\,\mathrm{mm}^3$ ($d_f = 66\,\mu\mathrm{m}$), $R_t = 201\,\mathrm{MPa}$.

The origin of failure, in these cases the flaw from which failure initiates, is marked in the pictures. Final failure initiates at surface defects in all unmodified fibres, with the defect size being critical for stress at failure. Since no rest lines are visible in the fracture surface, the crack growth rate is almost constant. The fibre in Figure 4.21a) has a very small volume and contains a very small surface defect and thus exhibits the highest failure stress. This is similar for the fibre shown in Figure 4.21d), for which a small surface defect is identified within a region of plastic deformation at failure at the fibre edge. For the fibre shown in Figure 4.21b), a larger defect results in a comparable low failure stress, which is even lower than that of the fibre shown in Figure 4.21c), although the latter one has a larger volume. But as can be seen in Figure 4.21c), the surface area defect is smaller, than that of the fibre in Figure 4.21b) containing a surface defect nearly twice as large. This is attributed to the manufacturing process, during which the size of flaws varies statistically, so that fibres of larger volume may as well contain a small defect. But in general, a trend of decreasing defect size with decreasing volume is observed. Therefore, these results are in good agreement with the theory of a statistical defect distribution [84] and the fractography results confirm the R_t versus volume behaviour described in section 4.5.1.

A representative fracture surface of a with 0.5 wt.% CB modified epoxy fibre is shown in Figure 4.22. Failure initiates at a surface defect that is larger than the nanoparticles or small CB agglomerates visible in the fracture surface. The fracture surface is rougher compared to that of neat epoxy, which indicates a potential for fracture toughness increase. Crack separation and crack propagation at different heights are visible and may act as energy dissipating damage mechanism at the globular shaped CB nanoparticles.

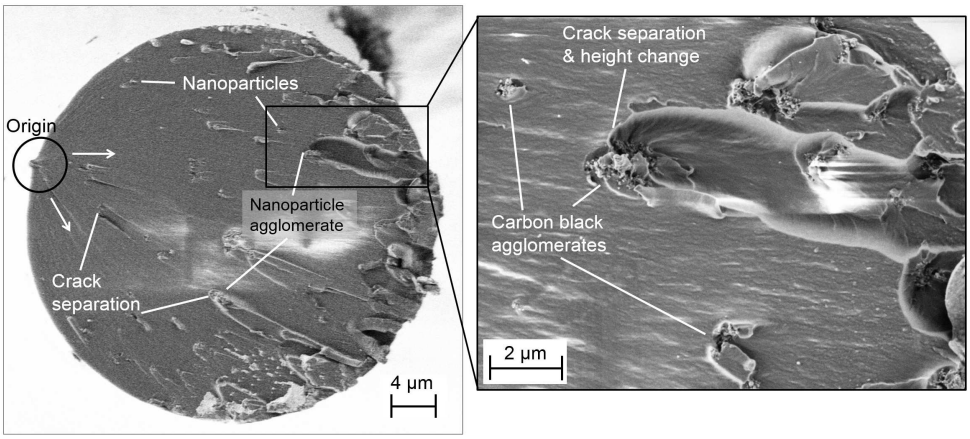

Figure 4.22: SEM image of a representative fracture surface of a with 0.5 wt.% CB modified epoxy fibre ($V = 0.06\,\mathrm{mm}^3$, $R_t = 226.11\,\mathrm{MPa}$), showing crack separation at CB particles and agglomerates.

Figure 4.23 shows representative fracture surfaces of CNT modified epoxy fibres. Failure initiates either at CNT agglomerates (refer to Figure 4.23a)) or at inclusions like amorphous carbon (Figure 4.23c)) or other foreign particles (Figure 4.23b)). These inclusions act like defects in the material and initiate failure due to local stress concentrations. An inclusion of foreign particles is shown in detail in Figure 4.23e). Failure initiation at an aggregate of amorphous carbon is presented in detail in Figure 4.23f).

Energy dispersive X-ray (EDX) analysis is performed in SEM to identify these two types of inclusions. The analysis reveals a high concentration of iron in the globular shaped inclusions. EDX analysis is also performed on pure, as received CNT. An SEM image of the pure CNT with the two types of inclusions is given in Figure 4.24 together with the results of an EDX line scan along the line marked in the image. The concentration of carbon is represented with a red line, the iron concentration with a yellow line. The globular particle on the right side exhibits a significantly higher iron concentration, whereas the particle of irregular structure on the left has a slightly higher carbon concentration compared to the surrounding CNT. The globular particle is therefore identified as a remnant with high iron content from the CNT production process, whereas the particle of irregular shape is amorphous carbon. The foreign particle inclusions found in the fracture surfaces of the fibres are thus assumed to be remnants from the ferrocene catalyst used in the CNT production process, because they occurred only in CNT modified fibres. Amorphous carbon is also a remnant from the CNT production process. The used CNT have a purity of 75 %. The remaining 25 % material are MWCNT, amorphous carbon or other impurities, according to the manufacturer.

The higher the CNT filler content, the higher the probability of such impurities being present in the fibre. If no inclusions are present, failure initiates at the largest CNT agglomerate in the fracture surface. Such a CNT agglomerate is shown in detail in Figure 4.23d). The presence of the impurities as failure initiating flaws reduces the true failure strength of the CNT modified fibres. By using CNT of higher purity for modification, even higher R_t values could be achieved for similar volumes. But despite this fact, higher R_t values compared to the unmodified resin are measured, which highlights the potential of SWCNT for improving mechanical properties of epoxy in small volumes. An increase in CNT weight fraction in the matrix increases the fracture surface roughness and thus indicates higher toughness [150, 236]. Crack separation at CNT aggregates is visible. Nanotubes that are pulled out of the fracture surface are also visible, the amount being significantly higher for 0.5 wt.% CNT compared to 0.05 wt.% CNT content. Pulled-out tubes are partly oriented in crack growth direction.

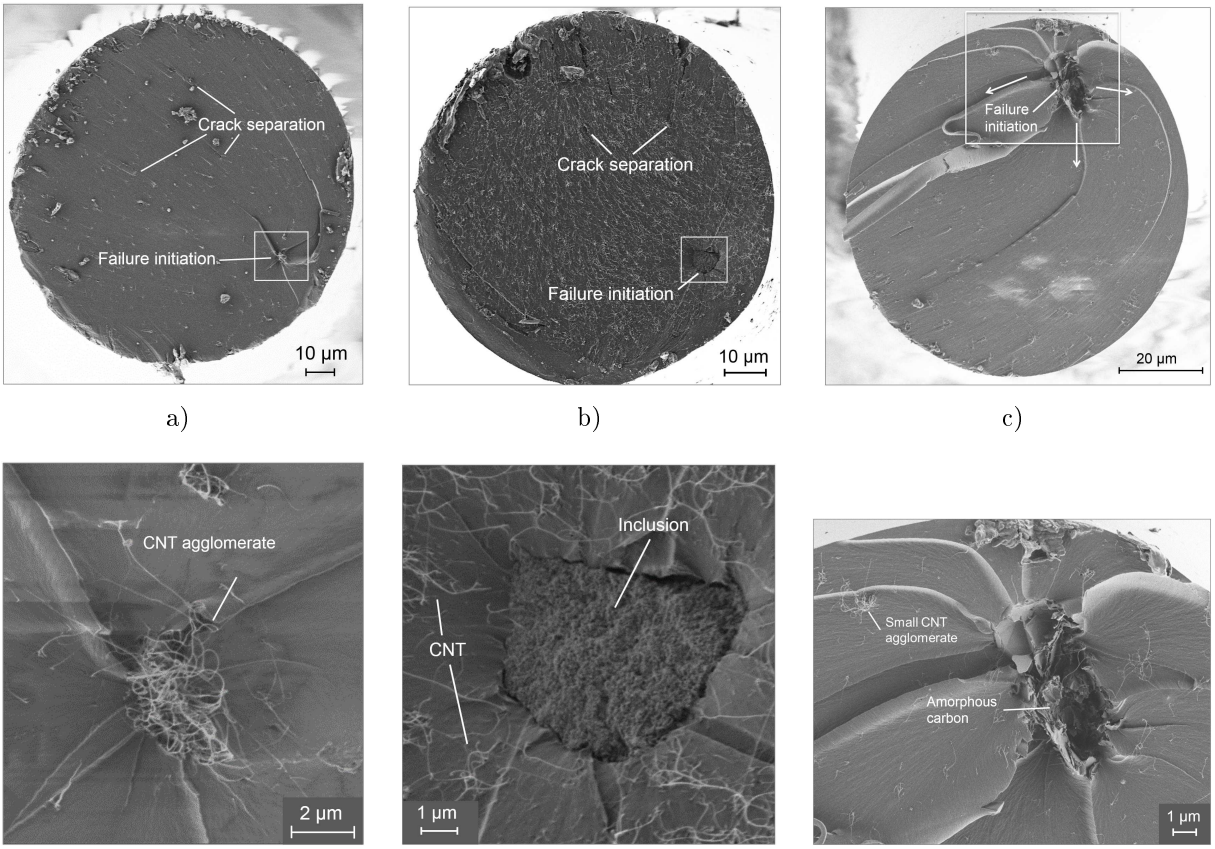

Figure 4.23: SEM images of representative fracture surfaces of epoxy fibres modified with carbon nanotubes:
a) Fibre modified with 0.05 wt.% CNT ($V = 0.91\,\mathrm{mm}^3$), showing crack initiation at a CNT agglomerate and crack separation at CNT particles ($R_t = 154.69\,\mathrm{MPa}$),
b) Fibre modified with 0.5 wt.% CNT ($V = 0.39\,\mathrm{mm}^3$), showing crack initiation at a non-carbon inclusion ($R_t = 126.57\,\mathrm{MPa}$),
c) Fibre modified with 0.05 wt.% CNT ($V = 0.31\,\mathrm{mm}^3$), showing crack initiation at an amorphous carbon inclusion ($R_t = 123.87\,\mathrm{MPa}$),
d) detail of the CNT agglomerate in a), e) detail of failure initiating inclusion in c), f) detail of failure initiating region in e).

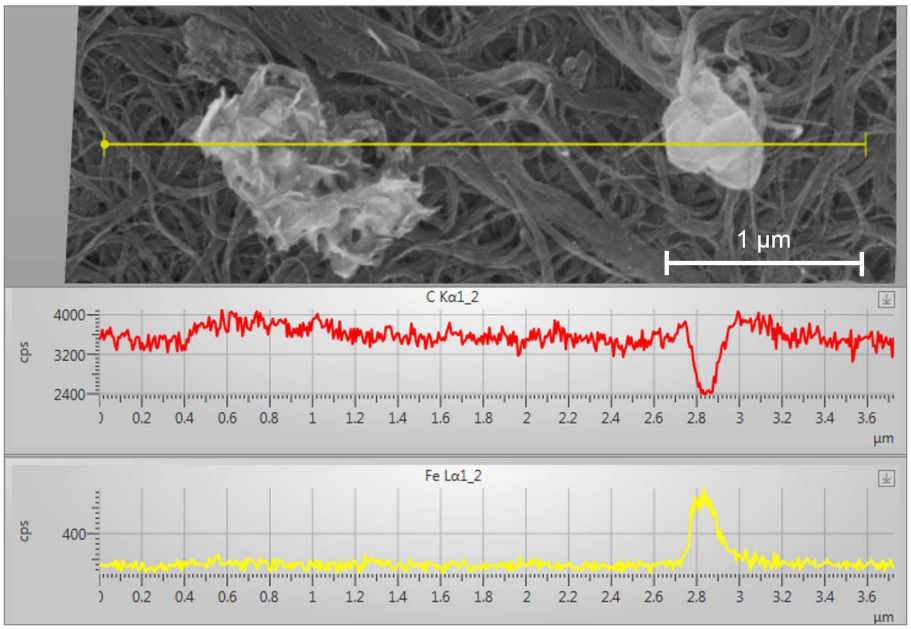

Figure 4.24: EDX line analysis of as received OCSiAl 75 % Tuball SWCNT including two different types of particles. Carbon concentration: red line, iron concentration: yellow line.

SEM images of the fracture surfaces of three FLG modified fibres of different diameter are shown in Figure 4.25. They failed at the stress levels given in the caption. Each fracture surface is representative for the respective range of true failure strength. The origin of failure initiation is marked in the images. Figures 4.25a) and 4.25b) show fibres with 0.05 wt.% FLG and Figure 4.25c) a fibre with 0.1 wt.% FLG dispersed in the matrix.

In contrast to the unmodified matrix fibres, where failure initiates from a surface defect, the crack initiates from the largest FLG nanoparticle aggregate in the fracture surface in all FLG modified specimens. As already discussed, the volume of FLG modified epoxy has minor influence on R_t, leaving particle size and orientation as reasons for the difference in strength. Failure initiates at the largest FLG particle or aggregate in the volume, similar to the largest flaw in the unmodified or CB modified matrix. But when comparing the two fibres shown in Figures 4.25b) and 4.25c), the FLG particles at the origin of failure have similar size. Despite having a smaller volume, the strength of the fibre in Figure 4.25b) is significantly lower, eliminating FLG particle size as the only explanation for this behaviour. Regarding the fracture surfaces of the other fibres, this trend is confirmed. Hence, not only the size of the FLG particle in relation to the fracture surface, but also its orientation with regard to the loading direction has an influence. Particle size is relevant for failure initiation, but its value alone is not the dominating factor for strength.

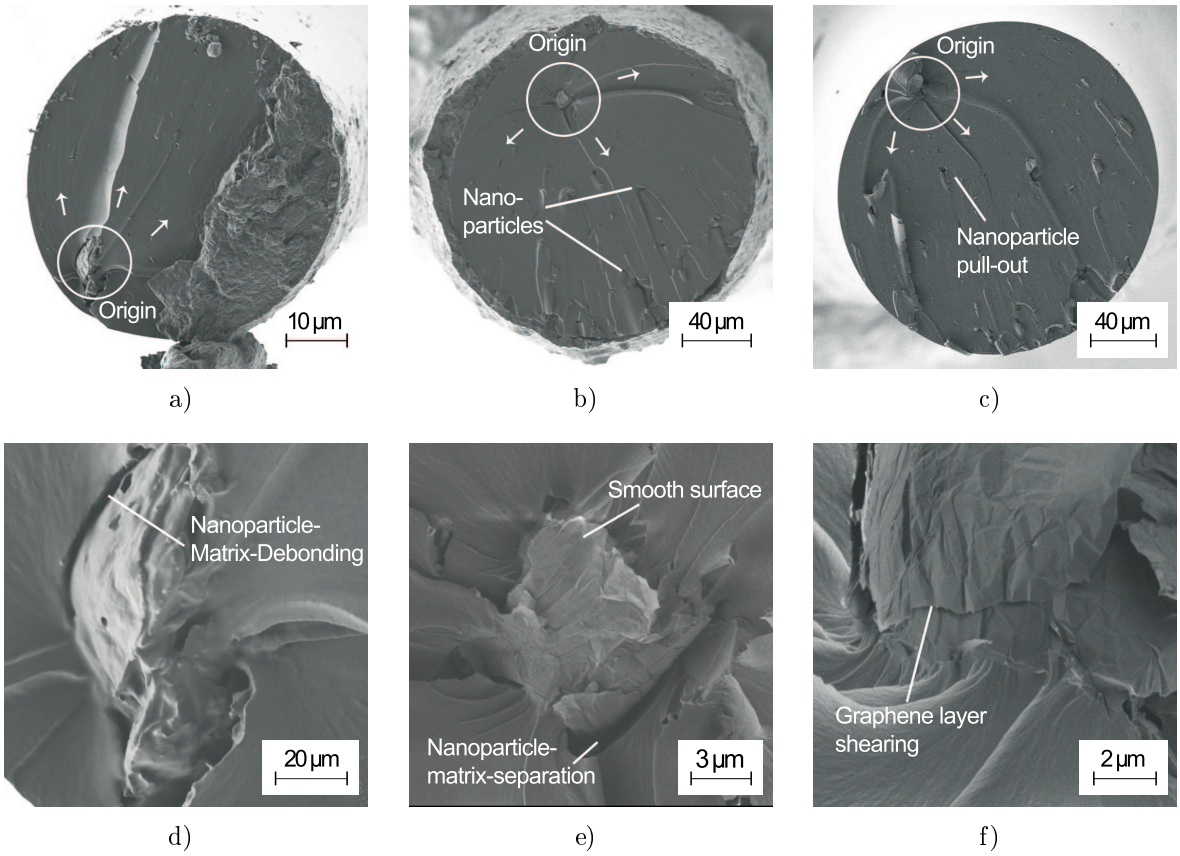

Figure 4.25: SEM images of the fracture surface of FLG modified matrix fibres of different volume V:
a) Fibre modified with 0.05 wt.% FLG ($V = 0.19\,\mathrm{mm}^3$, $d_f = 97\,\mu\mathrm{m}$, $R_t = 111\,\mathrm{MPa}$)
b) Fibre modified with 0.05 wt.% FLG ($V = 1.00\,\mathrm{mm}^3$, $d_f = 216\,\mu\mathrm{m}$, $R_t = 72\,\mathrm{MPa}$)
c) Fibre modified with 0.1 wt.% FLG ($V = 1.34\,\mathrm{mm}^3$, $d_f = 261\,\mu\mathrm{m}$, $R_t = 101\,\mathrm{MPa}$)
d) Detail of a), e) Detail of b), f) Detail of c)

In Figures 4.25d), 4.25e) and 4.25f), larger magnifications of the failure initiating nanoparticle in the fracture surfaces shown in Figures 4.25a), 4.25b) and 4.25c), respectively, are given. Different types of microdamage at the FLG nanoparticles are visible. Figure 4.25d) shows nanoparticle matrix debonding and a pull-out type of microdamage that occurs when the graphene flakes are orientated in loading direction, because the interfacial strength between graphene and matrix is lower than the strength of the covalent atomic bonds within the graphene layers. Figure 4.25e) shows a flat, smooth surface and nanoparticle matrix separation as well. The smooth surface indicates, that two layers of graphene are separated from each other. This type of microdamage is typical for graphene layers being orientated perpendicular to the loading direction. In this case, the Van-der-Waals bonds between two layers fail before or at the same stress as the graphene-matrix interface. In Figure 4.25f), shearing of two graphene layers orientated in an angle of approximately 45° to loading direction is visible. This is the case, when the Van-der-Waals bonds fail before the covalent bonds of the layers. Considering the tensile test results and the fractography analysis, the orientation of the largest particle has the highest influence on true failure strength.

In Figure 4.26, two FLG aggregates of similar size are visible in the fracture surface of one fibre. The graphene layers in the failure initiating particle are oriented nearly perpendicular to loading direction, whereas the layers in the other FLG particle are oriented parallel to loading direction. This confirms that despite the size of the particle, the orientation with regard to loading direction is critical. The large amount of FLG modified fibres prepared, allows to quantify the influence of particle or aggregate orientation on the true failure strength. Assuming that failure always initiates at the largest FLG particle or aggregate in the volume, fracture surfaces of several FLG modified specimens are analysed with regard to the orientation of the failure initiating FLG particle. The orientation of this particle related to loading direction is correlated with the volume and true failure strength of the respective specimen, as shown in Figure 4.27. True failure strength of the fibres with particles oriented perpendicular or diagonal to loading direction is limited to approximately $R_t = 105\,\mathrm{MPa}$. The layers oriented perpendicular to loading direction may separate at lower stresses due to the comparable weak Van-der-Waals forces between the layers and initiate failure. When the FLG particles are oriented with the layers in loading direction, the modified fibres exhibit true failure strength above $R_t = 105\,\mathrm{MPa}$ and up to $R_t = 140\,\mathrm{MPa}$. FLG particles oriented perpendicular to loading direction are observed only in fibres of larger volume. This can be explained by the fibre/FLG particle diameter ratio. If the fibre diameter approaches the lateral FLG dimensions, which may be up to 20 µm, the fibre is prone to break during the manufacturing process. Therefore,

in the smaller fibres produced, the largest FLG particles are oriented almost all in loading direction. With smaller volume, the probability of the comparable large FLG particles to be oriented transverse to loading direction decreases, leading to higher failure stress. This leads to the observed occurrence of parallel to loading direction oriented particles only in fibres with smaller volume.

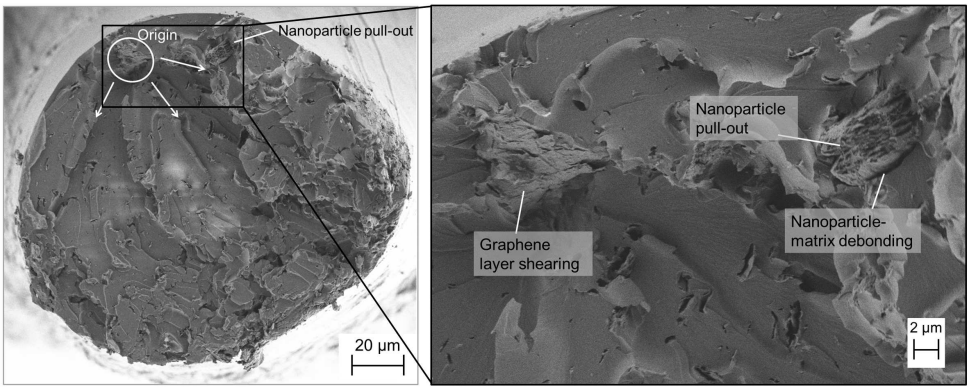

Figure 4.26: SEM image of a representative fracture surface of an epoxy fibre modified with 0.5 wt.% FLG ($V = 0.58\,\mathrm{mm}^3$, $R_t = 80.19\,\mathrm{MPa}$), showing crack initiation at an FLG particle, FLG pull-out failure mechanisms at another particle and a very rough fracture surface.

The fracture surface of all FLG modified fibres is rougher compared to the neat specimens. Crack deflection and crack bifurcation at FLG nanoparticles are clearly visible (refer to Figure 4.25b) and 4.25c)). With these findings, the mechanisms for crack propagation in graphene based nanoparticle modified epoxy, proposed by Chandrasekaran et al. [156], are confirmed experimentally in a very small fracture surface. Figure 4.26 shows an SEM image of a representative fracture surface of a fibre containing 0.5 wt.% FLG. Similar to the CNT modification, an increase in nanoparticle content leads to a rougher fracture surface. The damage mechanisms of nanoparticle pull-out, plastic void growth and graphene layer shearing at the FLG particles, already discussed in [9, 23, 156], are observed. Increasing nanofiller content increases the amount of matrix plastic deformation and hence the fracture surface roughness.

4.5.3 Influence of nanoparticle morphology on the damage process of epoxy in small volumes

Particle morphology has a clear influence on the size effect and the maximum true failure strength of modified epoxy. If nanoparticles or nanoparticle aggregates are larger than the statistically distributed defects always existent within the material, they initiate failure

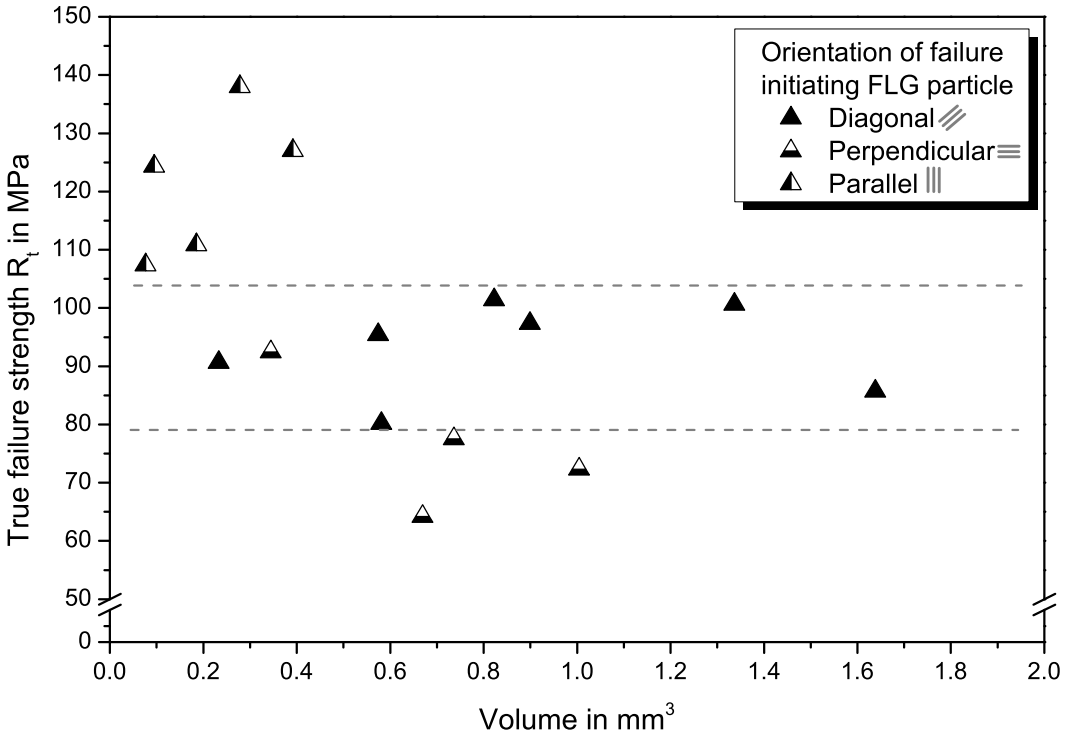

Figure 4.27: Influence of FLG-particle orientation with regard to loading direction on true failure strength for different volumes.

and thus neglect any size effect. This is the case for the comparable large FLG particles used in the present study. Otherwise, if nanoparticles are smaller than material defects, a size effect with increasing strength for decreasing volume exists. This is the case for CB particles or even small CB agglomerates and may increase the local strength in small volumes, e.g. between the fibres of FRP. According to the experimental results, a size effect is also observable for CNT modified epoxy if purity and dispersion are of high quality.

The SEM images show, that dispersion of CNT with the calendering method is very efficient even for CNT with a very high specific surface area (high aspect ratio). They are an optimum for mechanical and electrical properties, but difficult to disperse homogeneously in the matrix [135, 148]. Good dispersion is achieved for CB and FLG as well, confirming the three roll mill dispersion method as highly efficient for different particle morphologies [148, 237]. Although SWCNT have a high potential for increasing tensile strength [135], the presence of undesired remnants from the production process may counteract any enhancement, as is the case in several fibres in this study. Accordingly, in order to achieve an optimum in reinforcement, dispersion and purity of the nanoparticles are critical and should be considered carefully. Impurities from nanotube production act as

flaws within the material and oppose the desired enhancement. The observed failure initiation at CNT agglomerates is in accordance with other experimental results, e.g. from Bai and Allaoui [155].

The high values of true failure strength at smaller volumes for CB modified epoxy exhibit a certain potential for increasing mechanical properties of polymers and FRP with these comparable low-cost fillers. This is due to the fracture toughness increase, reported in [135]. The toughening mechanism of crack separation and plastic yielding of the matrix at the CB particles is shown in Figure 4.28 as a scheme and in an SEM image of a fracture surface. This is comparable to the mechanism shown by Haba et al. [237] for fullerene like tungsten disulfide (WS_2) particles that have similar morphology. Because of the globular shape of CB, additional energy dissipating mechanisms like pull-out or layer shearing are not available for this type of particles. Compared to the other particles investigated, the zone around a particle available for energy dissipation is very small, confirming the classification of a point-like 0D enhancement (refer to figure 2.8).

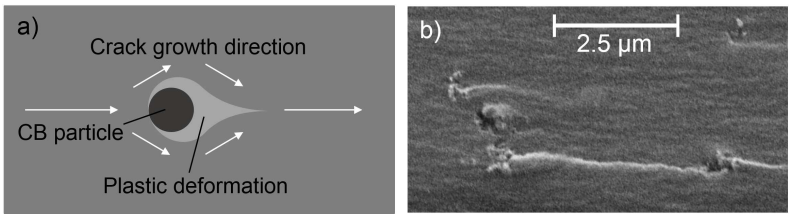

Figure 4.28: Damage mechanisms at carbon black particles: a) Scheme for crack separation at a CB nanoparticle or agglomerate, b) SEM image showing local matrix plastic deformation and crack separation at CB particles in a fibre fracture surface.

The highest true failure strength values of neat and CNT modified epoxy are in the same range, but those of the latter are measured in specimens of larger volume. The CNT modification therefore increases the tensile failure strength of polymers. What is reported in literature for bulk specimens [20, 135, 148–150, 157, 238] is now confirmed for very small, elongated volumes. Different energy dissipating, toughening mechanisms at the nanoscale are identified. Among these are nanotube fracture, crack bridging and nanotube pull-out, with the latter being most pronounced in the fracture surfaces of the fibres. A scheme (adapted from [135]) and SEM images showing the damage mechanisms at SWCNT in the fracture surface are given in Figure 4.29. Nanotube pull-out is the dominating mechanism at the nanoscale and it can only be effective in dissipating energy along the nanotube direction. Hence, the categorisation of CNT as 1D reinforcement (Figure 2.8) seems to be valid. The size effect - a significant increase in strength below

a certain volume - is valid for CNT modified polymer as well, but the volume, at which strength increases significantly, is shifted to higher values.

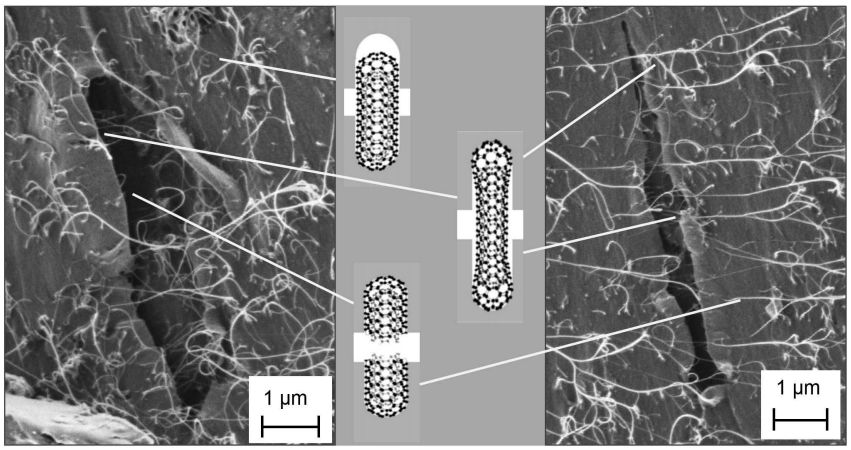

Figure 4.29: Different damage mechanisms at carbon nanotubes: schematic representation of the nano-damage mechanisms crack bridging, nanotube pull-out and nanotube fracture from [135] and SEM images of these mechanisms in the fracture surface of a matrix fibre modified with 0.5 wt.% CNT.

No significant size effect is observed for the FLG modified fibres. For most effective improvement of mechanical properties, a particle size close to the critical length is desired [162], but larger particles or aggregates may initiate failure in small volumes at lower stress, compared to the unmodified material. Hence, large particles may have negative effects on some mechanical properties. As determined with fractography, failure initiates at FLG particles or aggregates and not from a defect within the polymer, therefore the statistical defect distribution has only minor influence on the true failure strength in the fibrous specimens. The nanoparticles act as flaws in this context, counteracting any size effect due to differences in specimen volume, because there is always a nanoparticle and hence a crack initiating stress concentration present in the specimen. It is further assumed that failure initiates at the largest nanoparticle in the volume, similar to the largest flaw in brittle materials. From the lower strength of the modified fibres compared to the unmodified ones, it can be concluded that damage initiation at nanoparticles may lead to localised crack initiation in the small volume between the fibres in FRP at lower strength in static or at shorter time in cyclic tests.

A clear influence of the particle orientation with regard to loading direction is quantified. Orientation of the covalent bonds within the graphene layers of the largest particle in loading direction leads to damage initiation at higher stresses and thus, higher true failure strength. For diagonal or perpendicular orientation of the largest FLG particle, true failure strength of the specimens is limited to 105 MPa. This is the maximum global stress

value at which local layer shearing, layer separation or plastic yielding of the matrix occurs and initiates final failure. The damage mechanisms of FLG pull-out occurs at latest at a maximum stress of 140 MPa. Due to the high stiffness difference between fibre and matrix, local stress concentrations occur. Considering this, calculations of the maximum failure strength of either the Van-der-Waals bonds between the layers or the nanoparticle-matrix interface can be verified by using these experimental results.

In small elongated volumes, like in the spaces between the fibres in FRP, an orientation of the graphene layers perpendicular to the fibre axis in the modified layer is not possible, if lateral dimensions of the FLG particles are in the range of the fibre diameter. The results implicate that in FRP, larger particles are mostly oriented along the reinforcing fibres. In 0°-layers, the covalent bonds of the FLG particles are oriented in loading direction. In 90°-layers, the layers are oriented perpendicular to loading direction and may on one hand initiate local matrix failure, but on the other hand dissipate energy due to the shearing of the graphene layers and plastic deformation of the surrounding matrix, leading to enhanced mechanical properties observed when incorporated in FRP [11, 23].

When comparing the strength of the dog-bone specimens, the small increase in strength for some FLG modified specimens is in accordance with previous investigations on the effect of graphene nanoparticles on mechanical properties of polymer matrices. A positive influence of FLG nanoparticle modification has been reported by several authors [156–159, 235]. The increase in strength is attributed to a higher fracture toughness resulting from stress relieving mechanisms such as microdamage at the nanoparticles and crack separation and bifurcation [156]. In the nanoparticle modified fibres, the volume is too small for these stress relaxation mechanisms to be efficient, because any microdamage at a nanoparticle as first failure, results in final failure, leading to lower or equal strength compared with the unmodified fibres. Nonetheless, crack separation and bifurcation are clearly visible, confirming existing theories experimentally in a small fracture surface. In the larger volume of the dog-bone specimens, microdamage does not result in final failure, but reduces the stress, which, along with a lower crack growth rate, may lead to a higher strength compared to the unmodified material.

Different types of microdamage at FLG particles are observed that confirm existing models on damage mechanisms at layered particles. In Figure 4.30, a schematic representation of different types of microdamage at graphene nanoparticles, with SEM images showing these types of damage in the fracture surface of FLG modified matrix fibres, are given together with the corresponding strength of the pictured fibres in a strength versus volume diagram. The schematic representation is based on the work of Wittich et al. for layered

particles [161] and was already applied for explaining increased fatigue life of FLG modified FRP by Knoll et al. [23]. The type of microdamage depends on the orientation of the layers to the loading direction, as indicated in the scheme. Fibres, in which the graphene layers of the largest FLG particle in the fracture surface are orientated with their covalent bonds in loading direction, exhibit the highest strength. When the graphene layers of the largest particle within the fracture surface are orientated perpendicular to loading direction, the Van-der-Waals bonds between the layers carry the load, which results in lower strength (refer to the plot in Figure 4.30 c)). Thus, the true tensile strength is mostly determined by the orientation of the largest FLG nanoparticle with regard to loading direction, as presented in Figure 4.27. For best mechanical properties in a small polymer volume, for example the matrix between the fibres in FRP, the graphene layers should be orientated parallel to loading direction.

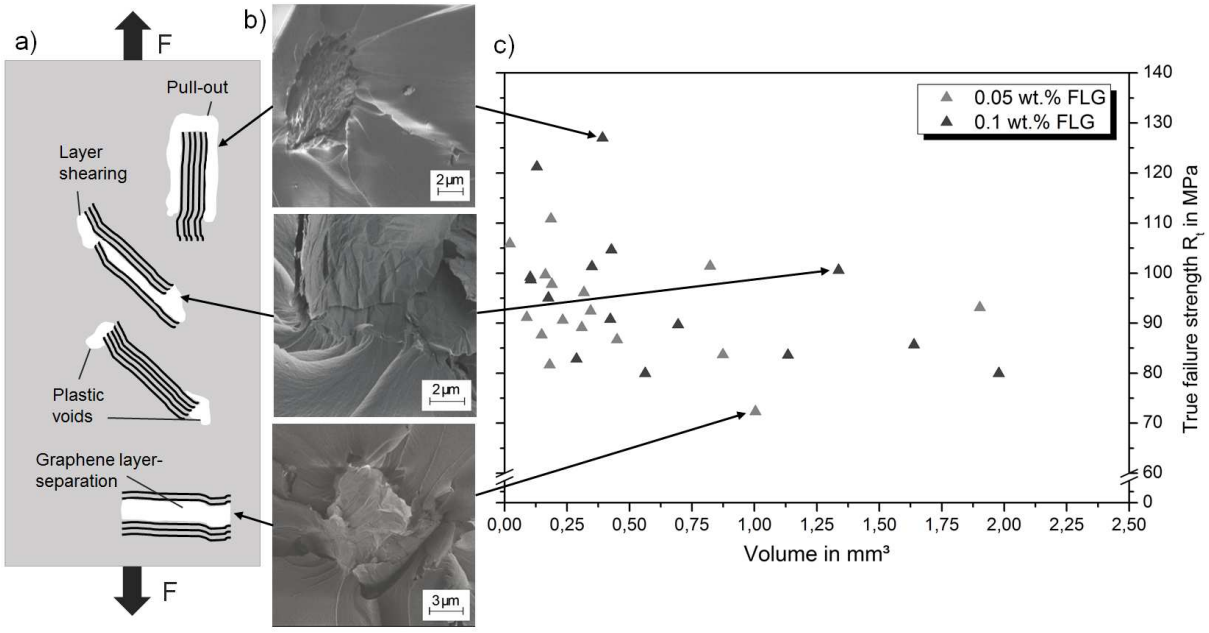

Figure 4.30: Different damage mechanisms at FLG nanoparticles in dependency of the particle orientation with regard to the loading direction
a) Schematic representation of the damage mechanisms after [23, 161]
b) SEM images of the fracture surface of three different FLG modified matrix fibres showing the mechanisms sketched in a)
c) True tensile strength versus specimen volume for the FLG modified fibres.

As expected, the fracture surface roughness increases with increasing filler content for all investigated particle morphologies. Comparing the plastic deformation of the matrix for the three types, FLG modification exhibits the highest amount of fracture surface deformation, whereas in CB modified specimens only rough spots at agglomerates are found, where the crack height is changed. CNT modification in general leads to higher amounts

of plastic deformation compared to CB, but pull-out of the nanotubes is the dominant mechanism. The nanotubes used in this study are quite long and pull-out length is high before breakage. According to analytical approaches by Greenfeld et al. [162], this should result in a significant increase in strength and toughness and explains both, the higher stress values compared to unmodified fibres of same volume and the shift of the strength increase, due to the size effect, to higher volumes. The higher fracture surface roughness for FLG in comparison to CNT corresponds well with a higher fracture toughness. Referring to Figure 2.11, an FLG modification results in higher fracture toughness than a modification with CNT.

The nanoparticle volume fraction may have a significant influence on mechanical properties of nanocomposites [135, 148, 156]. Regarding the size effect, no significant influence of a modification with FLG or CB nanoparticles is found. In FLG modified epoxy, a failure initiating particle is always available, neglecting any size effect, whereas for CB, the particles are smaller than material surface defects, resulting in a similar behaviour as the neat epoxy. With decreasing filling content, CNT modified epoxy exhibits less probability of agglomerates or impurities from manufacturing process, resulting in a more significant size effect. Nonetheless, if purity and dispersion are high enough, it is assumed that the CNT weight fraction has no significant influence on the size effect up to a certain volume fraction.

Concluding, the influence of the investigated particle morphologies on the size effect according to the experimental results is presented schematically in Figure 4.31. As there is a clear dependence on particle size, epoxy modified with smaller graphene particles than those used here may also exhibit a size effect.

4.6 Tailored FLG modification

From the investigation of small volumes by using epoxy fibres, FLG nanoparticles exhibit the most interesting failure mechanisms and properties for modification of FRP. This type of particles also leads to the highest increase in fracture toughness of epoxy in SENB experiments (refer to Figure 2.11). Since failure initiates at FLG particles, a relief of the fibre-matrix interface and a change in transverse cracking behaviour might be achieved. Furthermore, previous investigations [23, 183, 184] showed differences in the fatigue behaviour of FLG modified CFRP between tension-tension (t-t) and tension-compression (t-c) loading that need clarification with regard to the influence of FLG in the different layers. Therefore, the influence of an FLG modification of either 90°- or

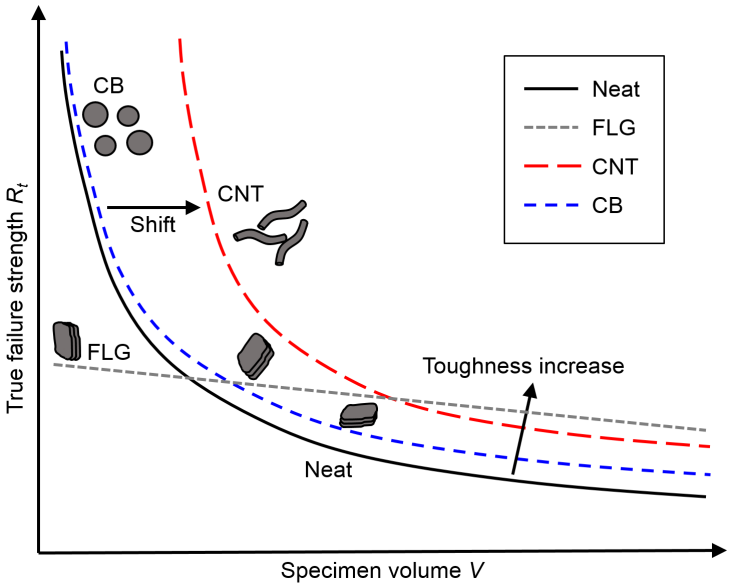

Figure 4.31: Influence of carbon nanoparticle morphology on the size effect of epoxy matrix nanocomposites.

0°-layers of cross-ply laminates is investigated. Most of the quasi static and fatigue tests presented within this chapter were carried out, presented and discussed within the scope of the master thesis of Schetle [239] and submitted for publication. Fractography of the fracture surfaces after failure by using SEM is carried out to analyse the influence of nanoparticles on the failure process and different damage types of cross-ply laminates.

4.6.1 Quasi-static tensile tests

Figure 4.32 shows representative stress-strain curves (Figure 4.32a)) and the related cumulative energy of the AE signals versus strain plots (Figure 4.32b)) for unmodified and tailored FLG modified cross-ply laminates. Results from the quasi-static tensile tests are summarised in Table 4.5. No significant change in strain to failure is observed with a nanoparticle modification. The FLG modified configurations show slightly higher values for the Young's modulus ($\approx +5.5$ %).

For specimens with unmodified 0°-layers (NNN and NGN), load drops and a decreasing slope of the stress-strain curve are observed above approx. 0.4 % strain. These load drops correlate with an abrupt increase in cumulated energy as visible in Figure 4.32b) and can be attributed to material degradation at higher strains by IFF, delaminations and breakage of single fibres or fibre bundles.

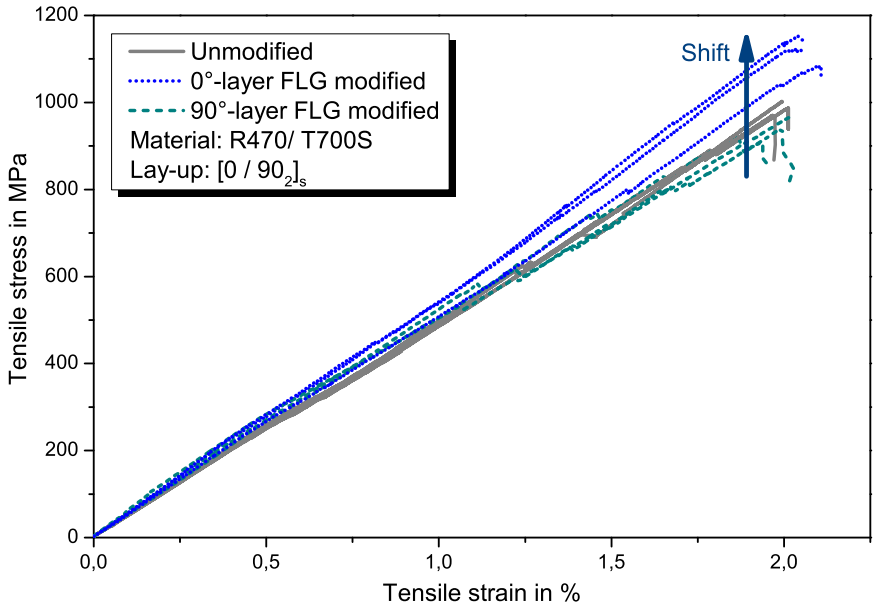

a)

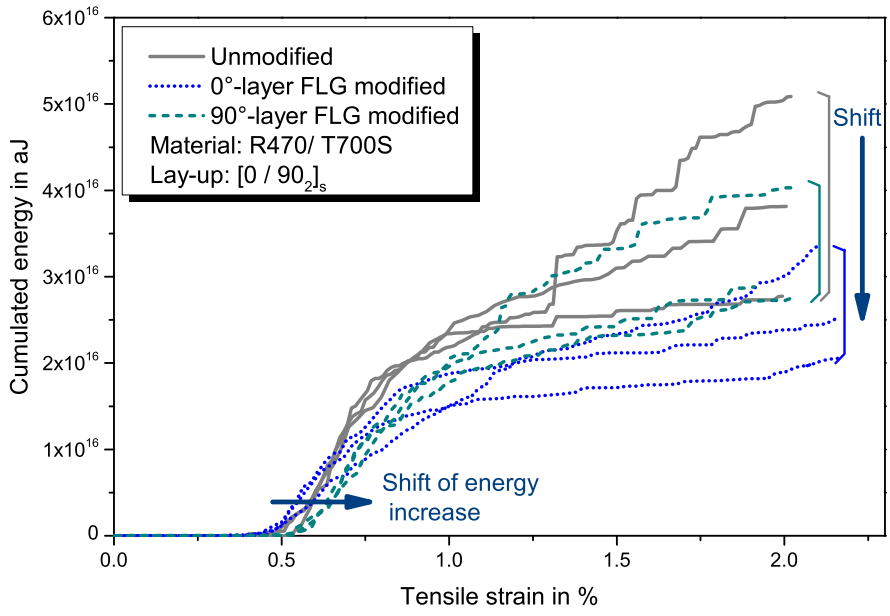

b)

Figure 4.32: Results from quasi-static tensile tests: representative stress-strain curves a) and the related cumulated energy versus strain curves b).

Table 4.5: Quasi-static tensile test results for tailored FLG modified cross-ply laminates (material: T700S / R470).

	Unmodified	**90°-modified**	**0°-modified**
Young's modulus / GPa	51.4 ± 2.8	54.4 ± 4.2	54.1 ± 2.5
Stress at failure initiation / MPa	273 ± 18	328 ± 20	284 ± 18
Tensile strength / MPa	947 ± 76	945 ± 40	1093 ± 58
Strain to failure / %	1.99 ± 0.02	1.95 ± 0.13	1.98 ± 0.09
Cumulated energy at failure / aJ	$(4.2 \pm 1.3) \cdot 10^{16}$	$(3.8 \pm 0.9) \cdot 10^{16}$	$(2.9 \pm 0.7) \cdot 10^{16}$

A significant difference in the slope of the stress-strain curves is observed for the 0°-layer modification. These specimen exhibit a linear stress-strain behaviour without any significant load drops until final failure that results in a higher tensile strength (+15.3 %) compared to the other configurations. This difference in the damage process is also visible in the AE cumulated energy (refer to Figure 4.32b)). Compared to the other configurations, the increase in accumulated energy for the 0°-layer modified specimens is less steep after the first increase, attributed to IFF, resulting in a lower value of accumulated energy at final failure. Fibre bundle breakage, that correlates with a significant increase in AE cumulated energy and a drop in the stress-strain curve, is hence suppressed for a long period of loading with a FLG modification of the 0°-layers.

The stress at IFF initiation can be determined from the increase in accumulated energy that correlates well with a slight decrease in the slope of the stress-strain curve. This slope decrease is also referred to as a "knee" and is typical for initiation of the first transverse cracks in cross-ply laminates [55, 220]. A modification of the 90°-layers with FLG nanoparticles (NGN) shifts the initiation of IFF to higher stresses (+20.2 %) compared to the unmodified reference (NNN). This shift in IFF initiation is also visible in the slope of the AE accumulated energy (refer to Figure 4.32b)), where the first steep increase in accumulated signal energy is shifted to higher strain values. Since IFF occurs mainly in the 90°-layers, no significant change is observed for a 0°-layer FLG modification, although the stress at IFF initiation is slightly higher (+4.0 %) compared to that of unmodified specimens. During the tensile tests, all configurations show similar AE signal frequencies, indicating similar damage types in general.

Photographs of representative specimens after final failure are shown in Figure 4.33 a) for a 90°-layer FLG modification (NGN) and in Figure 4.33 b) for an unmodified 90°-layer specimen (GNG in the image). All specimens with unmodified 90°-layer (NNN and GNG) look similar after final failure. An FLG nanoparticle modification of the 90°-layer significantly reduces the amount of transverse cracks spanning both the thickness and

width of the specimens, as can be seen from the smaller amount of 90°-layer fragments. Nonetheless, the total amount of IFF visible at the specimen edges is similar in all configurations. Transverse cracks can as well be observed at the edges within the remaining large parts after fracture of the 90°-layer modified plies. But these cracks do not span either thickness, width or both of the specimen completely, thus they are not visible as fully separated fragments after failure.

Figure 4.33: Photographs of representative CFRP cross-ply specimens after final failure: a) 90°-layer FLG modified, b) 0°-layers FLG modified, 90°-layer unmodified.

Figure 4.34 shows representative SEM images of the delamination fracture surface between the 0°-layer, visible in the images, and the 90°-layer. Figures 4.34 a) and b) show images of an unmodified NNN specimen, in Figure 4.34 c)-h) images of GNG specimens with the 0°-layer modified with FLG nanoparticles are shown. The fracture surface of unmodified specimens is comparable smooth with mostly adhesive fibre-matrix interface failure. Small, localised matrix remnants sticking on the fibres indicate regions of cohesive matrix failure. In contrast to that, delamination surfaces of modified specimens are rougher and exhibit both adhesive and large areas of cohesive failure. As shown in the detail in Figures 4.34 e),f),g), and h), FLG particles are found in the transition zone from adhesive to cohesive failure. Around these particles the matrix exhibits plastic deformation. The delamination surface of NGN specimens (90°-layer FLG modified) looks similar regarding roughness and the proportion of cohesive and adhesive failure. However, as shown in Figure 4.35, large remnants of the 90°-layer are visible on the fracture surface.

These are attributed to crack tip delaminations of transverse cracks in the 90°-layer that results in the delamination running partly through the 90°-layer.

4.6.2 Cyclic tests

In Figure 4.36 the cycles to failure for the two load levels and the three configurations are shown. A modification of the matrix with FLG nanoparticles reduces the fatigue lifetime under alternating loads ($R = -1$). The decrease is more pronounced for a 90°-modified layer showing a reduction of approximately -88 % at 215.0 MPa and -72 % at 228.3 MPa. These specimens exhibit the lowest cycles to failure at both load levels with a greater difference in comparison to the other configurations for the lower load level of 215.0 MPa.

Damage accumulation until final failure in cyclic tests is similar for the investigated configurations. Cracks in the form of IFF in the 90°-layer are the first observed damage type within the first load cycles. Amount and length of these transverse cracks increase with increasing cycles. Final failure is initiated by large delaminations between the 90°-layer and the 0°-layer. Shortly after delamination initiation, final failure of the specimen occurs in the form of buckling of the 0°-layer within the free area of the anti-buckling device. Hence, rupture of the specimens occurs under the compressive part of the loading. The delamination growth is pronounced for nanoparticle modified specimens resulting in shorter fatigue life at $R = -1$.

Development of 90°-layer transverse cracks at the edges with increasing load cycles during interrupted fatigue tests of one representative specimen of each configuration are presented in Figure 4.37. The FLG modified specimens exhibit slightly reduced amount of edge cracks in the 90°-layer. This is more pronounced for a modification of the 90°-layers (NGN) as it was already the case in the quasi-static tensile tests. Similar to the tensile tests, the IFF development is changed with slightly smaller amount of IFF at higher load cycles with a 90°-layer modification. As only the edge crack density is measured, no information about crack width or crack opening is obtained. Nonetheless, as transverse cracks initiate at the free edge of a specimen for the chosen geometry [5, 56], the value is a good indicator for transverse cracking behaviour in the 90°-layer.

Figure 4.38 shows the delamination fracture surface between the 0°- and the 90°-layer and the initial delamination at a transverse crack in the 90°-layer. Similar to the behaviour observed in the tensile tests (refer to Figure 4.35), the initial delamination at a crack tip is significantly larger for an FLG modified 90°-layer.

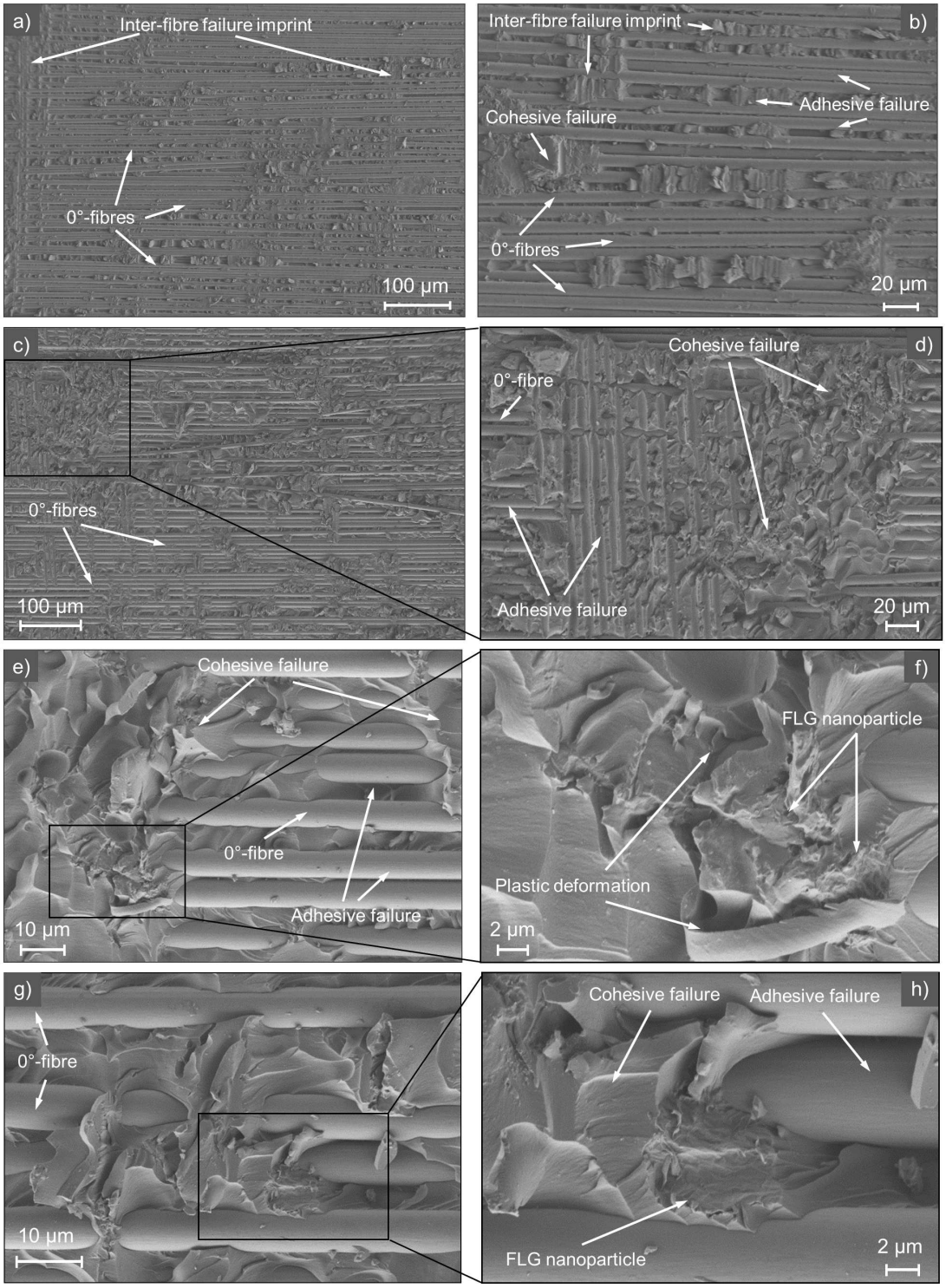

Figure 4.34: SEM images of the delamination fracture surface. The 0°-layer is shown for a) and b): unmodified specimens, c)-h): 0°-layer FLG modified specimens.

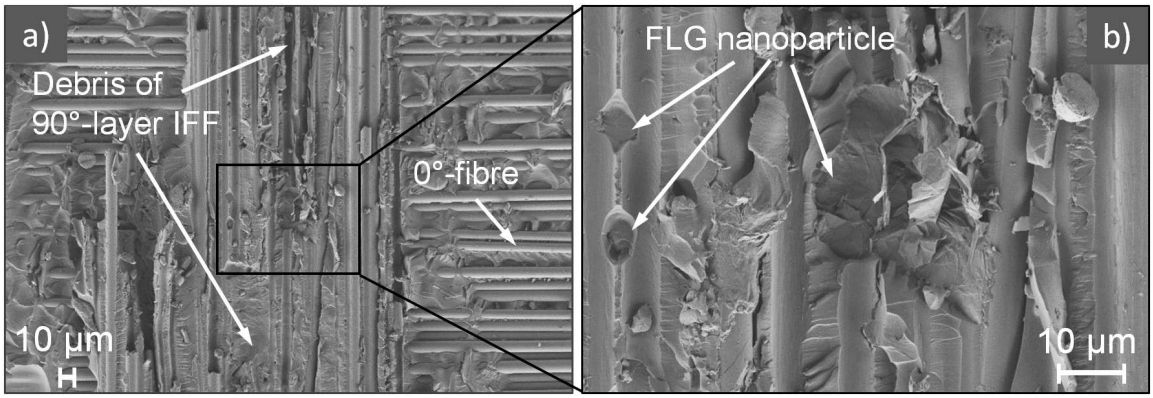

Figure 4.35: SEM images of the delamination fracture surface of a 90°-layer FLG modified matrix specimen. The 0°-layer is shown in a) an overview and b) detail of the interlaminar failure (delamination) originating in and partly running through the 90°-layer.

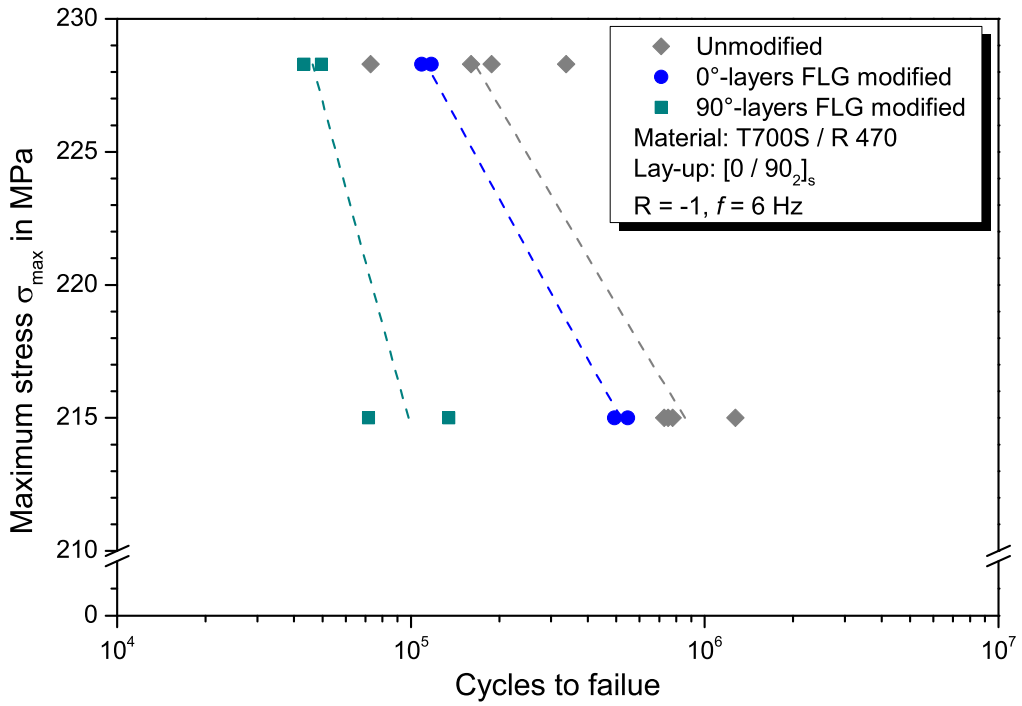

Figure 4.36: S-N curves of CFRP showing the influence of a matrix modification with FLG nanoparticles in the different layers of cross-ply laminates.

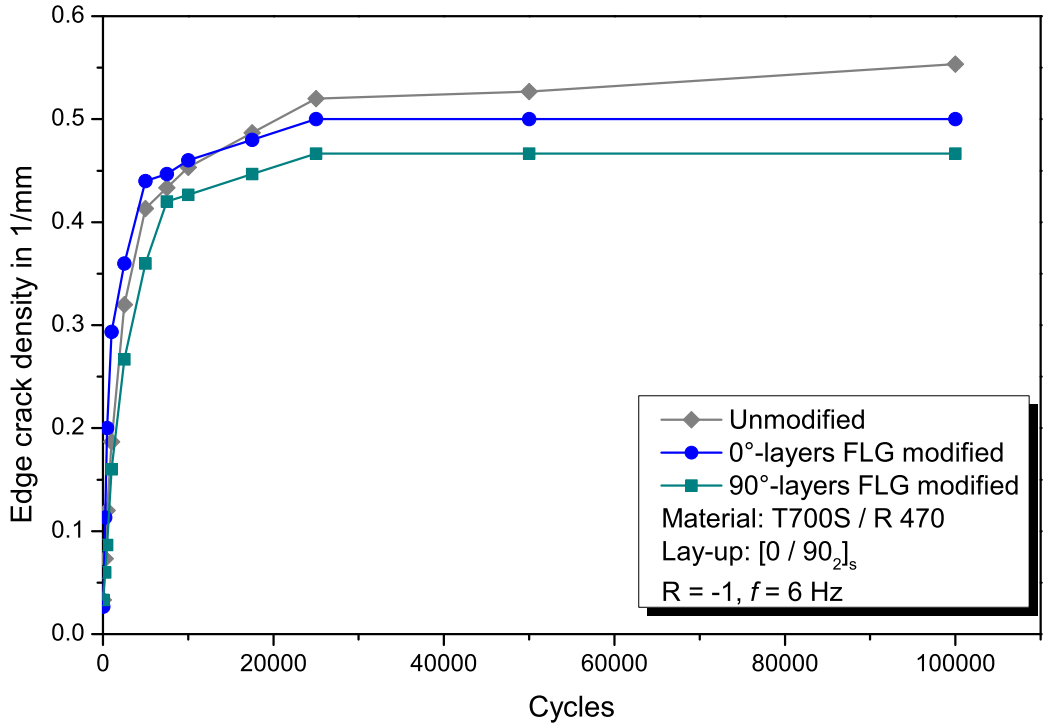

Figure 4.37: Development of 90°-layer transverse cracks with increasing load cycles in CFRP cross-ply laminates during interrupted fatigue tests of one representative specimen of each configuration.

For these NGN-specimens, crack tip delamination at IFF is approximately 80 µm larger per crack, resulting in a larger initial delamination surface over the length of the specimen and the observed larger crack distance.

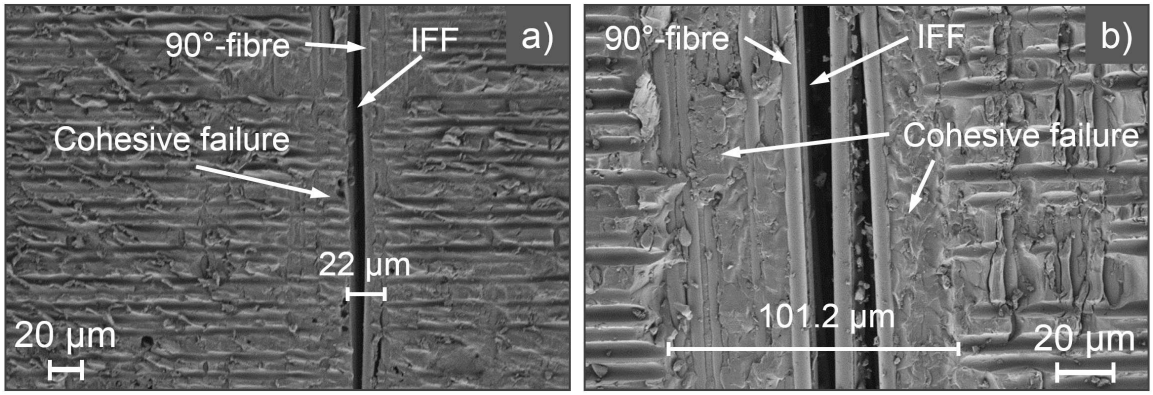

Figure 4.38: Fracture surfaces of the delamination between 0°- and 90°-layer. The 90°-layer with a typical initial delamination at IFF is shown for a) unmodified and b) FLG modified 90°-layer.

4.6.3 Influence of FLG nanoparticle modification on the failure process of CFRP cross-ply laminates

Regarding the influence of a nanoparticle modification in FRP, it is distinguished between an intralayer modification, where the nanoparticles are between the fibre filaments within a layer and where 0°- and 90°-layers are differentiated, and an interlayer modification, considering the influence of nanoparticles on interlaminar damage behaviour. As discussed in chapter 4.5, the efficiency of FLG nanoparticles in small volumes depends on the FLG orientation with regard to loading direction. The FLG particles are found in the transition zone between adhesive and cohesive crack growth and thus seem to initiate a change in crack height and propagation type. This is comparable to the toughening mechanisms in polymers [9, 156] and is valid also for very small volumes as they are present between the fibres in FRP, as shown in chapter 4.5.3.

Tensile properties of cross-ply laminates are dominated by the 0°-layers. The observed slight increase in Young's modulus can be explained by an increase in the matrix stiffness due to the nanoparticle modification, also reported for pure polymers [157, 240]. However, as stiffness is dominated by the 0°-fibres, the change is small. Strain to failure is dominated by the failure strain of the 0°-fibres and does not change with a modification, as the fibres are of the same type in all configurations. Therefore, the stress-strain curves of

specimens with unmodified 0°-layers show similar behaviour at higher strain levels shortly before final failure. The stepwise decrease of stress with increasing strain is attributed to delaminations and fibre bundle breakage. Surprisingly, the 0°-layer modified specimens exhibit linear stress-strain behaviour until final failure without any significant load drops. This observed difference in stiffness behaviour with increasing strain for a 0°-layer FLG modification can be explained by a reduction of fibre bundle failure due to the FLG particles being oriented along the fibre axis. This effect is schematically shown in Figure 4.39. Breakage of fibre bundles in the 0°-layers after single fibre breakage is reduced due to a better load redistribution via the stiff FLG particles oriented in loading direction between the fibres, resulting in higher tensile stress. This is analogue to the observed deflection of a delamination crack at FLG particles, resulting in cohesive instead of adhesive crack growth, as shown in Figure 4.34. In the 0°-layers, the strong covalent bonds lay in loading direction with the particles oriented parallel to the fibres and may act locally as a new load path next to a broken fibre, leading to a stress relief of the neighbouring fibres. In FRP with unmodified matrix, the load of a broken fibre is distributed evenly to the nearest, surrounding fibres, often leading to filament and bundle breakage because of an overload due to load sharing [75, 76, 241]. FLG particles between the fibres distribute the stress concentration over a broader length of the neighbouring fibres and hence act as local load paths and reduce the overload of the surrounding fibres after breakage of single fibres.

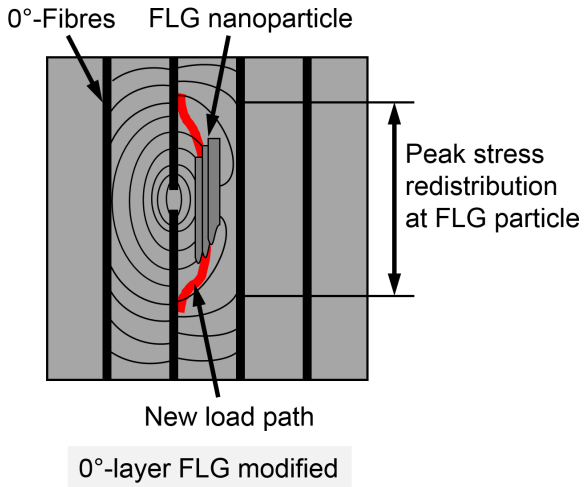

Figure 4.39: Scheme showing load and stress redistribution at an FLG nanoparticle next to a broken fibre filament in an FLG modified 0°-layer of a cross-ply laminate.

A top view of a 0°-layer, showing the influence of FLG nanoparticles on the load sharing at fibre breakage in dependence of the load level, is sketched in Figure 4.40. For a low load level, only the fibres with the lowest strength, determined by statistically distributed

defects, fail due to the external loading. Assuming the strength of the surrounding fibres is high enough, they carry the additional stress induced by load sharing at the broken fibre. Although the FLG particles lead to a better load redistribution, the influence on the macroscopic behaviour is negligible, because the external loading is too small for the mechanisms to be efficient (refer to Figure 4.40 a) and b)). For a high load level however, failure of the fibres with the lowest strength leads with a higher probability to filament and bundle breakage in the unmodified case, due to the additional load, distributed among the unbroken fibres next to the failed fibre via load sharing (Figure 4.40 c)) [75]. At the higher load level, the mechanisms of load redistribution and FLG particles acting locally as additional load paths (refer to Figure 4.39), may reduce the amount of fibre filament breakage, as shown schematically in Figure 4.40 d). This is an explanation for the observed behaviour observed here and in [23, 183], that the influence of an FLG modification is more pronounced with higher load level in fatigue tests.

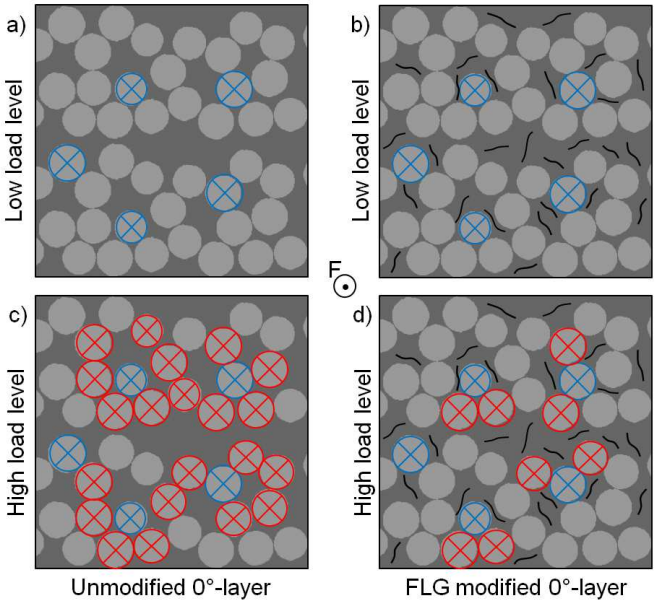

Figure 4.40: Scheme showing the influence of FLG nanoparticles on the load sharing at fibre breakage in a 0°-layer of a cross-ply laminate in dependence of the load level. ⊗ indicates a failed fibre and ⊗ marks fibres that fail due to an overload from local load sharing.

Regarding the 90°-layer fragments after final failure, a difference in IFF growth behaviour is visible when these layers are modified with FLG nanoparticles. The significantly smaller amount of 90°-layer fragments for NGN hints to broader transverse cracks with large crack tip delaminations in combination with distributed cracks that do not penetrate the layer in at least one dimension. The reasons for the significantly smaller amounts of transverse cracks penetrating both, width and thickness of the specimen and the corresponding larger

fragments can be explained by the damage mechanisms at the planar FLG flakes, analysed with fractography of the fracture surfaces. Due to energy dissipating microdamage such as layer shearing, matrix plastic deformation and plastic void growth at the FLG particles, the morphology of 90°-layer transverse cracking is changed to more intricate paths, which should imply more distributed damage instead of straight cracks. This leads to the observed delay in AE-cumulated energy increase and the smaller number of fragments after final failure. Distributed damage behaviour instead of large cracks has a potential for increasing the resistance of the 90°-layer against transverse cracking and reduction of stress concentrations without severe damage. Although IFF initiation as edge cracking is assumed to appear at the same strain level as the unmodified reference, the propagation of IFF through the width is shifted to higher stresses and is slower for embedded 90°-layers, as seen in the tensile tests for 90°-layer modified specimens. With the microdamage at the particles, an additional damage mechanisms is introduced into the composite and an increased material volume participates in the deformation process. The energy to initiate and propagate a transverse crack should be higher, because these types of local damage dissipate energy that is not available for crack initiation or growth. The delayed increase in AE cumulated energy with 90°-layer modification (refer to Figure 4.32b)), which is attributed to large IFF, confirms the shift of width penetrating IFF to a slightly higher strain level. This leads to the observed increase in the local stress-strength ratio to be exceeded for initiating a new crack and also contributes to a change in transverse crack morphology. Depending on FLG orientation, the aforementioned plastic voids at the particles initiate local matrix failure, which results in small, localised cracks. Hence, with the forming of small local cracks around FLG particles, the overall fracture surface is enlarged and smaller distributed cracks that do not penetrate the width or thickness of the 90°-layer are the result.

As shown in the SEM images (refer to Figures 4.35 and 4.38), the crack tip delamination is larger for 90°-layer modified specimens. The mechanisms explaining this observation are shown schematically in Figure 4.41 a) and b), in which through the thickness matrix cracking in a unmodified respectively FLG modified 90°-layer of a cross-ply laminate and the resulting initial delamination at the crack tip is displayed. Due to shear stresses at the tips of transverse cracks next to the adjacent layer, Y-shaped shear cracks may form next to the crack tip [242]. Figure 4.35 shows the SEM image of the sketched case in Figure 4.41 where the transverse crack is branched at FLG particles and a large amount of 90°-fibres stick to the 0°-layer. Growth of these shear cracks is favoured by FLG particles lying in the fracture plane and the plastic voids at the particles acting as small localised cracks. This leads to the observed increase in crack tip delamination area.

The load cannot be transferred from the 0°- to the 90°-layer in delaminated areas, resulting in larger distance between two transverse cracks. The observed reduction of fragments is thus caused by a combination of microdamage increasing the energy required for crack initiation and propagation as well as a different load introduction pattern between 90° and 0°-layer because of increased crack tip delaminations.

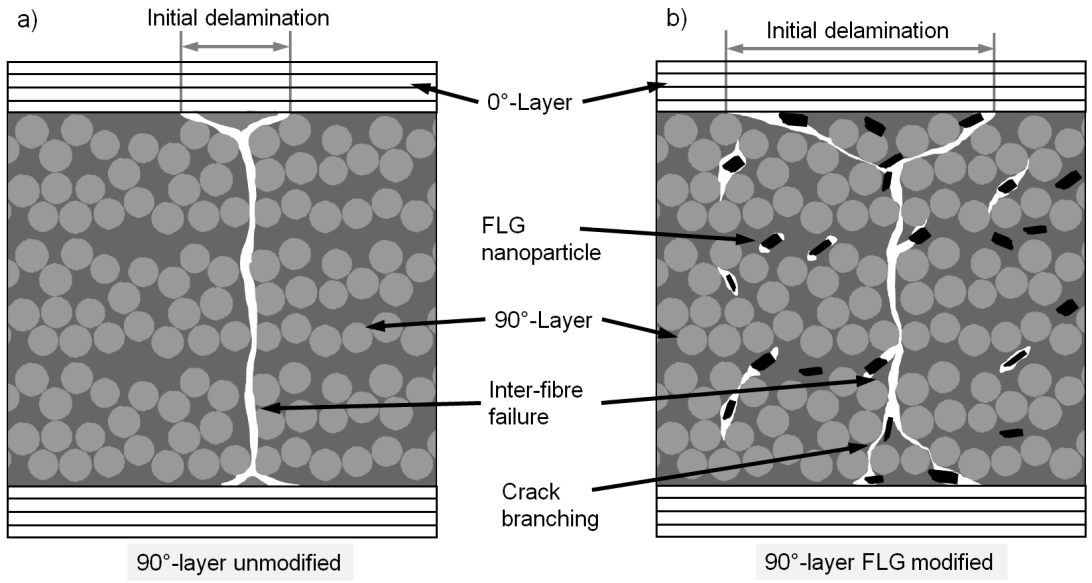

Figure 4.41: Scheme showing through the thickness matrix cracking in a) unmodified and b) FLG modified 90°-layer of a cross-ply laminate and the resulting initial delamination at the crack tip.

In cyclic tests, besides IFF in the 90°-layers, the interlaminar delamination crack growth plays in important role for fatigue degradation with increasing load cycles. For unmodified laminates, interfacial failure between fibre and matrix is the dominating crack propagation mechanisms, resulting in a comparably smooth fracture surface. Shear hackles that are typical for epoxy matrix shear failure [124, 243] are visible where the matrix sticks to the fibres. Both FLG modified specimen types exhibit rougher fracture surfaces. Surface roughness can be correlated with resistance against crack propagation and thus toughness [150, 236]. The matrix modification with FLG nanoparticles leads to a mixed, cohesive and adhesive, delamination failure. The additional energy dissipating damage mechanisms available with FLG particles in the matrix and the larger transverse crack tip delaminations lead also to a delayed initiation and larger distance of transverse cracks in cyclic tests with a 90°-layer modification. However, the observed larger crack tip delamination at IFF with a 90°-layer modification is problematic, because it promotes delamination growth and favours buckling failure under compressive loading. This results in lower cycles to failure in cyclic tests with alternating loading for the 90°-layer modified

specimens. These large initial delaminations and thus the decrease in fatigue life are more pronounced for a 90°-layer modification. It must be pointed out, that also the 0°-layer modified specimens exhibit a decrease in fatigue life compared to the unmodified reference, although the crack tip delamination size at 90°-layer IFF is in the same range. This is in contrast to previous results with the same material in the tension-tension regime ($R = 0.1$) [23], or for GNP modified GFRP under bending [185], where an increase in fatigue life with FLG modification of all layers is reported. But it agrees with previous results for the tension-compression regime ($R = -1$) [183, 184], where a slight decrease in fatigue lifetime with an FLG modification of all layers in cross-ply specimens of the same configuration and material is reported for a load level of 242 MPa (equivalent to 24 % mean tensile strength). This is attributed to lower mode I interlaminar fracture toughness values with the FLG modification (refer to chapter 2.3.2).

The observed behaviour that FLG modification has a more positive influence at higher load levels, in this case the decrease in fatigue life is smaller for the higher load level, agrees well with previous observations. In the t-t regime, the increase in fatigue life with an FLG modification is more pronounced at higher load levels [23] and in the t-c regime, no decrease at a load level of 326 MPa (34 % mean tensile strength) is measured [183, 184].

Possible explanations for the observed phenomenon of reduced fatigue life for GNG-specimens are, that under compression loading even small amounts of fibre misalignment strongly influence static and fatigue properties of composite laminates [41, 42, 244, 245]. Precise orientation of the fibres was pursued and although small amounts of fibre misalignment cannot be excluded completely from the manufacturing process, it should be the same for all configurations and can be disregarded as a reason for the observed change in fatigue life. Compression failure is also strongly influenced by delaminations between 0°/90°-layers and the difference between the t-t regime and the t-c regime can be explained with the difference in delamination growth behaviour. Under in-plane compression, delamination growth is mode I dominated, whereas in tension shear stresses dominate, leading to mostly mode II delamination growth.

As pointed out in the literature overview in section 2.3, the size of layered graphene based nanoparticles seems to be critical regarding their influence on delamination crack propagation. GNP with larger lateral dimensions tend to align with the carbon fibres in the interlayer and hence in crack growth direction, thereby generating numerous weak links. Particles with smaller lateral dimensions may also orient transverse to the interlayer plane, thus being an efficient obstacle for interlaminar crack growth under mode I.

The differences in the mode I fracture toughness of GNP modified CFRP between the studies from Kosmann et al. [183] (decrease in $G_{\mathrm{I},c}$ with modification) and Kostagiannakopoulou et al. [188, 189] (increase in $G_{\mathrm{I},c}$ with modification) can be explained by the difference in particle size. Furthermore, the particle orientation in the fracture plane may depend on the manufacturing method. If only the interlayer between two sublaminates is modified with GNP as in [190], this results in larger matrix volume between these two layers than typical for prepreg and a behaviour more comparable to a bulk volume. This explains the similar trend between bulk volume and FRP, with G_{Ic} increase and G_{IIc} decrease, in [190] and the deviation with other results for FRP [183, 188, 189], where G_{IIc} increases as well. Due to the larger volume between the layers, an orientation of the particles perpendicular to crack growth direction is possible and more probable compared to a complete modification using prepreg technique as done in [183, 188, 189]. Particles that lie with their lateral orientation perpendicular or at a certain angle $> 45°$ with regard to the interlaminar plane would result in an increase of mode I and a decrease of mode II interlaminar fracture toughness. The difference in manufacturing method hence explains the deviations in the findings reported in [190] and [183] for comparable particle size.

Schemes showing the influence of an FLG or GNP nanoparticle modification on interlaminar (delamination) crack growth are presented in Figure 4.42 for mode I loading and in Figure 4.43 for mode II loading. For these figures, manufacturing of modified FRP by the common techniques in industry like infusion, fibre winding, or prepreg techniques is assumed, which implies that larger GNP particles are oriented along the fibres in the interlayer. In Figure 4.42, the influence of particle size under mode I is shown. For smaller particles, a higher amount of energy dissipating failure mechanisms can be activated during crack propagation in the interlayer. For larger particles however, the crack may jump from one plastic void (weak link) at FLG particles lying in the process zone to the next. These plastic voids thus act as pre-cracks and facilitate delamination growth [183, 184]. Under mode II loading, crack growth is mainly by the forming of cusps in the matrix [124, 243]. In this case, larger particles oriented in plane between two layers hinder forming of these cusps, thereby increasing the energy required to propagate the crack. This is shown in the sketched detail in Figure 4.43 and is comparable to the mechanisms reported for layered silicate [192].

Under pure quasi-static or fatigue tensile loading, the negative effect of larger crack tip delamination at FLG modified 90°-layers is hence compensated by the increased resistance against mode II delamination growth. For (partly) compressive loading, FLG nanoparticles with large planar dimensions in the interlayer are detrimental, because they favour delamination growth. The experimental results show, that a tailored modification of single

layers may be advantageous in comparison to unmodified laminates or a modification of all layers, as long as compression loading is avoided. For improved delamination resistance under mode I loading, the lateral size of the layered nanoparticles should be preferably small.

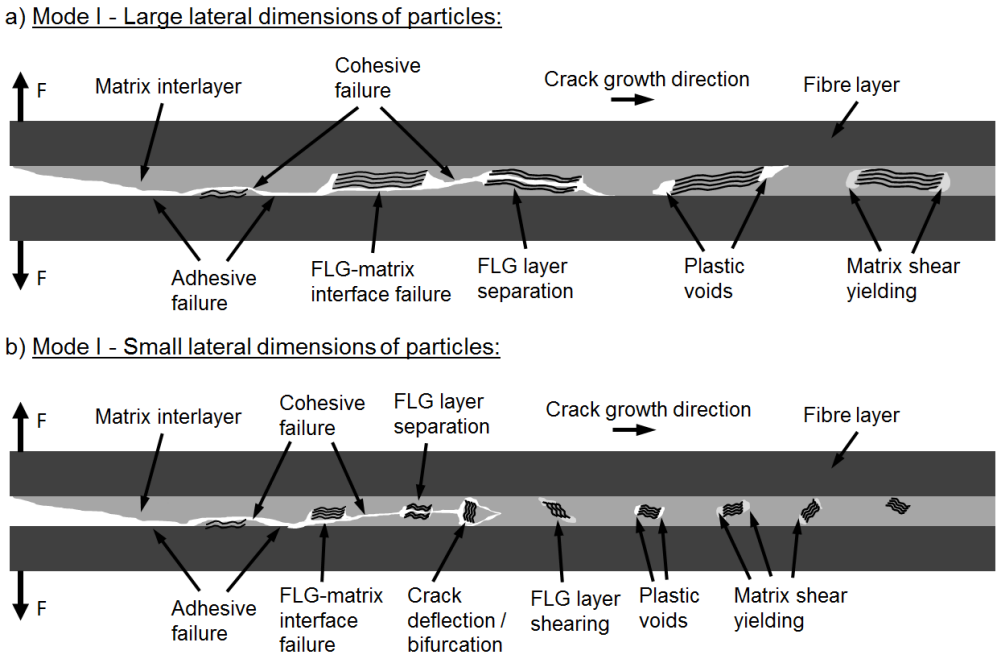

Figure 4.42: Scheme showing delamination crack growth under mode I with layered nanoparticles in the interlayer for particles with a) comparable large lateral dimensions b) small lateral dimensions.

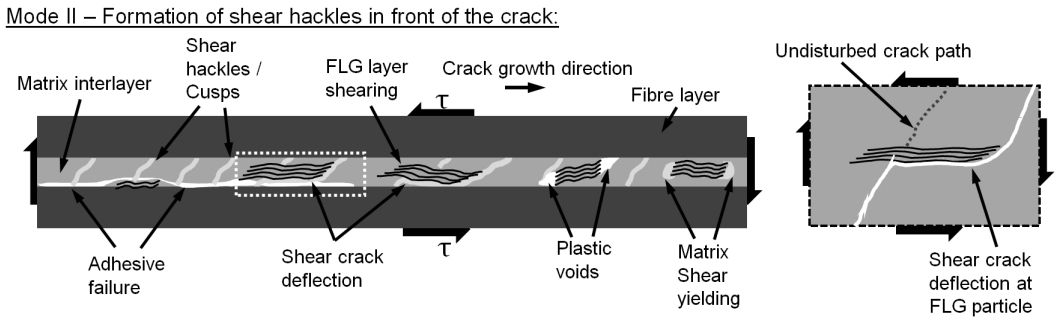

Figure 4.43: Scheme showing delamination crack growth under mode II with layered nanoparticles in the interlayer suppressing the forming of shear cusps.

5 Summary and conclusions

The research questions given in chapter 1 are addressed as follows. The observed influence of a FLG modification on the damage behaviour and mechanical properties of FRP can be explained with the results from the experiments and fractography analysis of single fibres, in which the local damage mechanisms at the particles can be clearly identified.

How does layer thickness scaling influence the mechanical properties and damage behaviour of FRP laminates?

A decrease in FRP layer thickness has a positive influence on the mechanical properties under a broad range of loading conditions, but results in a more brittle failure behaviour. At stress intensifications, a decreasing layer thickness results in higher notch sensitivity and has therefore a negative influence on the macroscopic mechanical properties. Two different aspects of layer thickness related scaling effects are investigated in detail and summarised as follows:

How does the transverse layer thickness in cross-ply laminates influence the initiation and propagation of IFF?

Decreasing the layer thickness has a positive influence on initiation and propagation of transverse cracking in FRP. As observed in experiments with model composites that allow exact observation of failure initiation, a decrease in transverse ply thickness shifts the initiation of fibre-matrix-debonding to higher global strain and thus the onset of IFF to higher loads. The subsequent damage development in the form of matrix cracks occurs in more regions but is less severe for thinner plies. For cross-ply laminates, a higher number but smaller transverse cracks and a delay in IFF initiation is observed. In addition, it is shown with AE analysis, that the transverse crack growth rate is slower with reduced layer thickness. A reduction of layer thickness hence increases the resistance against IFF and results in increased fatigue lifetime of composite parts made of thin-ply laminates.

How do layer thickness and stacking sequence influence the mechanical properties and damage process of laminates containing stress intensifications under compressive loading?

If stress concentrations are present, other factors than layer thickness also highly influence the damage behaviour and resulting mechanical properties. The experimental investigation on the influence of layer thickness and the position of the 0°-layers with an analysis of the failure process initiating at a stress concentration shows the influence of the FRP lay-up on mechanical properties and damage propagation. When regarding free edges or an impact damage as delamination inducing stress intensifications within a laminate, the position of the 0°-layer is critical for stability under compression and is thus more important than the layer thickness. Central 0°-layers show best results for OHC and CAI strength due to higher resistance against compressive buckling and better supporting effect by the adjacent layers. Nonetheless, open-hole and CAI strength are higher for thinner layers, when regarding laminates with distributed 0°-plies. This is due to a reduced delamination area resulting in a shorter unsupported length of the load bearing sublaminates. The statistical defect distribution and the increased *in situ* strength lead to a delayed damage initiation with decreasing layer thickness. Thus, the unnotched compressive strength increases with decreasing layer thickness.
With increasing layer thickness, damage in the form of IFF initiates at the stress concentration, e.g. a hole, at lower strains. This reduces the stress concentration factor and leads to a change from brittle to progressive delamination failure. In laminates with blocked plies, final failure is transverse to loading direction with an orientation along the ±45°-layers around the stress intensification that leads to a step in the fracture plane, whereas in laminates with distributes plies, final fracture occurs as one straight splitted crack transverse to loading direction. Although a more progressive failure process, as observed for higher layer thickness, is advantageous in some materials, because it results in the possibility to take measures for repair of replacement of the damaged part, a damage initiation at lower strains is mostly not acceptable for FRP and first ply failure is often a design criterion. This work may hence may help to select an appropriate stacking sequence in the design of FRP parts with stress intensifications or where impact damage cannot be excluded regarding compression behaviour.

What are promising nanoparticle morphologies for increasing fracture toughness of FRP?

With a carbon nanoparticle modification, multifunctional materials combining electrical conductivity for damage sensing with enhanced mechanical properties can be obtained.

Particle size, morphology and orientation are key factors in this context when regarding small volumes, because larger particles may initiate failure prior to material defects. A significant size effect that shows increasing tensile strength with decreasing volume due to a statistical defect distribution is identified for neat epoxy, which is according to Weibull's theory [84] and previous investigations for a different matrix system [73]. With a new concept of simultaneous testing of mechanical and electrical properties in small elongated volumes, the influence of carbon nanoparticle morphology with regard to failure initiation and damage mechanisms at the nanoscale and microscale is investigated. A clear size effect, similar to the unmodified material is measured for CB and CNT modified epoxy, whereas for a FLG modification, the used particle size is larger than material defects.
Larger FLG particles hence initiate failure prior to material defects and act as crack initiators and thus as flaws. The size of the particles is independent of specimen volume, so that the failure initiating as well as energy absorbing mechanisms are always available. In the fibres with their small volume and thus small crack area, this leads to failure initiation at the nanoparticles, counteracting any size effect due to a statistical defect distribution. In a bulk volume, energy dissipation mechanisms such as crack pinning, crack bifurcation and energy dissipation by micro-damage play a more important role, therefore higher values for tensile strength, compared to the neat matrix, are obtained with a nanoparticle modification.
No significant influence of filler content on the general behaviour with regard to the size effect is found for CB and FLG modification. The CNT modified epoxy shows a higher probability of impurities from CNT manufacturing process or small agglomerates with increasing particle weight fraction. For all investigated morphologies an increase in particle weight fraction increases fracture surface roughness and thus matrix plastic deformation during crack propagation.
Fractography analysis of SEM images shows different failure mechanisms at the nano- or micro-scale in dependence of the nanoparticle morphology. For CB modification, crack separation and local matrix plastic deformation dissipate additional energy during fracture. The dominant mechanism in CNT modified specimens is pull-out of nanoparticles, but crack bridging and nanotube rupture are also observed. For FLG modified epoxy, energy dissipating damage mechanisms are matrix shear yielding leading to plastic voids, graphene layer separation and shearing as well as pull-out of particles. Crack separation and crack bifurcation at FLG particles are observed as well. The mechanisms can be clearly identified in the small fracture surfaces. These local, distributed damage mechanisms dissipate energy, so that a carbon nanoparticle modification results in an increased fracture toughness of epoxy if the volume is large enough. For FLG, the orientation of the graphene layers with regard to loading direction is critical. Higher true failure strength is

measured with the largest particle oriented parallel to loading direction. With the identification of these single mechanisms, depending on the orientation of the graphene layers to the loading direction, theories and models about micro-damage at graphene nanoparticles are confirmed experimentally. From a design point of view, FLG and CNT are the most promising particle morphologies for improving mechanical properties, if CNT length is high enough and FLG are oriented in loading direction.

This work may thus be used as a base for developers to carefully select a nanoparticle reinforcement with regard to the desired properties and under the consideration of small volumes. For multifunctional polymer or FRP materials, CNT with a weight fraction above 0.3 wt.% are shown to be the most promising nanoparticle filler for improving both, electrical [195] and mechanical properties, even in small elongated volumes. With this modification, smart structures for health monitoring with improved mechanical properties can be designed.

Is a tailored nanoparticle modification of only some layers in a composite laminate promising for improving mechanical properties?

The modification with FLG nanoparticles influences the damage behaviour and final failure mode of CFRP. The presented tailored matrix modification approach allows exact analysis of the impact of a nanoparticle modification in either 0° or 90°-layers of CFRP cross-ply laminates on mechanical properties and damage mechanisms. A modification of the 0°-layers unexpectedly increases the quasi-static tensile strength, although dominated by fibre properties. Positive, crack stopping effects as well as negative effects, such as accelerated delamination growth are experimentally proven. Depending on the loading case, a tailored modification of single layers may be advantageous in comparison to unmodified or a modification of all layers. For quasi-static or cyclic tensile loading ($0 < R < 1$), a modification of the 90°-layers changes the transverse cracking behaviour and has the potential for delaying the initiation of IFF to higher loads. This could be useful for applications where IFF is a design criterion. For an increase in tension fatigue life of composite laminates, additionally a 0°-layer modification or a modification of all layers is promising. Furthermore, the crack growth through the material is slower and in the form of smaller cracks, leading to a significantly smaller amount of penetrating cracks. This is due to distributed micro-damage at the particles dissipating energy that is thus no longer available for intralaminar crack propagation. For an increase in fatigue life of composite laminates, a 0°-layer modification or a modification of all layers is most promising. Under partly compressive cyclic loading ($R < 0$) however, a FLG matrix modification is detrimental in both 0°-layers and 90°-layers and should be avoided. The comparable large FLG particles

are oriented along the fibres and in the 90°-layer promote large crack tip delamination. Interlaminar crack initiation and growth under mode I is favoured by FLG particles in the crack growth plane. Under compressive loading, this leads to delamination induced global loss of stability and fracture, with lower fatigue life in the t-c regime compared to unmodified laminates. Layered particles of smaller lateral dimensions however, may not exhibit this disadvantage and should be investigated further. With decreasing compression ratio of the alternating load case, the negative influences should diminish.

The dependency of interlaminar crack growth on the particle size and orientation with regard to the crack growth direction is analysed. A theoretical concept is given that explains the findings from the experiments presented here, as well as the at first sight opposing results presented in literature for mode I and mode II interlaminar (delamination) fracture toughness. For smaller particles, a higher amount of energy dissipating failure mechanisms can be activated during crack propagation in the interlayer under mode I. For larger particles that are oriented along the fibres and in line of the crack however, the crack may jump from one plastic void (weak link) at FLG particles lying in the process zone to the next. These plastic voids thus act as pre-cracks and facilitate delamination growth (refer to [183, 184]). Under mode II loading, larger particles oriented in plane between two layers hinder forming of shear cusps, thereby increasing the energy required to propagate the crack. Smaller particles are with higher probability oriented along the shear crack direction and their effect on mode II interlaminar toughness is hence negligible or even negative.

Following these remarks, the applicability of nanoparticle modified resin systems to improve the performance of FRP laminates is sensitive to the loading case. For laminates only loaded in tension a modification appears to be advantageous, whereas in case of bending or compression loads the effect of nano-particles is ambiguous and should be further clarified in future investigations.

5.1 Concluding remarks

From the respective examinations on layer-thickness effects and on the influence of a carbon nanoparticle modification with regard to damage behaviour and mechanical properties of CFRP, it can be concluded, that a combination of reduced ply thickness and matrix modification is promising for further improvement of composite materials. By modifying the matrix of thin-ply laminates, their high notch-sensitivity might be reduced with the distributed microdamage at the nanoparticles that dissipates energy, thereby reducing

local stress concentrations, e.g. at free edges like a hole. FLG nanoparticles with small or medium lateral dimensions are the most promising morphology for further investigations in this context. In Figure 5.1, the open-hole tensile fatigue behaviour for thick-ply and thin-ply CFRP laminates is shown schematically, as it is reported in literature [17]. The aim is to develop materials that comprise both the improved fatigue life of thin-ply laminates and a high resistance against premature failure at stress concentrations. The desired behaviour is shown in the diagram as a solid line. Considering also the potential of carbon nanoparticles for structural health monitoring, with the presented approach, multifunctional, self-monitoring materials with improved mechanical properties could be developed in the near future.

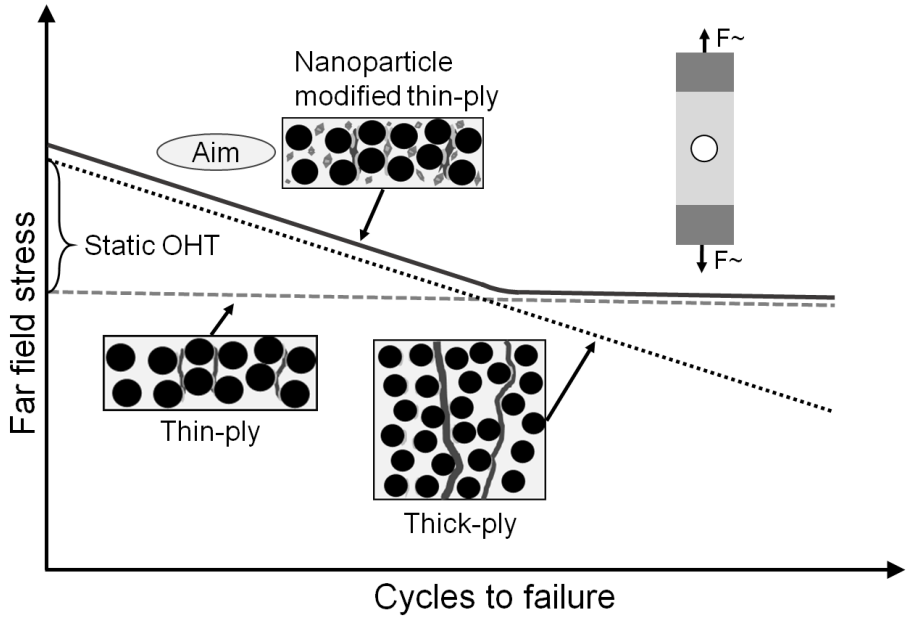

Figure 5.1: Scheme showing the potential of a carbon nanoparticle modification for reducing the notch sensitivity of thin-ply laminates and hence improving their mechanical properties with the presence of stress concentrations, e.g. an open hole.

6 Outlook

As is experimentally shown, decreasing the ply thickness and modification of the matrix with carefully selected nanoparticles has high potential for improving mechanical properties of FRP. The combination of the thin-ply technology by using a ply thickness below 50 µm with a nanoparticle modification would be the next step of research in this field. The microdamage at the nanoparticles is expected to release local stress concentration at free edges, counterbalancing the comparable high notch sensitivity of thin-ply laminates, which is one of their main disadvantages.

Incorporation of carbon nanoparticles also increases the thermal conductivity of polymers and FRP [170, 181, 246]. Hence, the influence of carbon nanoparticles on thermal residual stresses after curing of FRP is an interesting topic for further investigations. An increase in matrix thermal conductivity would result in a smaller difference between matrix and fibre thermal conductivity and thus in reduced thermal residual stresses. This should reduce local stresses after curing and lead to a slight delay of IFF initiation. The observed changes in transverse cracking behaviour in the 90°-layer with the FLG modification may also be partly attributed to reduced stress concentrations at the fibres, resulting from the decreased mismatch of the coefficients of thermal expansion.

For a more detailed investigation of the differences in transverse crack initiation and propagation in dependence of layer thickness or for investigating the influence of a nanoparticle matrix modification, continuous monitoring of internal damage during static or cyclic loading would give further insight on the influence of these variations on the damage behaviour of FRP. This could for example be achieved with X-ray Micro Computed Tomography (Micro-CT) measurements during quasi-static or cyclic tensile tests.

FLG nanoparticles with small lateral dimensions and CNT are the most promising nanoparticle morphology for improvement of FRP toughness and fatigue properties. A modification of thick-ply and thin-ply laminates and characterisation of their mechanical properties with a focus on OHT, impact and CAI as well as fatigue properties will give further insight on the potential of this material combination for highly loaded and reliable structural

parts. An evaluation of the combination of reduced ply thickness with a matrix modification is thus interesting from both a scientific and an industrial point of view. Due to the improved fatigue behaviour of thin-ply laminates but their notch and impact sensitivity, the toughening effect of a matrix modification is of particular interest for evaluation of fatigue after impact properties of unmodified and nanoparticle modified thin-ply laminates. Furthermore, this would be a common load case of structural parts. An experimental investigation to address this topic is currently in planning and will be carried out in the near future.

In addition, the influence of nanoparticle matrix modification on the interfacial strength and fibre-matrix debonding behaviour at the microscale is an interesting approach. This can be carried out either by single fibre fragmentation tests or in transverse tensile tests by using model composites with several fibres oriented transverse to loading direction and the particles in between these fibres [183]. Combining this approach with a crucifix specimen geometry as used in this thesis would allow for investigation of the fibre matrix debonding and IFF propagation under light microscopy in a defined area, where damage is expected to initiate. A mould for producing such specimens was already designed and some preliminary tests confirming the feasibility of the approach with model composites were executed.

An FEM model was developed that can be used for micromechanical investigation on transverse crack initiation and propagation in cross-ply laminates [222]. The model is currently complemented by incorporating thermal residual stresses, a statistical variation of the interfacial strength between fibres and matrix and the possibility to add regions with different properties into the matrix, representing the influence zone of flake-shaped nanoparticles, such as graphene based or silica nanoparticles. The FEM model may serve as a simulation tool to investigate the influence of ply thickness and matrix nanoparticle modification for finding the most promising combinations regarding damage propagation behaviour and mechanical properties, although limited to investigation of IFF in cross-ply laminates under tensile loading. The model with the unmodified matrix is validated by comparing its behaviour with experimental results for cross-ply laminates [222]. A quantitative validation of simulation results with nanoparticle modified matrix e.g. with the experimental results of FLG modified cross-ply laminates presented within this thesis is possible. With this model, different configurations could be analysed without any costly and time consuming test effort.

Continuation of this research is assured within the project "*Schadenstolerante dünnschichtige (Thin-Ply) Kohlenstofffaser-Kunststoff-Verbunde mit Graphen-verstärktem Matrixsystem*"

funded by DFG (FI688/5-1) in which the impact of a carbon nanoparticle matrix modification on the mechanical properties and damage behaviour of thin-ply laminates is investigated.

Bibliography

[1] D. J. Mortell, D. A. Tanner, C. T. McCarthy, In-situ sem study of transverse cracking and delamination in laminated composite materials, Composites Science and Technology 105 (2014) 118–126. doi:10.1016/j.compscitech.2014.10.012.

[2] C. Garnier, M.-L. Pastor, F. Eyma, B. Lorrain, The detection of aeronautical defects in situ on composite structures using non destructive testing, Composite Structures 93 (5) (2011) 1328–1336. doi:10.1016/j.compstruct.2010.10.017.

[3] L. Cheng, G. Y. Tian, Comparison of nondestructive testing methods on detection of delaminations in composites, Journal of Sensors 2012 (2012) 7. doi:10.1155/2012/408437.

[4] S. Gholizadeh, A review of non-destructive testing methods of composite materials, XV Portuguese Conference on Fracture, PCF 2016, 10-12 February 2016, Paco de Arcos, Portugal 1 (2016) 50–57. doi:10.1016/j.prostr.2016.02.008.

[5] A. Parvizi, K. W. Garrett, J. E. Bailey, Constrained cracking in glass fibre-reinforced epoxy cross-ply laminates, Journal of Materials Science 13 (1) (1978) 195–201. doi:10.1007/BF00739291.

[6] A. Hosoi, S. Sakuma, Y. Fujita, H. Kawada, Prediction of initiation of transverse cracks in cross-ply CFRP laminates under fatigue loading by fatigue properties of unidirectional CFRP in 90° direction, Composites Part A: Applied Science and Manufacturing 68 (2015) 398–405. doi:10.1016/j.compositesa.2014.10.022.

[7] S. Sihn, R. Y. Kim, K. Kawabe, S. W. Tsai, Experimental studies of thin-ply laminated composites, Composites Science and Technology 67 (6) (2007) 996–1008. doi:10.1016/j.compscitech.2006.06.008.

[8] R. J. Young, I. A. Kinloch, L. Gong, K. S. Novoselov, The mechanics of graphene nanocomposites: A review, Composites Science and Technology 72 (12) (2012) 1459–1476. doi:10.1016/j.compscitech.2012.05.005.

[9] M. Quaresimin, K. Schulte, M. Zappalorto, S. Chandrasekaran, Toughening mechanisms in polymer nanocomposites: From experiments to modelling, Composites Science and Technology 123 (2016) 187–204. doi:10.1016/j.compscitech.2015.11.027.

[10] B. T. Marouf, Y.-W. Mai, R. Bagheri, R. A. Pearson, Toughening of epoxy nanocomposites: Nano and hybrid effects, Polymer Reviews 56 (1) (2016) 70–112. doi:10.1080/15583724.2015.1086368.

[11] Y. Tang, L. Ye, Z. Zhang, K. Friedrich, Interlaminar fracture toughness and cai strength of fibre-reinforced composites with nanoparticles – a review, Composites Science and Technology 86 (2013) 26–37. doi:10.1016/j.compscitech.2013.06.021.

[12] C. Mittelstedt, W. Becker, Free-edge effects in composite laminates, Applied Mechanics Reviews 60 (5) (2007) 217–245. doi:10.1115/1.2777169.

[13] R. B. Pipes, N. J. Pagano, Interlaminar stresses in composite laminates under uniform axial extension, Journal of Composite Materials 4 (4) (1970) 538–548. doi:10.1177/002199837000400409.

[14] N. J. Pagano, R. B. Pipes, The influence of stacking sequence on laminate strength, Journal of Composite Materials 5 (1) (1971) 50–57. doi:10.1177/002199837100500105.

[15] K. Kawabe, S. Tomoda, Multi-filament split-yarn sheet and method and device for the manufacture thereof (patent) (2000).
URL https://www.google.com/patents/US6032342

[16] S. W. Tsai, S. Sihn, R. Y. Kim, Thin ply composites, in: 46th AIAA/ASME/ASCE/AHS/ASC Structures 2005, Structural Dynamics & Materials Conference, Austin, Texas, USA, 2005. doi:10.2514/6.2005-2005.
URL http://dx.doi.org/10.2514/6.2005-2005

[17] R. Amacher, J. Cugnoni, J. Botsis, L. Sorensen, W. Smith, C. Dransfeld, Thin ply composites: Experimental characterization and modeling of size-effects, Composites Science and Technology 101 (2014) 121–132. doi:10.1016/j.compscitech.2014.06.027.

[18] P. P. Camanho, A. Arteiro, A. Turon, J. Costa, E. G. Guillamet, Structural integrity of thin-ply laminates, JEC Composites Magazine (71) (2012) 91–92.

[19] H. Saito, M. Morita, K. Kawabe, M. Kanesaki, H. Takeuchi, M. Tanaka, I. Kimpara, Effect of ply-thickness on impact damage morphology in CFRP laminates, Journal of Reinforced Plastics and Composites 30 (13) (2011) 1097–1106. doi:10.1177/0731684411416532.

[20] B. Fiedler, F. H. Gojny, M. H. Wichmann, M. C. Nolte, K. Schulte, Fundamental aspects of nano-reinforced composites, Composites Science and Technology 66 (16) (2006) 3115–3125. doi:10.1016/j.compscitech.2005.01.014.

[21] C. Zweben, Is there a size effect in composites? designer's corner, Composites 25 (6) (1994) 451–454. doi:10.1016/0010-4361(94)90102-3.

[22] E. Pullicino, C. Soutis, M. Gresil, Gambling with graphene.... will it pay off?, JEC Composites Magazine (99) (2015) 41–44.

[23] J. B. Knoll, B. T. Riecken, N. Kosmann, S. Chandrasekaran, K. Schulte, B. Fiedler, The effect of carbon nanoparticles on the fatigue performance of carbon fibre reinforced epoxy, Composites Part A: Applied Science and Manufacturing 67 (2014) 233–240. doi:10.1016/j.compositesa.2014.08.022.

[24] H. Schürmann, Konstruieren Mit Faser-Kunststoff-Verbunden, 2nd Edition, VDI-Buch, Springer-Verlag, Berlin, 2008.

[25] M. Flemming, G. Ziegmann, S. Roth, Faserverbundbauweisen: Halbzeuge und Bauweisen, Springer-Verlag, Berlin, 1996.

[26] M. Flemming, G. Ziegmann, S. Roth, Faserverbundbauweisen: Fertigungsverfahren mit duroplastischer Matrix, Springer-Verlag, Berlin, 1999.

[27] T. Hobbiebrunken, M. Hojo, T. Adachi, C. de Jong, B. Fiedler, Evaluation of interfacial strength in cf/epoxies using fem and in-situ experiments, Composites Part A: Applied Science and Manufacturing 37 (12) (2006) 2248–2256. doi:10.1016/j.compositesa.2005.12.021.

[28] B. Fiedler, C. de Jong, T. Hobbiebrunken, M. Hojo, K. Schulte, Micro/macro-mechanical approach of first ply failure in CFRP, Journal of Materials Science 41 (20) (2006) 6760–6767. doi:10.1007/s10853-006-0215-4.

[29] I. M. Daniel, O. Ishai, Engineering mechanics of composite materials, Oxford University Press, New York, 1994.

[30] B. Fiedler, M. Hojo, S. Ochiai, K. Schulte, M. Ochi, Finite-element modeling of initial matrix failure in CFRP under static transverse tensile load, Composites Science and Technology 61 (1) (2001) 95–105. doi:10.1016/S0266-3538(00)00198-6.

[31] H. Zhang, M. L. Ericson, J. Varna, L. A. Berglund, Transverse single-fibre test for interfacial debonding in composites: 1. experimental observations, Composites Part A: Applied Science and Manufacturing 28 (4) (1997) 309–315. doi:10.1016/S1359-835X(96)00123-6.

[32] J. Varna, L. A. Berglund, M. L. Ericson, Transverse single-fibre test for interfacial debonding in composites: 2. modelling, Composites Part A: Applied Science and Manufacturing 28 (4) (1997) 317–326. doi:10.1016/S1359-835X(96)00125-X.

[33] K. Martyniuk, B. F. Sørensen, P. Modregger, E. M. Lauridsen, 3d in situ observations of glass fibre/matrix interfacial debonding, Composites Part A: Applied Science and Manufacturing 55 (2013) 63–73. doi:10.1016/j.compositesa.2013.07.012.

[34] M. F. Munoz-Velez, A. Valadez-Gonzalez, P. J. Herrera-Franco, Effect of fiber surface treatment on the incorporation of carbon nanotubes and on the micromechanical properties of a single-carbon fiber-epoxy matrix composite, Express Polymer Letters 11 (9) (2017) 704–718. doi:10.3144/expresspolymlett.2017.68.

[35] G. J. Dvorak, N. Laws, Analysis of progressive matrix cracking in composite laminates ii. first ply failure, Journal of Composite Materials 21 (4) (1987) 309–329. doi:10.1177/002199838702100402.

[36] D. Gross, T. Seelig, Fracture Mechanics, Springer-Verlag, Berlin, 2011. doi:10.1007/978-3-642-19240-1.

[37] B. W. Rosen, Mechanics of composite strengthening: American society for metals: Seminar on fiber composite materials (October 17, 1964).

[38] P. M. Moran, X. H. Liu, C. F. Shih, Kink band formation and band broadening in fiber composites under compressive loading, Acta Metallurgica et Materialia 43 (8) (1995) 2943–2958. doi:10.1016/0956-7151(95)00001-C.

[39] J. S. Poulsen, P. M. Moran, C. F. Shih, E. Byskov, Kink band initiation and band broadening in clear wood under compressive loading, Mechanics of Materials 25 (1) (1997) 67–77. doi:10.1016/S0167-6636(96)00043-9.

[40] N. A. Fleck, P. Jelf, P. Curtis, Compressive failure of laminated and woven composites: Compressive failure of laminated and woven composites, Journal of Composites, Technology and Research 17 (3) (1995) 212–220.

[41] B. Budiansky, N. A. Fleck, Compressive failure of fibre composites, Journal of the Mechanics and Physics of Solids 41 (1) (1993) 183–211. doi:10.1016/0022-5096(93)90068-Q.

[42] B. Budiansky, N. A. Fleck, J. C. Amazigo, On kink-band propagation in fiber composites, Journal of the Mechanics and Physics of Solids 46 (9) (1998) 1637–1653. doi:10.1016/S0022-5096(97)00042-2.

[43] W. V. Liebig, C. Leopold, K. Schulte, Photoelastic study of stresses in the vicinity of a unique void in a fibre-reinforced model composite under compression, Composites Science and Technology 84 (2013) 72–77. doi:10.1016/j.compscitech.2013.04.011.

[44] W. V. Liebig, K. Schulte, B. Fiedler, Hierarchical analysis of the degradation of fibre-reinforced polymers under the presence of void imperfections, Philosophical transactions. Series A, Mathematical, physical, and engineering sciences 374 (2071) (2016) 20150279. doi:10.1098/rsta.2015.0279.

[45] S. S. Shams, R. F. Elhajjar, Investigation into the effects of fiber waviness in standard notched composite specimens, CEAS Aeronautical Journal 6 (4) (2015) 541–555. doi:10.1007/s13272-015-0161-4.

[46] R. Gutkin, S. T. Pinho, P. Robinson, P. Curtis, On the transition from shear-driven fibre compressive failure to fibre kinking in notched CFRP laminates under longitudinal compression, Composites Science and Technology 70 (8) (2010) 1223–1231. doi:10.1016/j.compscitech.2010.03.010.

[47] R. Gutkin, S. T. Pinho, P. Robinson, P. Curtis, Micro-mechanical modelling of shear-driven fibre compressive failure and of fibre kinking for failure envelope generation in CFRP laminates, Composites Science and Technology 70 (8) (2010) 1214–1222. doi:10.1016/j.compscitech.2010.03.009.

[48] M. Richardson, M. J. Wisheart, Review of low-velocity impact properties of composite materials, Composites Part A: Applied Science and Manufacturing 27 (12) (1996) 1123–1131. doi:10.1016/1359-835X(96)00074-7.

[49] Guynn, E., T. K. O'Brien, The influence of lay-up and thickness on composite impact damage and compression strength, in: 26th Structures, Structural Dynamics, and Materials Conference, Structures, Structural Dynamics, and Materials and Co-located Conferences, American Institute of Aeronautics and Astronautics, 1985. doi:10.2514/6.1985-646.
URL http://dx.doi.org/10.2514/6.1985-646

[50] J. C. Prichard, P. J. Hogg, The role of impact damage in post-impact compression testing, Composites 21 (6) (1990) 503–511. doi:10.1016/0010-4361(90)90423-T.

[51] V. J. Hawyes, P. T. Curtis, C. Soutis, Effect of impact damage on the compressive response of composite laminates, Composites Part A: Applied Science and Manufacturing 32 (9) (2001) 1263–1270. doi:10.1016/S1359-835X(01)00072-0.

[52] N. Tai, M. Yip, J. Lin, Effects of low-energy impact on the fatigue behavior of carbon/epoxy composites, Composites Science and Technology 58 (1) (1998) 1–8. doi:10.1016/S0266-3538(97)00075-4.

[53] N. Kosmann, B. T. Riecken, H. Schmutzler, J. B. Knoll, K. Schulte, B. Fiedler, Evaluation of a critical impact energy in GFRP under fatigue loading, Composites Science and Technology 102 (2014) 28–34. doi:10.1016/j.compscitech.2014.07.010.

[54] N. Kosmann, Einfluss von Defekten auf das Degradationsverhalten faserverstärkter Kunststoffe. (Dissertation), TuTech-Verlag, 2015.

[55] K. W. Garrett, J. E. Bailey, Multiple transverse fracture in 90 cross-ply laminates of a glass fibre-reinforced polyester, Journal of Materials Science 12 (1) (1977) 157–168. doi:10.1007/BF00738481.

[56] A. Parvizi, J. E. Bailey, On multiple transverse cracking in glass fibre epoxy cross-ply laminates, Journal of Materials Science 13 (10) (1978) 2131–2136. doi:10.1007/BF00541666.

[57] J. E. Bailey, P. Curtis, A. Parvizi, On the transverse cracking and longitudinal splitting behaviour of glass and carbon fibre reinforced epoxy cross ply laminates and the effect of poisson and thermally generated strain, Proceedings of the Royal Society of London A: Mathematical, Physical and Engineering Sciences 366 (1727) (1979) 599–623. doi:10.1098/rspa.1979.0071.

[58] R. Talreja, Fatigue of composite materials: damage mechanisms and fatigue-life diagrams, Proceedings of the Royal Society of London A: Mathematical, Physical and Engineering Sciences 378 (1775) (1981) 461. doi:10.1098/rspa.1981.0163.

[59] K. L. Reifsnider, K. Schulte, J. C. Duke, Long-term fatigue behavior of composite materials, in: T. K. O'Brien (Ed.), Long-Term Behavior of Composites, ASTM International, 1983, pp. 136–159. doi:10.1520/STP31820S.

[60] K. L. Reifsnider, R. Jamison, Fracture of fatigue-loaded composite laminates, International Journal of Fatigue 4 (4) (1982) 187–197. doi:10.1016/0142-1123(82)90001-9.

[61] A. Hosoi, K. Kurihara, N. Sato, H. Kawada, Prediction of initiation of transverse cracks in cross-ply CFRP laminates under fatigue loading, International Journal of The Institute of Materials Malaysia (IJIMM) 1 (2) (2015) 157–164.

[62] A. A. Griffith, The phenomena of rupture and flow in solids, Philosophical Transactions of the Royal Society of London A: Mathematical, Physical and Engineering Sciences 221 (582-593) (1921) 163–198. doi:10.1098/rsta.1921.0006.

[63] A. J. Kinloch, R. J. Young, Fracture Behaviour of Polymers, Springer Netherlands, Dordrecht, 1995.

[64] M. R. Wisnom, Jones, M. I., Size effects in interlaminar tensile and shear strength of unidirectional glass fibre/epoxy, Journal of Reinforced Plastics and Composites 15 (1) (1996) 2–15. doi:10.1177/073168449601500101.

[65] J. Lee, C. Soutis, Thickness effect on the compressive strength of T800/924C carbon fibre-epoxy laminates, Composites Part A: Applied Science and Manufacturing 36 (2) (2005) 213–227. doi:10.1016/j.compositesa.2004.06.010.

[66] J. Lee, C. Soutis, A study on the compressive strength of thick carbon fibre-epoxy laminates, Composites Science and Technology 67 (10) (2007) 2015–2026. doi:10.1016/j.compscitech.2006.12.001.

[67] M. R. Wisnom, B. Khan, S. R. Hallett, Size effects in unnotched tensile strength of unidirectional and quasi-isotropic carbon/epoxy composites, Composite Structures 84 (1) (2008) 21–28. doi:10.1016/j.compstruct.2007.06.002.

[68] R. W. Hertzberg, R. P. Vinci, J. L. Hertzberg, Deformation and fracture mechanics of engineering materials, 5th Edition, Wiley-VCH.

[69] P. Rose, Hochfeste C-Fasern auf PAN-Basis, Einsatzformen und Eigenschaften im CFK-Verbund, in: Verarbeiten und Anwenden kohlenstoffaserverstärkter Kunststoffe, VDI-Verlag, Düsseldorf, 1981, pp. 5–39.

[70] D. J. Thorne, Carbon fibres with large breaking strain, Nature 248 (5451) (1974) 754–756. doi:10.1038/248754a0.

[71] D. J. Thorne, Distribution of internal flaws in acrylic fibers, Journal of Applied Polymer Science 14 (1) (1970) 103–113. doi:10.1002/app.1970.070140111.

[72] A. Towse, K. Potter, M. R. Wisnom, R. D. Adams, Specimen size effects in the tensile failure strain of an epoxy adhesive, Journal of Materials Science 33 (17) (1998) 4307–4314. doi:10.1023/A:1004487505391.

[73] T. Hobbiebrunken, B. Fiedler, M. Hojo, M. Tanaka, Experimental determination of the true epoxy resin strength using micro-scaled specimens, Composites Part A: Applied Science and Manufacturing 38 (3) (2007) 814–818. doi:10.1016/j.compositesa.2006.08.006.

[74] H. E. Daniels, The statistical theory of the strength of bundles of threads. I, Philosophical Transactions of the Royal Society of London A: Mathematical, Physical and Engineering Sciences 183 (995) (1945) 405. doi:10.1098/rspa.1945.0011.

[75] B. W. Rosen, Tensile failure of fibrous composites, AIAA Journal 2 (11) (1964) 1985–1991. doi:10.2514/3.2699.

[76] C. Zweben, B. W. Rosen, A statistical theory of material strength with application to composite materials, Journal of the Mechanics and Physics of Solids 18 (3) (1970) 189–206. doi:10.1016/0022-5096(70)90023-2.

[77] D. Hull, Matrix-dominated properties of polymer matrix composite materials, Materials Science and Engineering: A 184 (2) (1994) 173–183. doi:10.1016/0921-5093(94)91030-8.

[78] D. F. Adams, T. R. King, D. M. Blackketter, Evaluation of the transverse flexure test method for composite materials, Composites Science and Technology 39 (4) (1990) 341–353. doi:10.1016/0266-3538(90)90080-O.

[79] T. K. O'Brien, S. A. Salpekar, Scale effects on the transverse tensile strength of graphite/epoxy composites: Presented at the 11th ASTM Symposium on Composite Materials: Testing and Design, Pittsburgh, USA, NASA technical memorandum (1992).

[80] M. R. Wisnom, Size effects in tensile, compressive and interlaminar failure of unidirectional composites, American Society of Mechanical Engineers, Aerospace Division (Publication) AD 55.

[81] S. Mespoulet, Through-thickness test methods for laminated composite materials: (PhD Thesis), University of London, 1998.

[82] T. K. O'Brien, A. D. Chawan, K. DeMarco, I. Paris, Influence of specimen preparation and specimen size on composite transverse tensile strength and scatter, NASA Langley Technical Report NASA TM-2001-211030 (2001) (ARL-TR-2540).

[83] W. V. Liebig, C. Leopold, T. Hobbiebrunken, B. Fiedler, New test approach to determine the transverse tensile strength of CFRP with regard to the size effect, Composites Communications 1 (2016) 54–59. doi:10.1016/j.coco.2016.09.003.

[84] W. Weibull, A statistical distribution function of wide applicability, Journal of Applied Mechancis 18 (1951) 293–29.

[85] L. Sutherland, R. Shenoi, S. Lewis, Size and scale effects in composites: I. literature review, Composites Science and Technology 59 (2) (1999) 209–220. doi:10.1016/S0266-3538(98)00065-7.

[86] D. L. Flaggs, M. H. Kural, Experimental determination of the in situ transverse lamina strength in graphite/epoxy laminates, Journal of Composite Materials 16 (2) (1982) 103–116. doi:10.1177/002199838201600203.

[87] P. P. Camanho, C. G. Dávila, S. T. Pinho, L. Iannucci, P. Robinson, Prediction of in situ strengths and matrix cracking in composites under transverse tension and in-plane shear, CompTest 2004 37 (2) (2006) 165–176. doi:10.1016/j.compositesa.2005.04.023.

[88] A. Arteiro, G. Catalanotti, A. R. Melro, P. Linde, P. P. Camanho, Micro-mechanical analysis of the in situ effect in polymer composite laminates, Composite Structures 116 (2014) 827–840. doi:10.1016/j.compstruct.2014.06.014.

[89] T. A. Sebaey, J. Costa, P. Maimí, Y. Batista, N. Blanco, J. A. Mayugo, Measurement of the in situ transverse tensile strength of composite plies by means of the real time monitoring of microcracking, Composites Part B: Engineering 65 (2014) 40–46. doi:10.1016/j.compositesb.2014.02.001.

[90] T. Okabe, H. Imamura, Y. Sato, R. Higuchi, J. Koyanagi, R. Talreja, Experimental and numerical studies of initial cracking in CFRP cross-ply laminates, Composites Part A: Applied Science and Manufacturing 68 (2015) 81–89. doi:10.1016/j.compositesa.2014.09.020.

[91] A. Arteiro, G. Catalanotti, J. Xavier, P. P. Camanho, Notched response of non-crimp fabric thin-ply laminates, Composites Science and Technology 79 (2013) 97–114. doi:10.1016/j.compscitech.2013.02.001.

[92] A. Arteiro, G. Catalanotti, J. Xavier, P. P. Camanho, Notched response of non-crimp fabric thin-ply laminates: Analysis methods, Composites Science and Technology 88 (2013) 165–171. doi:10.1016/j.compscitech.2013.09.003.

[93] C. Furtado, A. Arteiro, G. Catalanotti, J. Xavier, P. P. Camanho, Selective ply-level hybridisation for improved notched response of composite laminates, Composite Structures 145 (2016) 1–14. doi:10.1016/j.compstruct.2016.02.050.

[94] T. Yokozeki, T. Aoki, T. Ishikawa, Transverse Crack Propagation in the Specimen Width Direction of CFRP Laminates under Static Tensile Loadings, Journal of Composite Materials 36 (17) (2002) 2085–2099. doi:10.1177/0021998302036017978.

[95] H. Saito, H. Takeuchi, I. Kimpara, Experimental evaluation of the damage growth restraining in 90° layer of thin-ply CFRP cross-ply laminates, Advanced Composite Materials 21 (1) (2012) 57–66. doi:10.1163/156855112X629522.

[96] C. Baker, G. N. Morscher, V. V. Pujar, J. R. Lemanski, Transverse cracking in carbon fiber reinforced polymer composites: Modal acoustic emission and peak frequency analysis, Composites Science and Technology 116 (2015) 26–32. doi:10.1016/j.compscitech.2015.05.005.

[97] H. M. EL-Dessouky, C. A. Lawrence, Ultra-lightweight carbon fibre/thermoplastic composite material using spread tow technology, Composites Part B: Engineering 50 (2013) 91–97. doi:10.1016/j.compositesb.2013.01.026.

[98] G. Czél, M. R. Wisnom, Demonstration of pseudo-ductility in high performance glass/epoxy composites by hybridisation with thin-ply carbon prepreg, Composites Part A: Applied Science and Manufacturing 52 (2013) 23–30. doi:10.1016/j.compositesa.2013.04.006.

[99] K. Masania, R. Geissberger, D. Stefaniak, C. Dransfeld, Steel foil reinforced composites: experimental and numerical study of strength, plasticity and ply size effects, in: O. von Estorff, F. Thielecke (Eds.), Proceedings of the 5th International Workshop on Aircraft System Technologies, Berichte aus der Luft- und Raumfahrttechnik, Shaker, Herzogenrath, 2015.

[100] H. Saito, H. Takeuchi, I. Kimpara, A study of crack suppression mechanism of thin-ply carbon-fiber-reinforced polymer laminate with mesoscopic numerical simulation, Journal of Composite Materials 48 (17) (2014) 2085–2096. doi:10.1177/0021998313494430.

[101] G. Guillamet, A. Turon, J. Costa, J. Renart, P. Linde, J. A. Mayugo, Damage occurrence at edges of non-crimp-fabric thin-ply laminates under off-axis uniaxial loading, Composites Science and Technology 98 (2014) 44–50. doi:10.1016/j.compscitech.2014.04.014.

[102] Y. Yuan, X. Yao, B. Liu, H. Yang, H. Imtiaz, Failure modes and strength prediction of thin ply CFRP angle-ply laminates, Composite Structures 176 (2017) 729–735. doi:10.1016/j.compstruct.2017.06.005.

[103] Y. Nishikawa, K. Okubo, T. Fujii, K. Kawabe, Fatigue crack constraint in plain-woven CFRP using newly-developed spread tows, The Third International Conference on Fatigue of Composites 28 (10) (2006) 1248–1253. doi:10.1016/j.ijfatigue.2006.02.010.

[104] International Organization for Standardization, DIN EN ISO 527-4 Plastics - Determination of tensile properties - Part 4: Test conditions for isotropic and orthotropic fibre-reinforced plastic composites (1997).

[105] T. Yokozeki, Y. Aoki, T. Ogasawara, Experimental characterization of strength and damage resistance properties of thin-ply carbon fiber/toughened epoxy laminates, Composite Structures 82 (3) (2008) 382–389. doi:10.1016/j.compstruct.2007.01.015.

[106] M. R. Wisnom, S. R. Hallett, C. Soutis, Scaling effects in notched composites, Journal of Composite Materials 44 (2) (2010) 195–210. doi:10.1177/0021998309339865.

[107] B. Kötter, D. Polyak, J. Körbelin, B. Fiedler, Influence of ply thickness in CFRP laminates on failure initiation, propagation and mechanical properties: 7th International Conference on Fatigue of Composites (ICFC 7) (2018).

[108] M. R. Wisnom, Size effects in the testing of fibre-composite materials, Composites Science and Technology 59 (13) (1999) 1937–1957. doi:10.1016/S0266-3538(99)00053-6.

[109] C. Soutis, Measurement of the static compressive strength of carbon-fibre/epoxy laminates, Composites Science and Technology 42 (4) (1991) 373–392. doi:10.1016/0266-3538(91)90064-V.

[110] J. Lee, C. Soutis, Measuring the notched compressive strength of composite laminates: Specimen size effects, Composites Science and Technology 68 (12) (2008) 2359–2366. doi:10.1016/j.compscitech.2007.09.003.

[111] C. Soutis, J. Lee, Scaling effects in notched carbon fibre/epoxy composites loaded in compression, Journal of Materials Science 43 (20) (2008) 6593–6598. doi:10.1007/s10853-008-2807-7.

[112] A. Arteiro, G. Catalanotti, A. R. Melro, P. Linde, P. P. Camanho, Micro-mechanical analysis of the effect of ply thickness on the transverse compressive strength of polymer composites, Composites Part A: Applied Science and Manufacturing 79 (2015) 127–137. doi:10.1016/j.compositesa.2015.09.015.

[113] C. Soutis, N. A. Fleck, P. A. Smith, Failure prediction technique for compression loaded carbon fibre-epoxy laminate with open holes, Journal of Composite Materials 25 (11) (1991) 1476–1498. doi:10.1177/002199839102501106.

[114] G. H. Erçin, P. P. Camanho, J. Xavier, G. Catalanotti, S. Mahdi, P. Linde, Size effects on the tensile and compressive failure of notched composite laminates, Composite Structures 96 (2013) 736–744. doi:10.1016/j.compstruct.2012.10.004.

[115] H. Suemasu, H. Takahashi, T. Ishikawa, On failure mechanisms of composite laminates with an open hole subjected to compressive load, Composites Science and Technology 66 (5) (2006) 634–641. doi:10.1016/j.compscitech.2005.07.042.

[116] J. Wang, P. Callus, M. Bannister, Experimental and numerical investigation of the tension and compression strength of un-notched and notched quasi-isotropic laminates, Composite Structures 64 (3–4) (2004) 297–306. doi:10.1016/j.compstruct.2003.08.012.

[117] E. Fuoss, P. V. Straznicky, C. Poon, Effects of stacking sequence on the impact resistance in composite laminates - part 1: parametric study, Composite Structures 41 (1) (1998) 67–77. doi:10.1016/S0263-8223(98)00036-1.

[118] E. V. González, P. Maimí, P. P. Camanho, C. S. Lopes, N. Blanco, Effects of ply clustering in laminated composite plates under low-velocity impact loading, Composites Science and Technology 71 (6) (2011) 805–817. doi:10.1016/j.compscitech.2010.12.018.

[119] E. V. González, P. Maimí, P. P. Camanho, A. Turon, J. A. Mayugo, Simulation of drop-weight impact and compression after impact tests on composite laminates, Composite Structures 94 (11) (2012) 3364–3378. doi:10.1016/j.compstruct.2012.05.015.

[120] D. Bull, S. Spearing, I. Sinclair, Observations of damage development from compression-after-impact experiments using ex situ micro-focus computed tomography, Composites Science and Technology 97 (2014) 106–114. doi:10.1016/j.compscitech.2014.04.008.

[121] E. Fuoss, P. V. Straznicky, C. Poon, Effects of stacking sequence on the impact resistance in composite laminates. part 2: prediction method, Composite Structures 41 (2) (1998) 177–186. doi:10.1016/S0263-8223(98)00037-3.

[122] T. Yokozeki, A. Kuroda, A. Yoshimura, T. Ogasawara, T. Aoki, Damage characterization in thin-ply composite laminates under out-of-plane transverse loadings, Composite Structures 93 (1) (2010) 49–57. doi:10.1016/j.compstruct.2010.06.016.

[123] R. Olsson, A. André, P. Hellström, Analytical modelling and FE simulation of impact response and damage growth in a thin-ply laminate, in: ICCM-20 - 20th International Conference on Composite Materials, Copenhagen, Denmark, 2015.

[124] E. S. Greenhalgh, C. Rogers, P. Robinson, Fractographic observations on delamination growth and the subsequent migration through the laminate, Composites Science and Technology 69 (14) (2009) 2345–2351. doi:10.1016/j.compscitech.2009.01.034.

[125] A. K. Geim, K. S. Novoselov, The rise of graphene, Nature Materials 6 (3) (2007) 183–191. doi:10.1038/nmat1849.

[126] K. S. Novoselov, A. K. Geim, S. V. Morozov, D. Jiang, Y. Zhang, S. V. Dubonos, I. V. Grigorieva, A. A. Firsov, Electric field effect in atomically thin carbon films, Science 306 (5696) (2004) 666. doi:10.1126/science.1102896.

[127] H. W. Kroto, J. R. Heath, S. C. O'Brien, R. F. Curl, R. E. Smalley, C60: Buckminsterfullerene, Nature 318 (1985) 162–163.

[128] H. Hanaei, M. K. Assadi, R. Saidur, Highly efficient antireflective and self-cleaning coatings that incorporate carbon nanotubes (CNTs) into solar cells: A review, Renewable and Sustainable Energy Reviews 59 (2016) 620–635. doi:10.1016/j.rser.2016.01.017.

[129] T.-H. Hsieh, A. J. Kinloch, K. Masania, A. C. Taylor, S. Sprenger, The mechanisms and mechanics of the toughening of epoxy polymers modified with silica nanoparticles, Polymer 51 (26) (2010) 6284–6294. doi:10.1016/j.polymer.2010.10.048.

[130] R. P. Singh, M. Zhang, D. Chan, Toughening of a brittle thermosetting polymer: Effects of reinforcement particle size and volume fraction, Journal of Materials Science 37 (4) (2002) 781–788. doi:10.1023/A:1013844015493.

[131] T. Liu, W. C. Tjiu, Y. Tong, C. He, S. S. Goh, T.-S. Chung, Morphology and fracture behavior of intercalated epoxy/clay nanocomposites, Journal of Applied Polymer Science 94 (3) (2004) 1236–1244. doi:10.1002/app.21033.

[132] M. Zappalorto, M. Salviato, M. Quaresimin, Mixed mode (I + II) fracture toughness of polymer nanoclay nanocomposites, Engineering Fracture Mechanics 111 (2013) 50–64. doi:10.1016/j.engfracmech.2013.09.006.

[133] E. H. Backes, F. R. Passador, C. Leopold, B. Fiedler, L. A. Pessan, Electrical, thermal and thermo-mechanical properties of epoxy/multi-wall carbon nanotubes/mineral fillers nanocomposites, Journal of Composite Materials 74 (7) (2018) 2513–2533. doi:10.1177/0021998318763497.

[134] L.-C. Tang, Y.-J. Wan, D. Yan, Y.-B. Pei, L. Zhao, Y.-B. Li, L.-B. Wu, J.-X. Jiang, G.-Q. Lai, The effect of graphene dispersion on the mechanical properties of graphene/epoxy composites, Carbon 60 (2013) 16–27. doi:10.1016/j.carbon.2013.03.050.

[135] F. H. Gojny, M. H. Wichmann, B. Fiedler, K. Schulte, Influence of different carbon nanotubes on the mechanical properties of epoxy matrix composites – a comparative study, Composites Science and Technology 65 (15–16) (2005) 2300–2313. doi:10.1016/j.compscitech.2005.04.021.

[136] D. C. Davis, J. W. Wilkerson, J. Zhu, D. O. Ayewah, Improvements in mechanical properties of a carbon fiber epoxy composite using nanotube science and technology, Composite Structures 92 (11) (2010) 2653–2662. doi:10.1016/j.compstruct.2010.03.019.

[137] B. Ahmadi-Moghadam, M. Sharafimasooleh, S. Shadlou, F. Taheri, Effect of functionalization of graphene nanoplatelets on the mechanical response of graphene/epoxy composites, Materials & Design 66, Part A (2015) 142–149. doi:10.1016/j.matdes.2014.10.047.

[138] P.-C. Ma, N. A. Siddiqui, G. Marom, J.-K. Kim, Dispersion and functionalization of carbon nanotubes for polymer-based nanocomposites: A review, Composites Part A: Applied Science and Manufacturing 41 (10) (2010) 1345–1367. doi:10.1016/j.compositesa.2010.07.003.

[139] L. S. Schadler, L. C. Brinson, W. G. Sawyer, Polymer nanocomposites: A small part of the story, JOM 59 (3) (2007) 53–60. doi:10.1007/s11837-007-0040-5.

[140] R. Nadiv, G. Shachar, S. Peretz-Damari, M. Varenik, I. Levy, M. Buzaglo, E. Ruse, O. Regev, Performance of nano-carbon loaded polymer composites: Dimensionality matters, Carbon 126 (2018) 410–418. doi:10.1016/j.carbon.2017.10.039.

[141] M. Mecklenburg, A. Schuchardt, Y. K. Mishra, S. Kaps, R. Adelung, A. Lotnyk, L. Kienle, K. Schulte, Aerographite: Ultra lightweight, flexible nanowall, carbon microtube material with outstanding mechanical performance, Advanced Materials 24 (26) (2012) 3486–3490. doi:10.1002/adma.201200491.

[142] S. Chandrasekaran, W. V. Liebig, M. Mecklenburg, B. Fiedler, D. Smazna, R. Adelung, K. Schulte, Fracture, failure and compression behaviour of a 3d interconnected carbon aerogel (aerographite) epoxy composite, Composites Science and Technology 122 (2016) 50–58. doi:10.1016/j.compscitech.2015.11.002.

[143] R. Schueler, J. Petermann, K. Schulte, H.-P. Wentzel, Agglomeration and electrical percolation behavior of carbon black dispersed in epoxy resin, Journal of Applied Polymer Science 63 (13) (1997) 1741–1746. doi:https://doi.org/10.1002/(SICI)1097-4628(19970328)63:13.

[144] D. Zhang, L. Ye, S. Deng, J. Zhang, Y. Tang, Y. Chen, CF/EP composite laminates with carbon black and copper chloride for improved electrical conductivity and interlaminar fracture toughness, Composites Science and Technology 72 (3) (2012) 412–420. doi:10.1016/j.compscitech.2011.12.002.

[145] M. H. Wichmann, J. Sumfleth, F. H. Gojny, M. Quaresimin, B. Fiedler, K. Schulte, Glass-fibre-reinforced composites with enhanced mechanical and electrical properties – benefits and limitations of a nanoparticle modified matrix, Engineering Fracture Mechanics 73 (16) (2006) 2346–2359. doi:10.1016/j.engfracmech.2006.05.015.

[146] S. Iijima, Helical microtubules of graphitic carbon, Nature 354 (6348) (1991) 56–58. doi:10.1038/354056a0.

[147] S. Iijima, T. Ichihashi, Single-shell carbon nanotubes of 1-nm diameter, Nature 363 (6430) (1993) 603–605. doi:10.1038/363603a0.

[148] F. H. Gojny, M. H. Wichmann, U. Köpke, B. Fiedler, K. Schulte, Carbon nanotube-reinforced epoxy-composites: enhanced stiffness and fracture toughness at low nanotube content, Composites Science and Technology 64 (15) (2004) 2363–2371. doi:10.1016/j.compscitech.2004.04.002.

[149] T.-H. Hsieh, A. J. Kinloch, A. C. Taylor, I. A. Kinloch, The effect of carbon nanotubes on the fracture toughness and fatigue performance of a thermosetting epoxy polymer, Journal of Materials Science 46 (23) (2011) 7525–7535. doi:10.1007/s10853-011-5724-0.

[150] M. Shtein, R. Nadiv, N. Lachman, H. Daniel Wagner, O. Regev, Fracture behavior of nanotube–polymer composites: Insights on surface roughness and failure mechanism, Composites Science and Technology 87 (2013) 157–163. doi:10.1016/j.compscitech.2013.07.016.

[151] N. Lachman, D. H. Wagner, Correlation between interfacial molecular structure and mechanics in CNT/epoxy nano-composites, Composites Part A: Applied Science and Manufacturing 41 (9) (2010) 1093–1098. doi:10.1016/j.compositesa.2009.08.023.

[152] F. H. Gojny, J. Nastalczyk, Z. Roslaniec, K. Schulte, Surface modified multi-walled carbon nanotubes in CNT/epoxy-composites, Chemical Physics Letters 370 (5–6) (2003) 820–824. doi:10.1016/S0009-2614(03)00187-8.

[153] W. Zhang, R. C. Picu, N. Koratkar, The effect of carbon nanotube dimensions and dispersion on the fatigue behavior of epoxy nanocomposites, Nanotechnology 19 (28) (2008) 285709.

[154] M.-F. Yu, O. Lourie, M. J. Dyer, K. Moloni, T. F. Kelly, R. S. Ruoff, Strength and breaking mechanism of multiwalled carbon nanotubes under tensile load, Science 287 (5453) (2000) 637. doi:10.1126/science.287.5453.637.

[155] J. B. Bai, A. Allaoui, Effect of the length and the aggregate size of mwnts on the improvement efficiency of the mechanical and electrical properties of nanocomposites - experimental investigation, Composites Part A: Applied Science and Manufacturing 34 (8) (2003) 689–694. doi:10.1016/S1359-835X(03)00140-4.

[156] S. Chandrasekaran, N. Sato, F. Tölle, R. Mülhaupt, B. Fiedler, K. Schulte, Fracture toughness and failure mechanism of graphene based epoxy composites, Composites Science and Technology 97 (2014) 90–99. doi:10.1016/j.compscitech.2014.03.014.

[157] M. A. Rafiee, J. Rafiee, Z. Wang, H. Song, Z.-Z. Yu, N. Koratkar, Enhanced mechanical properties of nanocomposites at low graphene content, ACS Nano 3 (12) (2009) 3884–3890. doi:10.1021/nn9010472.

[158] M. A. Rafiee, J. Rafiee, I. Srivastava, Z. Wang, H. Song, Z.-Z. Yu, N. Koratkar, Fracture and fatigue in graphene nanocomposites, Small 6 (2) (2010) 179–183. doi:10.1002/smll.200901480.

[159] D. R. Bortz, E. G. Heras, I. Martin-Gullon, Impressive fatigue life and fracture toughness improvements in graphene oxide/epoxy composites, Macromolecules 45 (1) (2011) 238–245. doi:10.1021/ma201563k.

[160] M.-Y. Shen, T.-Y. Chang, T.-H. Hsieh, Y.-L. Li, C.-L. Chiang, H. Yang, M.-C. Yip, Mechanical properties and tensile fatigue of graphene nanoplatelets reinforced polymer nanocomposites, Journal of Nanomaterials 2013 (4) (2013) 1–9. doi:10.1155/2013/565401.

[161] H. Wittich, K. Hedicke, V. Altstädt, C. Mehler, Optimierung des Gefüges von Nanoplättchen aus Schichtsilikaten in Polymeren im Hinblick auf ihre mikromechanische Wirkung: Presented at 14. Symposium: Verbundwerkstoffe und Werkstoffverbunde, Vienna, Austria (2003).

[162] I. Greenfeld, H. D. Wagner, Nanocomposite toughness, strength and stiffness: role of filler geometry, Nanocomposites 1 (1) (2015) 3–17. doi:10.1179/2055033214Y.0000000002.

[163] H. D. Wagner, P. M. Ajayan, K. Schulte, Nanocomposite toughness from a pull-out mechanism, Composites Science and Technology 83 (2013) 27–31. doi:10.1016/j.compscitech.2013.04.017.

[164] H. Liu, L. C. Brinson, Reinforcing efficiency of nanoparticles: A simple comparison for polymer nanocomposites, Composites Science and Technology 68 (6) (2008) 1502–1512. doi:10.1016/j.compscitech.2007.10.033.

[165] V. Mirjalili, M. Yourdkhani, P. Hubert, Dispersion stability in carbon nanotube modified polymers and its effect on the fracture toughness, Nanotechnology 23 (31) (2012) 315701.

[166] G. Dai, Mishnaevsky Jr. , Leon, Graphene reinforced nanocomposites: 3d simulation of damage and fracture, Computational Materials Science 95 (2014) 684–692. doi:10.1016/j.commatsci.2014.08.011.

[167] ASTM international, ASTM-D5045 Test methods for plane-strain fracture toughness and strain energy release rate of plastic materials (2014). doi:10.1520/D5045-14.

[168] S. Chandrasekaran, C. Seidel, K. Schulte, Preparation and characterization of graphite nano-platelet (GNP)/epoxy nano-composite: Mechanical, electrical and thermal properties, European Polymer Journal 49 (12) (2013) 3878–3888. doi:10.1016/j.eurpolymj.2013.10.008.

[169] S. Chatterjee, F. A. Nüesch, B. Chu, Comparing carbon nanotubes and graphene nanoplatelets as reinforcements in polyamide 12 composites, Nanotechnology 22 (27) (2011) 275714.

[170] X. Du, H. Zhou, W. Sun, H.-Y. Liu, G. Zhou, H. Zhou, Y.-W. Mai, Graphene/epoxy interleaves for delamination toughening and monitoring of crack damage in carbon fibre/epoxy composite laminates, Composites Science and Technology 140 (2017) 123–133. doi:10.1016/j.compscitech.2016.12.028.

[171] I. Zaman, T. T. Phan, H.-C. Kuan, Q. Meng, L. T. Bao La, L. Luong, O. Youssf, J. Ma, Epoxy/graphene platelets nanocomposites with two levels of interface strength, Polymer 52 (7) (2011) 1603–1611. doi:10.1016/j.polymer.2011.02.003.

[172] M. R. Ayatollahi, S. Shadlou, M. M. Shokrieh, M. Chitsazzadeh, Effect of multi-walled carbon nanotube aspect ratio on mechanical and electrical properties of epoxy-based nanocomposites, Polymer Testing 30 (5) (2011) 548–556. doi:10.1016/j.polymertesting.2011.04.008.

[173] B. C. Kim, S. W. Park, D. G. Lee, Fracture toughness of the nano-particle reinforced epoxy composite, Fourteenth International Conference on Composite Structures 86 (1) (2008) 69–77. doi:10.1016/j.compstruct.2008.03.005.

[174] L. Liu, L. Li, Y. Gao, L. Tang, Z. Zhang, Single carbon fiber fracture embedded in an epoxy matrix modified by nanoparticles, Composites Science and Technology 77 (2013) 101–109. doi:10.1016/j.compscitech.2012.12.015.

[175] J. Zhang, S. Deng, Y. Wang, L. Ye, L. Zhou, Z. Zhang, Effect of nanoparticles on interfacial properties of carbon fibre–epoxy composites, Composites Part A: Applied Science and Manufacturing 55 (2013) 35–44. doi:10.1016/j.compositesa.2013.08.005.

[176] Y. Tian, H. Zhang, Z. Zhang, Influence of nanoparticles on the interfacial properties of fiber-reinforced-epoxy composites, Composites Part A: Applied Science and Manufacturing 98 (2017) 1–8. doi:10.1016/j.compositesa.2017.03.007.

[177] E. Mannov, H. Schmutzler, S. Chandrasekaran, C. Viets, S. Buschhorn, F. Tölle, R. Mülhaupt, K. Schulte, Improvement of compressive strength after impact in fibre reinforced polymer composites by matrix modification with thermally reduced graphene oxide, Composites Science and Technology 87 (2013) 36–41. doi:10.1016/j.compscitech.2013.07.019.

[178] V. Kostopoulos, A. Baltopoulos, P. Karapappas, A. Vavouliotis, A. Paipetis, Impact and after-impact properties of carbon fibre reinforced composites enhanced with multi-wall carbon nanotubes, Composites Science and Technology 70 (4) (2010) 553–563. doi:10.1016/j.compscitech.2009.11.023.

[179] D. Bull, S. Spearing, I. Sinclair, The role of particle-toughening in improving post-impact compressive strength, in: ECCM16 - 16th European Conference on Composite Materials, Sevilla, Spain, 2014.

[180] J.-B. Moon, M.-G. Kim, C.-G. Kim, S. Bhowmik, Improvement of tensile properties of CFRP composites under LEO space environment by applying MWNTs and thin-ply, Composites Part A: Applied Science and Manufacturing 42 (6) (2011) 694–701. doi:10.1016/j.compositesa.2011.02.011.

[181] B. Zhang, R. Asmatulu, Soltani, S. A., Le, L. N., Kumar, S. S. A., Mechanical and thermal properties of hierarchical composites enhanced by pristine graphene and graphene oxide nanoinclusions, Journal of Applied Polymer Science 131 (19) (2014) n/a. doi:10.1002/app.40826.

[182] C. M. Manjunatha, A. C. Taylor, A. J. Kinloch, S. Sprenger, The tensile fatigue behaviour of a silica nanoparticle-modified glass fibre reinforced epoxy composite, Composites Science and Technology 70 (1) (2010) 193–199. doi:10.1016/j.compscitech.2009.10.012.

[183] J. B. Kosmann, Impact of Carbon Nanoparticles on Fatigue Properties and Damage Mechanisms of Carbon Fibre-Reinforced Epoxy. (Dissertation), TuTech Innovation, 2017.

[184] J. Kosmann, C. Leopold, K. Schulte, B. Fiedler, Damage initiation and failure mechanisms of carbon nanoparticle modified CFRP up to very high cycle fatigue loading: Final Report (Project SPP-1466) (2018).

[185] F. Yavari, M. A. Rafiee, J. Rafiee, Z.-Z. Yu, N. Koratkar, Dramatic increase in fatigue life in hierarchical graphene composites, ACS Appl. Mater. Interfaces 2 (10) (2010) 2738–2743. doi:10.1021/am100728r.

[186] N. Sato, M. Hojo, M. Nishikawa, Intralaminar fatigue crack growth properties of conventional and interlayer toughened CFRP laminate under mode I loading, Composites Part A: Applied Science and Manufacturing 68 (2015) 202–211. doi:10.1016/j.compositesa.2014.09.031.

[187] G. Dai, L. Mishnaevsky, Fatigue of multiscale composites with secondary nanoplatelet reinforcement: 3d computational analysis, Composites Science and Technology 91 (2014) 71–81. doi:10.1016/j.compscitech.2013.11.024.

[188] C. Kostagiannakopoulou, T. H. Loutas, G. Sotiriadis, A. Markou, V. Kostopoulos, On the interlaminar fracture toughness of carbon fiber composites enhanced with graphene nano-species, Composites Science and Technology 118 (2015) 217–225. doi:10.1016/j.compscitech.2015.08.017.

[189] C. Kostagiannakopoulou, X. Tsilimigkra, G. Sotiriadis, V. Kostopoulos, Synergy effect of carbon nano-fillers on the fracture toughness of structural composites, Composites Part B: Engineering 129 (2017) 18–25. doi:10.1016/j.compositesb.2017.07.012.

[190] B. Ahmadi-Moghadam, F. Taheri, Influence of graphene nanoplatelets on modes I, II and III interlaminar fracture toughness of fiber-reinforced polymer composites, Engineering Fracture Mechanics 143 (2015) 97–107. doi:10.1016/j.engfracmech.2015.06.026.

[191] B. Ahmadi-Moghadam, F. Taheri, Fracture and toughening mechanisms of GNP-based nanocomposites in modes I and II fracture, Engineering Fracture Mechanics 131 (2014) 329–339. doi:10.1016/j.engfracmech.2014.08.008.

[192] M. Quaresimin, R. J. Varley, Understanding the effect of nano-modifier addition upon the properties of fibre reinforced laminates, Composites Science and Technology 68 (3–4) (2008) 718–726. doi:10.1016/j.compscitech.2007.09.005.

[193] S. Brunauer, P. H. Emmett, E. Teller, Adsorption of gases in multimolecular layers, J. Am. Chem. Soc. 60 (2) (1938) 309–319. doi:10.1021/ja01269a023.

[194] ASTM international, ASTM D3379-75 Test method for tensile strength and youngs modulus for high-modulus single-filament materials (withdrawn 1998) (1975). doi:10.1520/D3379-75R89E01.

[195] C. Leopold, T. Augustin, T. Schwebler, J. Lehmann, W. V. Liebig, B. Fiedler, Influence of carbon nanoparticle modification on the mechanical and electrical properties of epoxy in small volumes, Journal of Colloid and Interface Science 506 (2017) 620–632. doi:10.1016/j.jcis.2017.07.085.

[196] International Organization for Standardization, DIN EN ISO 527-2 Plastics - Determination of tensile properties - Part 2: Test conditions for moulding and extrusion plastics (2012).

[197] S. Ogihara, Y. Sakamoto, J. Koyanagi, Evaluation of interfacial tensile strength in glass fiber/epoxy resin interface using the cruciform specimen method, Journal of Solid Mechanics and Materials Engineering 3 (9) (2009) 1071–1080. doi:10.1299/jmmp.3.1071.

[198] AIRBUS S.A.S, AITM 1-0008 Fibre Reinforced Plastics - Determination of Plain, Open Hole and Filled Hole Compression Strength. (2004).

[199] ASTM international, ASTM D7136 Test method for measuring the damage resistance of a fiber-reinforced polymer matrix composite to a drop-weight impact event (2015). doi:10.1520/D7136_D7136M-15.

[200] ASTM international, ASTM D7137 Test method for compressive residual strength properties of damaged polymer matrix composite plates (2012). doi:10.1520/D7137_D7137M-12.

[201] German Institute for Standardisation, DIN EN 3615 Fibre reinforced plastics - Determination of the conditions of exposure to humid atmosphere and of moisture absorption (Withdrawn) (1999).

[202] German Institute for Standardisation, DIN EN 2564 Aerospace series - Carbon fibre laminates - Determination of the fibre-, resin- and void contents (1998).

[203] A. Frick, C. Stern, Einführung in die Kunststoffprüfung: Prüfmethoden und Anwendungen, Hanser Fachbuchverlag, München, 2017.

[204] W. Grellmann, S. Seidler, Kunststoffprüfung, 3rd Edition, Hanser, München, 2015.

[205] B. Fiedler, K. Schulte, Photo-elastic analysis of fibre-reinforced model composite materials, Composites Science and Technology 57 (8) (1997) 859–867. doi:10.1016/S0266-3538(96)00177-7.

[206] W. V. Liebig, C. Viets, K. Schulte, B. Fiedler, Influence of voids on the compressive failure behaviour of fibre-reinforced composites, Composites Science and Technology 117 (2015) 225–233. doi:10.1016/j.compscitech.2015.06.020.

[207] C. U. Große, M. Ohtsu, Acoustic Emission Testing: Basics for Research - Applications in Civil Engineering, 1st Edition, Springer-Verlag, Berlin, 2008.

[208] The Japanese Society for Non-Destructive Inspection, Practical acoustic emission testing, Springer, Tokyo, 2016.

[209] N. Qing-Qing, J. Eiichi, Acoustic emission and fracture of carbon fiber reinforced thermosoftening plastic (CFRTP) materials under monotonous tensile loading, Engineering Fracture Mechanics 45 (5) (1993) 611–625. doi:10.1016/0013-7944(93)90267-V.

[210] Y. Mizutani, K. Nagashima, M. Takemoto, K. Ono, Fracture mechanism characterization of cross-ply carbon-fiber composites using acoustic emission analysis, NDT & E International 33 (2) (2000) 101–110. doi:10.1016/S0963-8695(99)00030-4.

[211] P. F. Liu, J. K. Chu, Y. L. Liu, J. Y. Zheng, A study on the failure mechanisms of carbon fiber/epoxy composite laminates using acoustic emission, Materials & Design 37 (2012) 228–235. doi:10.1016/j.matdes.2011.12.015.

[212] N. Kosmann, J. Karsten, M. Schuett, K. Schulte, B. Fiedler, Determining the effect of voids in GFRP on the damage behaviour under compression loading using acoustic emission, Composites Part B: Engineering 70 (2015) 184–188. doi:10.1016/j.compositesb.2014.11.010.

[213] P. J. de Groot, P. A. Wijnen, R. B. Janssen, Real-time frequency determination of acoustic emission for different fracture mechanisms in carbon/epoxy composites, Composites Science and Technology 55 (4) (1995) 405–412. doi:10.1016/0266-3538(95)00121-2.

[214] R. Gutkin, C. J. Green, S. Vangrattanachai, S. T. Pinho, P. Robinson, P. T. Curtis, On acoustic emission for failure investigation in CFRP: Pattern recognition and peak frequency analyses, Mechanical Systems and Signal Processing 25 (4) (2011) 1393–1407. doi:10.1016/j.ymssp.2010.11.014.

[215] N. Hsu, R. Breckenridge, Characterization and calibration of acoustic emission sensors, Materials Evaluation 39 (1981) 60–68.

[216] C. Leopold, M. Schütt, W. V. Liebig, T. Philipkowski, J. Kürten, K. Schulte, B. Fiedler, Compression fracture of CFRP laminates containing stress intensifications, Materials (Basel, Switzerland) 10 (9). doi:10.3390/ma10091039.

[217] R. Reichelt, Scanning electron microscopy, in: P. W. Hawkes, J. C. H. Spence (Eds.), Science of Microscopy, Springer, New York, 2007, pp. 133–272. doi:10.1007/978-0-387-49762-4_3.

[218] W. Zhou, Z. L. Wang (Eds.), Advanced scanning microscopy for nanotechnology: Techniques and applications, Springer, New York, 2007.

[219] C. Leopold, W. V. Liebig, S. Harder, B. Fiedler, Influence of ply thickness on the fibre matrix debonding, in: ICCM-20 - 20th International Conference on Composite Materials, Copenhagen, Denmark, 2015.
URL http://iccm20.org/fullpapers/file?f=Dlkm27wmdd

[220] A. Puck, Das 'Knie' im Spannungs-Dehnungs-Diagramm und Rissbildung bei Glasfaser/Kunststoffen, Kunststoffe 58 (12) (1968) 886.

[221] W. Weibull, A statistical theory of the strength of materials, Royal Swedish Institute for Engineering Research 151 (1939) 1–45.

[222] C. Leopold, S. Harder, C. Buggisch, W. V. Liebig, B. Fiedler, Influence of 90°-layer thickness on damage initiation and propagation in CFRP cross-ply laminates, in: European Conference on Composite Materials, ECCM (Ed.), ECCM17: Munich, Germany, 26-30th June 2016, 2016.

[223] J.-M. Berthelot, Transverse cracking and delamination in cross-ply glass-fiber and carbon-fiber reinforced plastic laminates: Static and fatigue loading, Applied Mechanics Reviews 56 (1) (2003) 111–147. doi:10.1115/1.1519557.

[224] J. Varna, R. Joffe, N. V. Akshantala, R. Talreja, Damage in composite laminates with off-axis plies, Composites Science and Technology 59 (14) (1999) 2139–2147. doi:10.1016/S0266-3538(99)00070-6.

[225] P. W. Manders, T.-W. Chou, F. R. Jones, J. W. Rock, Statistical analysis of multiple fracture in 0°/90°/0° glass fibre/epoxy resin laminates, Journal of Materials Science 18 (10) (1983) 2876–2889. doi:10.1007/BF00700768.

[226] Z. Hashin, Analysis of cracked laminates: a variational approach, Mechanics of Materials 4 (2) (1985) 121–136. doi:10.1016/0167-6636(85)90011-0.

[227] J. Varna, L. A. Berglund, A model for prediction of the transverse cracking strain in cross-ply laminates, Journal of Reinforced Plastics and Composites 11 (7) (1992) 708–728. doi:10.1177/073168449201100701.

[228] M. Herráez, D. Mora, F. Naya, C. S. Lopes, C. González, J. LLorca, Transverse cracking of cross-ply laminates: A computational micromechanics perspective, Composites Science and Technology 110 (2015) 196–204. doi:10.1016/j.compscitech.2015.02.008.

[229] P. E. Reed, S. Turner, Flexed plate impact, part 7. low energy and excess energy impacts on carbon fibre-reinforced polymer composites, Composites 19 (3) (1988) 193–203. doi:10.1016/0010-4361(88)90237-6.

[230] D. Gross, W. Hauger, J. Schröder, Technische Mechanik 2: Elastostatik, 12th Edition, Springer-Lehrbuch, Springer-Verlag, Berlin, 2014.

[231] C. Leopold, W. V. Liebig, H. Wittich, B. Fiedler, Size effect of graphene nanoparticle modified epoxy matrix, Composites Science and Technology 134 (2016) 217–225. doi:10.1016/j.compscitech.2016.08.022.

[232] H. Gao, B. Ji, I. L. Jäger, E. Arzt, P. Fratzl, Materials become insensitive to flaws at nanoscale: Lessons from nature, Proceedings of the National Academy of Sciences of the United States of America 100 (10) (2003) 5597–5600. doi:10.1073/pnas.0631609100.

[233] J. Bauer, A. Schroer, R. Schwaiger, I. Tesari, C. Lange, L. Valdevit, O. Kraft, Push-to-pull tensile testing of ultra-strong nanoscale ceramic–polymer composites made by additive manufacturing, Extreme Mechanics Letters 3 (2015) 105–112. doi:10.1016/j.eml.2015.03.006.

[234] J. Bauer, A. Schroer, R. Schwaiger, O. Kraft, Approaching theoretical strength in glassy carbon nanolattices, Nature Materials 15 (4) (2016) 438–443.

[235] Y. Liu, H. Wu, G. Chen, Enhanced mechanical properties of nanocomposites at low graphene content based on in situ ball milling, Polymer Composites 37 (4) (2016) 1190–1197. doi:10.1002/pc.23283.

[236] K. Arakawa, K. Takahashi, Relationships between fracture parameters and fracture surface roughness of brittle polymers, International Journal of Fracture 48 (2) (1991) 103–114. doi:10.1007/BF00018393.

[237] D. Haba, A. J. Brunner, G. Pinter, Dispersion of fullerene-like WS2 nanoparticles within epoxy and the resulting fracture mechanics, Composites Science and Technology 119 (2015) 55–61. doi:10.1016/j.compscitech.2015.09.013.

[238] F. H. Gojny, M. H. Wichmann, B. Fiedler, W. Bauhofer, K. Schulte, Influence of nano-modification on the mechanical and electrical properties of conventional fibre-reinforced composites, Composites Part A: Applied Science and Manufacturing 36 (11) (2005) 1525–1535. doi:10.1016/j.compositesa.2005.02.007.

[239] A. Schetle, Influence of graphene nanoparticle matrix modification of either the 0°- or the 90°- layer of CFRP cross-ply laminates on the mechanical properties and failure propagation under static and cyclic loads, Master thesis, Hamburg University of Technology (2016).

[240] Z. Li, R. J. Young, N. R. Wilson, I. A. Kinloch, C. Vallés, Z. Li, Effect of the orientation of graphene-based nanoplatelets upon the Young's modulus of nanocomposites, Composites Science and Technology 123 (2016) 125–133. doi:10.1016/j.compscitech.2015.12.005.

[241] K. Schulte, B. Fiedler, Structure and properties of composite materials, 2nd Edition, Vol. 11 of Technisch-wissenschaftliche Schriftenreihe / TUHH Polymer Composites, TuTech-Innovation GmbH, Hamburg, 2010.

[242] R. Talreja, C. V. Singh, Damage and failure of composite materials, Cambridge University Press, Cambridge and New York, 2012.

[243] B. Fiedler, M. Hojo, S. Ochiai, K. Schulte, M. Ando, Failure behavior of an epoxy matrix under different kinds of static loading, Composites Science and Technology 61 (11) (2001) 1615–1624. doi:10.1016/S0266-3538(01)00057-4.

[244] P. Berbinau, C. Soutis, P. Goutas, P. Curtis, Effect of off-axis ply orientation on 0°-fibre microbuckling, Composites Part A: Applied Science and Manufacturing 30 (10) (1999) 1197–1207. doi:10.1016/S1359-835X(99)00026-3.

[245] P. Berbinau, C. Soutis, I. A. Guz, Compressive failure of 0°unidirectional carbon-fibre-reinforced plastic (CFRP) laminates by fibre microbuckling, Composites Science and Technology 59 (9) (1999) 1451–1455. doi:10.1016/S0266-3538(98)00181-X.

[246] S.-Y. Yang, W.-N. Lin, Y.-L. Huang, H.-W. Tien, J.-Y. Wang, C.-C. M. Ma, S.-M. Li, Y.-S. Wang, Synergetic effects of graphene platelets and carbon nanotubes on the mechanical and thermal properties of epoxy composites, Carbon 49 (3) (2011) 793–803. doi:10.1016/j.carbon.2010.10.014.

Supervised student theses and research projects

Tugsbold Boldbaatar: Mechanical Properties of Thin-Ply Laminates. Bachelor thesis, Hamburg University of Technology 2015

Jan-Niklas Heitmann: Einfluss der Schichtdicke auf das Verhalten von CFK-Laminaten mit einer zentralen Bohrung unter Zugbelastung. Bachelor thesis, Hamburg University of Technology, 2015

Timo Philipkowski: Einfluss der Schichtdicke auf die mechanischen Eigenschaften von CFK-Laminaten mit einer zentralen Bohrung unter Druckbelastung. Bachelor thesis, Hamburg University of Technology, 2015

Roy Poels: Experimentelle Untersuchung des Einflusses der Schichtdicke auf die Schadensentwicklung in GFK Modell-Probekörpern. Bachelor thesis, Hamburg University of Technology, 2015

Sergej Harder: Numerische Betrachtung des Einflusses der Schichtdicke von Kreuzverbunden unter Berücksichtigung des nicht-linearen Werkstoffverhaltens der Matrix. Research project, Hamburg University of Technology, 2015

Christina Buggisch: Einfluss der Schichtdicke der 90° Schicht auf die Schadensentwicklung und die mechanischen Eigenschaften von CFK Kreuzverbundlaminaten unter Zuglast. Bachelor thesis, Hamburg University of Technology, 2015

Jonas Kürten: Einfluss der Schichtdicke von CFK-Laminaten auf die Restdruckfestigkeit nach einem Schlagschaden. Bachelor thesis, Hamburg University of Technology, 2015

Benno von Essen: Untersuchung des Volumeneffektes von Nanopartikel-modifizierter Epoxidmatrix im Einzelfaser-Zugversuch. Bachelor thesis, Hamburg University of Technology, 2015

Sergej Harder: Optimierung eines numerischen Modells von FKV Kreuzverbund-Laminaten und Vergleich mit experimentellen Untersuchungen, Master thesis, Hamburg University of Technology, 2015

Merle Braatz: Mikromechanische Simulation von Graphen-Nanopartikeln in Epoxidharzmatrix. Bachelor thesis, Hamburg University of Technology, 2016

Tjark Ole Green: Untersuchung des Einflusses der 90° Schichtdicke auf die mechanischen Eigenschaften von CFK Kreuzverbundlaminaten. Bachelor thesis, Hamburg University of Technology, 2016

Andreas Schetle: Einfluss einer Matrixmodifikation mit Graphen-Nanopartikeln von CFK-Kreuzverbundlaminaten auf die mechanischen Eigenschaften und die Schadensausbreitung unter statischer und zyklischer Last. Master thesis, Hamburg University of Technology, 2016

Jonas Lehmann: Einfluss von Füllgrad und Partikelgeometrie auf die elektrischen Eigenschaften von Kohlenstoff-Nanopartikel modifizierter Epoxidmatrix im Einzelfaser Zugversuch. Bachelor thesis, Hamburg University of Technology, 2016

Thomas Schwebler: Einfluss von Füllgrad und Partikelgeometrie auf die mechanischen Eigenschaften von Kohlenstoff-Nanopartikel-modifizierter Epoxidmatrix im Einzelfaser-Zugversuch. Bachelor thesis, Hamburg University of Technology, 2016

Timo Philipkowski: Validierung analytischer Modelle zur Vorhersage der Druckfestigkeit von Faser-Kunstoff-Verbunden. Research project, Hamburg University of Technology, 2016

Martina Schulze: Experimentelle Untersuchung des Einflusses von Kohlenstoff-Nanopartikeln in Epoxidmatrix auf die Faser-Matrix-Ablösung und die Schadensentwicklung in GFK Modell-Probekörpern. Bachelor thesis, Hamburg University of Technology, 2017

Christina Buggisch: Überblick über analytische Kriterien zur Bewertung der Auswirkungen der Zwischenfaserbruchmorphologie auf das weitere Versagen von Faser-Kunststoff-Verbunden. Research project, Hamburg University of Technology, 2017

Galin Gichev: Extension of a FE-model for studying the influence of a nanoparticle-modified matrix on the damage development in fibre reinforced plastics. Bachelor thesis, Hamburg University of Technology, 2018

Vita

Name:	Christian Leopold
Date of Birth	30.05.1984
Place of birth:	Lübeck, Germany
Since 03.2014	Research assistant at Institute of Polymer and Composites, Hamburg University of Technology (TUHH)
07.2012 - 02.2014	Research engineer at Alten Technology GmbH
10.2005 - 05.2012	Study in Mechanical Engineering, specialisation in Mechanical Engineering Design with focus on Aircraft Systems Engineering. Degree: Diploma (Dipl.-Ing.)
08.2004 - 08.2005	Civilian service, Die Brücke Lübeck
06.1991 - 07.2004	Freie Waldorfschule, Lübeck, degree: Abitur